Universiteit Utrecht

Graduate School of Natural Sciences
Institute for Theoretical Physics

Master's Thesis

Quantum Null Energy Condition in the holographic dual of Gauss-Bonnet gravity

Author:
Ferran del Moral Méndez

under the supervision of

Dr. Wilke van der Schee
Dr. Umut Gürsoy

MSc. in Theoretical Physics

June 30, 2019

Universiteit Utrecht

A mis padres y hermana, en cuyos hombros siempre estoy subido.

A mis abuelos. Siento que siempre me acabe marchando de nuevo.

"*Science is a way of life. Science is a perspective. Science is the process that takes us from confusion to understanding in a manner that's precise, predictive and reliable - a transformation, for those lucky enough to experience it, that is empowering and emotional.*"

Brian Greene

Abstract

The Quantum Null Energy Condition (QNEC) is the extension of the classical Null Energy Condition (NEC) into the quantum physics regime. This new energy condition relates the classical NEC to the second derivative of an entanglement entropy in the corresponding null direction k^μ: $\langle T_{\mu\nu}k^\mu k^\nu\rangle \geq \frac{\hbar}{2\pi\sqrt{h}}\frac{d^2S}{d\lambda^2}$. In this thesis, we perform an explicit computation of the QNEC for two different geometries of the entangling region in which we compute the entanglement entropy, namely strip-like and spherical regions, and we do so by considering both Einstein-Hilbert and Gauss-Bonnet holographies. We show that, in Einstein-Hilbert holography, for the strip-like regions the QNEC is always trivially satisfied while for spheres we can encounter a saturation of the inequality depending on how we choose the null direction k^μ. This saturation will not show up in the Gauss-Bonnet holography setup and, instead, we will find that the QNEC is violated depending on the sign of the Gauss-Bonnet coupling. Therefore, this results may add more arguments to the already existing discussion on whether the field theory dual to Gauss-Bonnet gravity is actually physical or not.

Acknowledgements

This thesis is the result of ten months of work and, although my name is the only one appearing in the cover, it would not be a reality if it were not for the people that supported and helped me along this journey.

First of all, I want to thank my supervisor Wilke van der Schee for all the time he invested into the project, always giving me clear explanations and motivating enriching discussions. I really appreciate the availability to meet and discuss every time I needed it, even if we had to skype from different continents.

I would also like to thank to my parents and sister all the effort they have done and all the support they have shown during all these years. Without them I would not have been able to travel all the way to the Netherlands to do this Master in the first place.

Last, but not least, I would like to thank Jans for this last year and a half. With no doubt, you are the main reason why I have enjoyed this time so much. Thank you for always believing in me. You are amazing!

Contents

1. Introduction

Among all the energy conditions, the Null Energy Condition (NEC), $T_{\mu\nu}k^\mu k^\nu \geq 0$, plays a central role in the context of General Relativity. It is not only logical and robust, but also underlies many important results, such as the singularity theorems, the area theorems or the cosmological censorship. Apart from that, it also plays an important role in AdS/CFT correspondence, since imposing the NEC in the bulk has some consequences in the boundary theory such as the holographic c-theorems. However, the NEC not always holds for all unitary QFTs. In other words: the NEC can be violated in quantum systems.

In 2016 Bousso, et.al. [1] proposed a new quantum version of this NEC, the Quantum Null Energy Condition (QNEC), based on a conjecture for a quantum version of the Focusing theorem. This QNEC, which is supposed to hold true for any unitary QFT, relates the expectation value of the energy density $\langle T_{\mu\nu}k^\mu k^\nu\rangle$ at a point p with the entanglement entropy S of a region. More precisely, consider that we divide the spacetime into two regions with a surface $\partial\mathcal{A}$ that crosses at the point p. Furthermore, consider now that we vary this surface at the point p in a null direction. Then, the QNEC states that the expectation value of the energy density at the point p is bounded from below by the second derivative of the entanglement entropy of one of the two regions of spacetime with respect to this null variation:

$$\langle T_{\mu\nu}k^\mu k^\nu\rangle \geq \frac{1}{2\pi\sqrt{h}}\frac{d^2S}{d\lambda^2} \ , \tag{1.1}$$

where h is the determinant of the metric of $\partial\mathcal{A}$ and λ parametrizes the variation. Thus, the QNEC is interesting, not only because it is believed to be satisfied for QFTs, but also because of the role that the entanglement entropy plays in it, since the latter is thought to be essential to understand the emergence of gravity in holographic theories.

The actual computation of the entanglement entropy is, in general, extremely difficult to perform. However, in 2006, Ryu and Takayanagi [2] proposed a formula, based on the Hawking entropy formula, to compute the entanglement entropy by means of the AdS/CFT correspondence, i.e. the holographic entanglement entropy. This prescription states that the entanglement entropy of a region $\mathcal{A}$ is given by the area of the minimal area surface $\mathcal{E}_\mathcal{A}$ which lives in the bulk manifold and limits with $\partial\mathcal{A}$ at the boundary. In other words:

$$S = \frac{\text{Area}(\mathcal{E}_\mathcal{A})}{4G_N^{(D)}} \ . \tag{1.2}$$

This prescription, then, reduces the question of studying the QNEC to study how this bulk minimal surfaces vary when we vary the entangling surfaces at the boundary.

An explicit computation of the QNEC has only been done in very few particular cases and this is going to be actually the goal of this thesis. More precisely, in this thesis we will study how the QNEC inequality behaves depending on the geometry of the entangling surface $\partial\mathcal{A}$ and the variations that we are allow to do to them. In particular, we are interested in studying the QNEC for strip-like and sphere-like entangling regions. Not only that but, since we will need to compute the holographic entanglement entropy, we will also study how the QNEC behaves in a holographic setup that involves higher derivative gravity in the bulk. We are going to do that by considering CFTs that are holographically dual to Gauss-Bonnet gravity, which is the the most general higher derivative gravity theory in 5 dimensions that yields second order equations of motion. This gravity theory has some very interesting properties, but probably the main interesting one is that it depends on a coupling constant that, in order to ensure that the boundary theory does not break causality, has to be bounded both from below and above. Therefore, it will be interesting to see how the QNEC behaves with respect to this coupling.

In order to make sure that all the preliminaries that are necessary to understand the QNEc are explained, the thesis will be structured as follows:

- In chapter 2 we will review the classical energy conditions and briefly comment why and when the NEC is violated. Then, the last part of this section will be dedicated to review the work of Bousso, et.al in [1] to understand where the original idea of the QNEC comes from.
- In chapter 3 we will review the concept of entanglement entropy paying special attention on how to compute it when we are in the case of a continuous QFT. Here we will also present the main important properties that the entanglement entropy has.
- Before talking on how to actually compute the entanglement entropy with holography we will first introduce the basic concepts of holography. This will be done in chapter 4 where we will give a brief review of [3] where the idea of the AdS/CFT correspondence was first proposed. In the end of this chapter we will also explain how the tress-energy tensors of the bulk and the boundary are related, which will be of a great importance for our computations later.
- In chapter 5 we will review the important features of Gauss-Bonnet gravity and derive the metric for Ads-type black branes and AdS vacuum. Here, we will also discuss the bounds of the coupling constant of the theory and how it affects the boundary field theory.
- In chapter 6 we will review the different prescriptions of the holographic entanglement entropy and review their derivations and generalizations to holographic setups with higher derivative gravity. In the ending section of this chapter we will also discuss how can we compute this holographic entanglement entropy using numerical methods. This will be useful for the last chapters of the thesis.
- In chapter 7 we will finally review an holographic proof on the QNEC that does not require the Bousso conjecture to work. Also in this chapter we will review the work done by van der Schee and Ecker [4] where they studied the QNEC explicitly for strip-like entangling regions. By doing hat, we realized that they did not take into

account all possible null variations of the entangling surface, so we generalize their work to complete that part. Last, but not least, we also perform the computation of the QNEC for sphere-like entangling surfaces. All of this computations are done for the case of a thermal plasma state in the CFT and using the numerical method described in the previous chapter.

- Finally, in chapter 8 we perform the computation of the QNEC in a holographic setup with Gauss-Bonnet gravity taking the same state and geometries as in the previous chapter.

2. Energy conditions

2.1 What are the energy conditions?

In General Relativity, sometimes it is useful to think about Einstein's equation without specifying the source from which the energy-momentum tensor $T_{\mu\nu}$ is derived. This allow us to work with arbitrary geometries, since any metric at all is a solution of Einstein's equation when we leave $T_{\mu\nu}$ free of constrains. Then, we only need to define $T_{\mu\nu}$ as being equal to the Einstein tensor $G_{\mu\nu}$. Nevertheless, even without specifying a specific and "realistic" model of matter source, we can impose some energy conditions to restrict the form of $T_{\mu\nu}$. In general words, this conditions are scalar restrictions that describe well-established physical properties common to most of the states of matter while, at the same time, they are restrictive enough to rule out unphysical solutions of Einstein's equation.

To construct these scalars we contract $T_{\mu\nu}$ with timelike vectors t^μ or null vectors k^μ. In order to gain some physical understanding, we take as an example an energy-momentum tensor broadly used in General Relativity, specially in cosmology, which is the perfect fluid $T_{\mu\nu}$ tensor

$$T_{\mu\nu} = (p + \rho)U_\mu U_\nu + p g_{\mu\nu} \tag{2.1}$$

where U_μ is the fluid velocity, ρ is the energy density, p is the pressure and $g_{\mu\nu}$ is the spacetime metric. Obviously, the perfect fluid is just an example used to understand better the physical implications of the conditions but these ones are imposed in the same way to any arbitrary energy-momentum tensor.

There are several energy conditions. Here I present some of the more popular ones:

- The **Weak Energy Condition (WEC)**: $T_{\mu\nu}t^\mu t^\nu \geq 0$ or, for the perfect fluid example, $\rho \geq 0$ and $\rho + p \geq 0$.
- The **Null Energy Condition (NEC)**: $T_{\mu\nu}k^\mu k^\nu \geq 0$ or, for our case in consideration, $\rho + p \geq 0$. As a difference with the WEC, now the energy density can be negative as long as the pressure compensates.
- The **Dominant Energy Condition (DEC)**: $T_{\mu\nu}t^\mu t^\nu \geq 0$ and $T_{\mu\nu}T^\nu{}_\lambda t^\mu t^\lambda \leq 0$, i.e. $T^{\mu\nu}t_\mu$ is not spacelike and, therefore, it doesn't flow faster than light. For a perfect fluid, the combination of this conditions is equivalent to the restriction $\rho \geq |p|$.

- The **Null Dominant Energy Condition (NDEC)** is the DEC condition contracting the energy-momentum tensor with null vectors instead of timelike ones: $T_{\mu\nu}k^\mu k^\nu \geq 0$ and $T_{\mu\nu}T^\nu{}_\lambda k^\mu k^\nu \leq 0$. The implication in the perfect fluid case is that the same condition as in the DEC holds but negative energy densities are allowed as long as they obey $\rho = -p$.
- The **Strong Energy Condition (SEC)**: $T_{\mu\nu}t^\mu t^\nu \geq \frac{1}{2}T^\lambda{}_\lambda t^\sigma{}_\sigma$ or, in other words, $\rho + p \geq 0$ and $\rho + 3p \geq 0$. It can be shown that this condition implies that gravitation is attractive [5].

All of this conditions, plotted in figure 2.1, are local and can be easily generalized to integral or "averaged" expressions by integrating them along timelike or null geodesics (or surfaces). For example, the averaged null energy condition, or ANEC, can be defined as the NEC averaged along a null geodesic as

$$\int_{-\infty}^{\infty} T_{\mu\nu}k^\mu k^\nu d\lambda \geq 0 \tag{2.2}$$

where k^μ is the tangent vector to the geodesic and λ is an affine parameter.

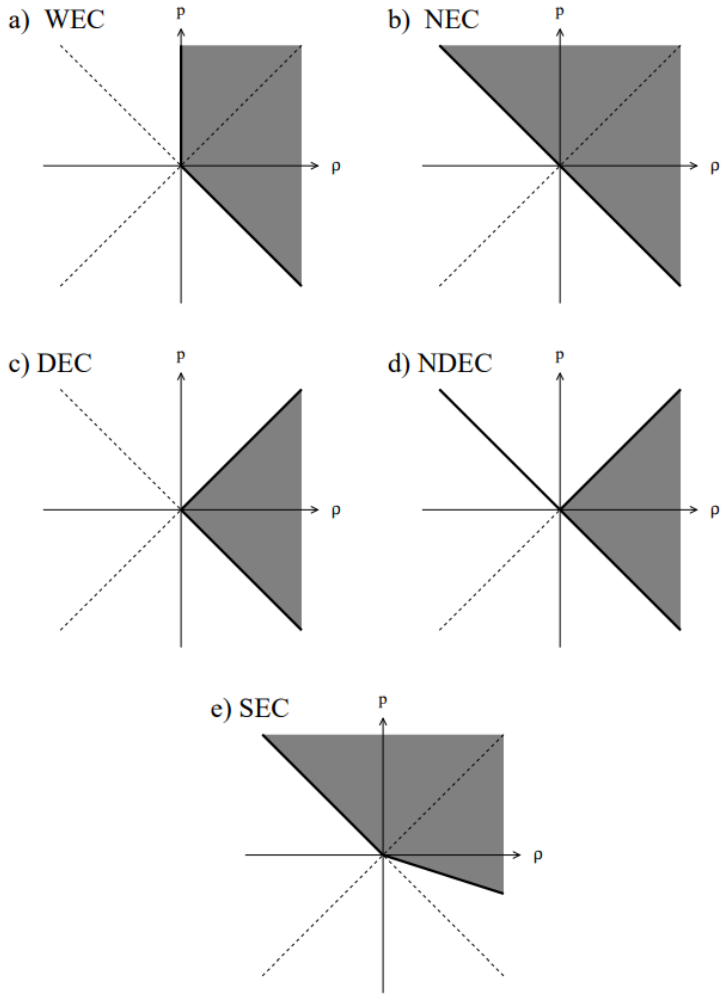

Figure 2.1: Energy conditions applied to perfect fluids. In grey the allowed values for the energy density ρ and the pressure p [6].

2.2 The NEC and its violation

Among the energy conditions discussed above, the NEC plays an important role in General Relativity, and the main reasons for it being interesting are two. First of all, originally, the common believe was that the NEC could not be violated in a reasonable theory, with the possible exception of a scalar field with arbitrary gravity coupling [7]. Second, the NEC is crucial in several General Relativity results such as the Penrose singularity theorem [8], the topological censorship [9], the chronology protection theorem [10], and others. In particular, the Penrose singularity theorem says that any trapped surface in space contains a singularity in the future. In a spherically symmetric situation, this means that all light rays emanating from a spheric trapped surface will propagate towards its centre. Examples of it are a sphere inside the Schwarzschild black hole horizon or a contracting sphere of spatially flat homogeneous isotropic Universe of radius greater than the Hubble parameter. Therefore, for theories where NEC holds, there is always a singularity inside a black hole and a contracting universe always ends in a singularity and, by time reversal symmetry, any expanding universe has a singularity in the past.

On the other hand, it is known since long ago that the NEC is violated in quantum field theories [11] (one can find several examples where this occurs in [12, 13]) and, therefore, the NEC should be replaced for a new condition. Several conditions, such as the averaged null energy condition (ANEC) [14–16] or the "quantum inequalities" [17,18], have been recently suggested to replace the NEC. Even though, in [19] it is shown that some classical results from General Relativity can be recovered from imposing the ANEC instead of the NEC, the main problem that this two proposals have is that they involve integrating $\langle T_{\mu\nu}k^\mu k^\nu\rangle$ over a region of spacetime and, consequently, we are not able to recover those classical results for which point-wise conditions are necessary. It was while studying how to unify the Bousso bound and the classical focusing theorem that Bousso, et.al. [1] proposed a quantum and local version of the NEC, the Quantum Null Energy Condition (QNEC), for the first time. This condition states that the energy density at a point is bounded below by the second derivative evaluated at the same point of an appropriate entropy. In the next section I mention, briefly, how Bousso's work motivates the QNEC.

2.3 Motivating the QNEC

The generalization of the NEC to the QNEC came from the work of Bousso et al. when they proposed a quantum version (or, more precisely, a semiclassical version) of the Classical Focussing Theorem. To understand what this theorem states, first consider a congruence of light-rays emanating orthogonally to a codimension-2 spacelike hypersurface. Then we can define the scalar expansion θ to be

$$\theta \equiv \nabla_a k^a \tag{2.3}$$

where k^a is the tangent vector to the congruence. Then, we can determine how θ will evolve along the congruence using the Raychaudhuri equation

$$\frac{d\theta}{d\lambda} = -\frac{1}{D-2}\theta^2 - \sigma_{ab}\sigma^{ab} + \omega_{ab}\omega^{ab} - R_{ab}k^a k^b \ . \tag{2.4}$$

Where λ is the affine parameter that characterizes the null geodesic, D is the spacetime dimensions, σ_{ab} is the trace-free symmetric part of the null extrinsic curvature $\nabla_a k_b$, ω_{ab}

is the antisymmetric rotation tensor $\omega_{ab} = \nabla_{[a}k_{b]}$ and R_{ab} is the Ricci tensor.

In a non-rotating spacetime satisfying the NEC and Einstein gravity the right hand side of equation (2.4) is strictly negative and, therefore

$$\frac{d\theta}{d\lambda} \leq 0 \ . \tag{2.5}$$

This is known as the Classical Focusing Theorem, and it implies that light rays can focus but not anti-focus, which, at the same time, implies that the area of the black hole horizon cannot decrease, at least classically. However, Bekenstein's proposal that black holes have an entropy proportional to their area [20,21],

$$S = \frac{A}{4G\hbar} \tag{2.6}$$

and the later calculations of the black hole temperature and radiation done by Hawking [22,23] meant that black hole can actually evaporate and therefore the area of their horizon shrinks decreasing their entropy. To avoid violation of the second law of thermodynamics, Bekenstein introduced the semi-classical concept of generalized entropy [24], defined as the sum of the black hole entropy plus the entropy of matter in the exterior of the black hole S_{out}, i.e.

$$S_{\text{gen}} = \frac{A}{4G\hbar} + S_{\text{out}} \ , \tag{2.7}$$

and stated that its the combination of the two kinds of entropies what has to always increase. Therefore, he proposed what is known as the generalized second law of black hole thermodynamics:

$$dS_{\text{gen}} \geq 0 \ . \tag{2.8}$$

Although Newton's constant G and S_{out} are cut-off dependent, the combined divergences of the gravitational and matter entropy to form S_{gen} cancel [25,26]. That makes the generalized entropy a very interesting notion since it is finite, and this suggests that, unlike S_{out} and $A/4G\hbar$, S_{gen} could refer to some information present in the full quantum gravity theory.

In 2015 Bousso, Fisher, Leichenauer and Wall [1] used the idea of S_{gen} to propose an universal inequality that unified both the classical focusing theorem with the Bousso bound. The latter one conjectures that given a light-sheet, which is a non-expanding null hypersurface, the entropy on it cannot be greater than the area of its initial cross-section in Planck units, namely $S \leq A/4G\hbar$. But since quantum fluctuations can have negative energy, the NEC can be violated and therefore the classical focusing theorem fails at the semi-classical level. Because of that, Bousso et.al. used the concept of S_{gen} to formulate a novel Quantum Focusing Conjecture (QFC) that substitutes the old scalar expansion θ for a new quantum expansion Θ.

The formulation of the QFC begins with a spacelike codimension-2 surface σ, which does not need to be connected nor a compact surface, that splits a Cauchy surface Σ into two portions and a null vector field k^μ normal to σ. Therefore, σ can be thought to be a cut of the null surface N generated by k^μ. It is here where the concept of a S_{gen} comes into account, since we can arbitrarily choose any of the two portions of Σ to be Σ_{out} and define the generalized entropy to be the sum of the gravitational entropy S_{grav}, defined as local geometric terms integrated over σ, plus the matter entropy S_{out} in the Σ_{out} region (see figure 2.2) The terms for the S_{grav} can be obtained from the low-energy

effective action for the metric, and are known explicitly for a wide class of actions. With this construction, the S_{gen} has the same properties of the original one defined in equation (2.7), namely it is cut-off independent and it obeys the second law of thermodynamics, i.e. equation (2.8).

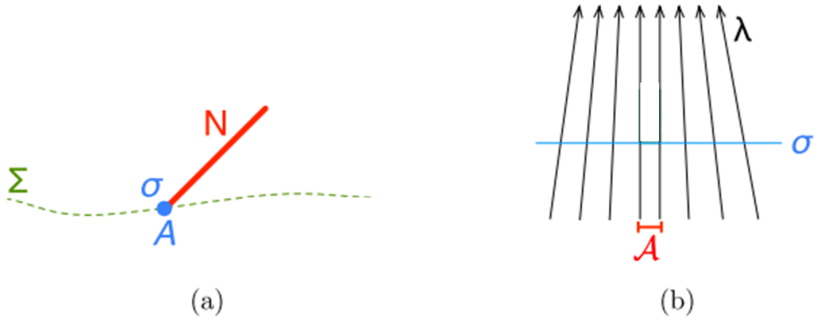

Figure 2.2: (a) The Cauchy surface Σ is divided into two regions Σ_{in} and Σ_{out} by the spatial surface σ of area A. Which one is Σ_{in} and Σ_{out} is arbitrary. N is the surface generated by the null vector field k^{μ} normal to σ. The generalized entropy is defined as $S_{\text{gen}} = S_{\text{grav}} + S_{\text{out}}$, where S_{out} is the matter entropy in Σ_{out} and S_{grav} is derived from the action for the metric of σ.
(b) N is formed by the null generators separated an infinitesimal distance $\mathcal{A}$. The deformation of σ is done along the affine parameter λ

With the definitions given above and being y a point on σ, we can see that for each y there passes a null generator of N. Then, we take λ to be an affine parameter along this generator beginning with $\lambda = 0$ at σ and $\lambda > 0$ away from σ. With this, σ is characterized by the coordinates y and N by (y, λ).

As mentioned above, σ splits the Cauchy surface Σ in two, but so it does any slice of N defined by $(y, \lambda = V)$. Therefore, these slices of N can be defined by a positive function $V(y) > 0$. Thus, $V(y)$ is the argument of the generalized entropy functional:

$$S_{\text{gen}}\left[V(y)\right] = S_{\text{grav}}\left[V(y)\right] + S_{\text{out}}\left[V(y)\right] \ . \tag{2.9}$$

The quantum expansion Θ is defined in the same way as the classical expansion, by deforming a slice of N in the neighborhood of y_1. Therefore, we can obtain Θ by just differentiating S_{gen} with respect to $V(y)$ [1]:

$$\Theta\left[V(y); y_1\right] \equiv \frac{4G\hbar}{\sqrt{h}} \frac{\delta S_{\text{gen}}}{\delta V(y_1)} \tag{2.10}$$

where $\sqrt{h}$ is the area element of the metric on σ and it is included to make sure that the derivative is taken per unit of geometrical area and not coordinate area.

The leading term of S_{grav} is $A\left[V(y)\right]/4G\hbar$, where A is the area of the slice of N that splits Σ. This means that in the classical limit, where $G\hbar \to 0$, the matter entropy S_{out} does not contribute to Θ and this reduces to the classical scalar expansion θ, for each point y_1. In other words, Θ relates to θ as

$$\Theta\left[V(y); y_1\right] = \theta(y_1) + \dots \ . \tag{2.11}$$

With this novel definition of the Quantum Expansion, Bousso et al. proposed a generalization of the Classical Focusing Theorem to a semi-classical regime. They named

it the *Quantum Focusing Conjecture* (QFC), and it states that the Quantum Expansion cannot increase at y_1 if the slice of N defined by $V(y)$ is deformed along y_2:

$$\frac{\delta}{\delta V(y_2)}\Theta\left[V(y);y_1\right] = \frac{\delta}{\delta V(y_2)}\frac{4G\hbar}{\sqrt{h}}\frac{\delta S_{\text{gen}}}{\delta V(y_1)} \leq 0 \ . \tag{2.12}$$

It is of particular interest to look at, what they named, the "diagonal" case, i.e. $y_1 = y_2$. In this case the surface σ is deformed along a single null generator. Therefore, from now on we are going to work with ordinary derivatives with respect to the affine parameter λ on the null geodesic. Using equations (2.9) and (2.10) and writing the term S_{grav} as $A\left[V(y)\right]/4G\hbar$, we can finally write the Quantum Expansion as

$$\Theta = \theta + \frac{4G\hbar}{\mathcal{A}}\frac{dS_{\text{out}}}{d\lambda} \tag{2.13}$$

where $\mathcal{A}$ is the infinitesimal unit area. Then the QFC becomes

$$\begin{aligned} 0 \geq \frac{d\Theta}{d\lambda} &= \frac{d\theta}{d\lambda} + \frac{4G\hbar}{\mathcal{A}}\left(\frac{d^2S_{\text{out}}}{d\lambda^2} - \frac{dS_{\text{out}}}{d\lambda}\theta\right) \\ &= -\frac{1}{2}\theta^2 - \sigma^2 - 8\pi G\left\langle T_{\mu\nu}k^\mu k^\nu\right\rangle + \frac{4G\hbar}{\mathcal{A}}\left(\frac{d^2S_{\text{out}}}{d\lambda^2} - \frac{dS_{\text{out}}}{d\lambda}\theta\right) \end{aligned} \tag{2.14}$$

where σ is the shear and $\langle T_{\mu\nu}k^\mu k^\nu\rangle$ is the expectation value of the stress-energy tensor contracted with two null vectors k^μ. In the classical limit $\hbar \to 0$ one can consider that the shear σ and the expansion θ vanish at a point p and, therefore, one can recover the NEC:

$$\langle T_{kk}\rangle \equiv \langle T_{\mu\nu}k^\mu k^\nu\rangle \geq 0 \ . \tag{2.15}$$

Choosing again both $\sigma = \theta = 0$ but not taking the limit $\hbar \to 0$ implies a new local energy condition: the novel *Quantum Null Energy Condition* (QNEC) [1]

$$\langle T_{kk}\rangle \geq \lim_{\mathcal{A}\to 0}\frac{\hbar}{2\pi\mathcal{A}}\frac{d^2S_{\text{out}}}{d\lambda^2} \tag{2.16}$$

Rewriting the expression in terms of the area element of the metric on σ instead of in terms of the infinitesimal area $\mathcal{A}$ we obtain the most common expression to write the QNEC:

$$\langle T_{kk}\rangle \geq \frac{\hbar}{2\pi\sqrt{h}}\frac{d^2S}{d\lambda^2} \ . \tag{2.17}$$

Where, from now on, S stands for S_{out}.

Unlike the NEC, the QNEC is a statement about quantum field theory, since equation does not depend on G nor on higher curvature terms. Thus, we can think of it as the quantum version of the NEC.

3. Entanglement Entropy

In the previous section I presented the QNEC (equation (2.17)), which relates the energy density of a given state to an entropy S which is the matter entropy outside of a bounded region. A rigorous definition of he entropy S can be given in terms of the von Neumann entropy of the state on the exterior of this bounded region, and this is usually known as the entanglement entropy. Since this concept is of crucial relevance for this thesis, in this chapter I will review the chapter 2 of [27] to present some basic concepts of entanglement entropy as well as some mathematical techniques that will be useful in future parts of the thesis.

3.1 Discrete QFTs

To start a discussion on entanglement entropy, let's fist focus on discrete systems. Assume that we have a lattice with spacing ϵ and that at each site we have a finite-dimensional Hilbert space $\mathcal{H}_\alpha$, where α indexes the lattice sites. Then, a pure state of the system is given by an element of the tensor product space

$$|\Psi\rangle \in \otimes_\alpha \mathcal{H}_\alpha \ . \tag{3.1}$$

The entanglement entropy accounts for how entangled a subset of the degrees of freedom of the whole system is with the rest of it. To study this, we divide the lattice sites into two sets by drawing a boundary across the lattice. o the region inside the boundary we call it $\mathcal{A}$, to the one outside $\mathcal{A}^c$ and to the boundary $\partial\mathcal{A}$. Then, with this partition of the system, the Hilbert space decomposes in

$$\otimes_\alpha \mathcal{H}_\alpha = \mathcal{H}_\mathcal{A} \otimes \mathcal{H}_{\mathcal{A}^c} \ . \tag{3.2}$$

Now, given the bipartition of the system and the subsequent partition of the Hilbert space we can construct an operator that acts only in one of the subspaces (in this case $\mathcal{H}_\mathcal{A}$) by tracing out the other subspace (in this case $\mathcal{H}_{\mathcal{A}^c}$). This operator is the so-called *reduced density matrix* $\rho_\mathcal{A}$, which is expressed as

$$\rho_\mathcal{A} = \mathrm{Tr}_{\mathcal{A}^c} \left(|\Psi\rangle \langle\Psi| \right) \ . \tag{3.3}$$

From this definition we can clearly see that $\rho_\mathcal{A}$ captures the degrees of freedom in $\mathcal{A}$ ignoring what happens in $\mathcal{A}^c$. To quantify the amount of entanglement between the degrees of freedom of both regions we use the von Neumann entropy of the reduced

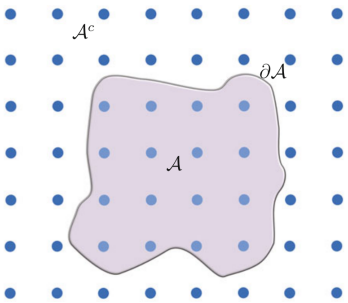

Figure 3.1: Partition of the lattice system into $\mathcal{A}$ and $\mathcal{A}^c$ separated by the surface $\partial\mathcal{A}$ [27].

density matrix, which is nothing more than the *entanglement entropy*:

$$S_{\mathcal{A}} = -\mathrm{Tr}_{\mathcal{A}} \left(\rho_{\mathcal{A}} \log \rho_{\mathcal{A}}\right) \ . \tag{3.4}$$

For future reference in this thesis, it is also useful to define another 'type' of entropies called the Rényi entropies. They are defined as

$$S_{\mathcal{A}}^{(q)} = \frac{1}{1-q} \log \mathrm{Tr} \left(\rho_{\mathcal{A}}{}^q\right) \tag{3.5}$$

where in principle $q \in \mathbb{Z}_+$ but often it is convenient to analytically continue q to $q \in \mathbb{R}_+$, as we will see in next section. The important aspect that we should stress here is that, by taking the limit $q \to 1$ the Rényi entropies converge to the von Neumann entropy

$$S_{\mathcal{A}} = \lim_{q \to 1} S_{\mathcal{A}}^{(q)} \ . \tag{3.6}$$

It is worth noting that, in the case that our whole system is in a pure state $|\Psi\rangle$, then we can write the wave function, using Schmidt decomposition, as

$$|\Psi\rangle = \sum_i \lambda_i \, |\alpha_i\rangle_{\mathcal{A}} \, |\beta_i\rangle_{\mathcal{A}^c} \ , \tag{3.7}$$

where $|\alpha_i\rangle_{\mathcal{A}}$ and $|\beta_i\rangle_{\mathcal{A}^c}$ are the eigenstates of $\rho_{\mathcal{A}}$ and $\rho_{\mathcal{A}^c}$ respectively and λ_i the eigenvalues. The key point here is that, for a pure state, the eigenvalues of $\rho_{\mathcal{A}}$ are the same as the ones for $\rho_{\mathcal{A}^c}$ and therefore we have that $S_{\mathcal{A}}^{(q)} = S_{\mathcal{A}^c}^{(q)}$ for all q.

3.2 Continuum QFTs

To generalize the discussion in the previous section to non-discrete QFTs we can take the limit when the lattice spacing vanishes, $\epsilon \to 0$. The entanglement entropy in a d-dimensional spacetime $\mathcal{B}_d$ is defined from the wave functional of the system $\Psi\left[\Phi(x)\right]$, where $\Phi(x)$ are the fields in the system and x are the coordinates that label a location for a given time, in a similar way as before.

If we take $\mathcal{B}_d$ to be globally hyperbolic, we can define simultaneity by choosing a Cauchy slice Σ_{d-1} where a state of the system is defined (note that x are the coordinates that label the positions on Σ_{d-1}). Then, we can perform a bipartition like in the previous section by just choosing a spacetime region $\mathcal{A}$ on the Cauchy slice in such a way that

$\mathcal{A} \cup \mathcal{A}^c = \Sigma_{d-1}$ (see figure 3.2(a)). With this partition we can separate dields into two sets by looking at their domains of support, $\Phi(x) = \{\Phi_{\mathcal{A}}(x), \Phi_{\mathcal{A}^c}(x)\}$.

The first step to compute the entanglement entropy in $\mathcal{A}$ is to construct the reduced density matrix operator $\rho_{\mathcal{A}}$ on a $(d-1)$-dimensional Cauchy slice, say $\Sigma_{t=0}$. This operator acts on $\mathcal{H}_{\mathcal{A}}$ and, therefore, its matrix elements should be defined by their action on the $\Phi_{\mathcal{A}}(x)$ fields. For this case, where we have continuous fields, to trace over the region $\mathcal{A}^c$ we need to integrate over all field configurations in that domain, and this path integral can be regularized by imposing the boundary conditions for the $\Phi_{\mathcal{A}}(x)$ fields

$$\Phi_{\mathcal{A}}|_{t=0^-} \equiv \Phi_- \quad \text{and} \quad \Phi_{\mathcal{A}}|_{t=0^+} \equiv \Phi_+ \ . \tag{3.8}$$

Thus, the expression for the path integral is

$$\begin{aligned} (\rho_{\mathcal{A}})_{\mp} &= \int [\mathcal{D}\Phi]\, e^{-S_{\mathrm{QFT}}[\Phi]} \delta_E\left(\Phi_{\mp\mathcal{A}}\right) \\ \delta_E\left(\Phi_{\mp\mathcal{A}}\right) &\equiv \delta\left(\Phi_{\mathcal{A}}(t=0^-) - \Phi_-\right) \delta\left(\Phi_{\mathcal{A}}(t=0^+) - \Phi_+\right) \ , \end{aligned} \tag{3.9}$$

where S_{QFT} stands for the action of the system as a difference of S which will be reserved for the von Neumann entropy and the subscript E stands for the Euclidean path integral (since this is the best framework for states with time reversal symmetry).

For states with non-trivial time dependence, i.e. without time reversal symmetry, the above formulation of the path integral needs to be modified to account for the fact that one cannot use information about the entire spacetime $\mathcal{B}_d$ without violating causality. To know the reduced density matrix for any given time $\rho_{\mathcal{A}}(t)$ we cannot use any information referring at later times $t' > t$. To deal with this problem here I will present the Schwinger-Keldysh formalism, which idea is to only consider evolving initial conditions from a time $t' < t$ up to the instant we want to compute $\rho_{\mathcal{A}}(t)$. To do that, we consider the causal past of the Cauchy slice $J^-[\Sigma_{t=0}]$, but instead of evolving from there to the causal future, we retract the evolution back to the initial state (see figure 3.2(b)). This way, we end up with two copies of $J^-[\Sigma_{t=0}]$ glued together on $\Sigma_{t=0}$, which can be simply seen as two copies of the same system.

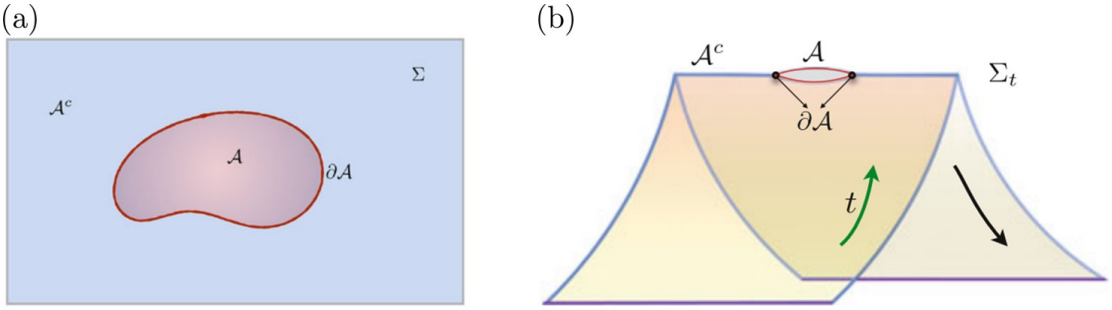

Figure 3.2: **(a)** Schematic representation of the bipartition of the Cauchy slice $\Sigma_{t=0}$ into $\mathcal{A}$ and $\mathcal{A}^c$. **(b)** Schwinger-Keldysh construction to compute $\rho_{\mathcal{A}}(t)$ for states with non-trivial time dependence [27].

Using the same reasoning as before, to compute the reduced density matrix we should open the path integral around $\mathcal{A}$ and impose boundary conditions like the ones in equation (3.8). In this case, we adopt the notation in [27] and label the two copies of the system with L and R, where the right fields evolve forward in time from the initial state to $\Sigma_{t=0}$ and the left ones are evolved backwards in time. Also, because of the path

integral is computed for a real time [28], we should include the usual i factor. With all of this in mind, the reduced density matrix is given by [27]

$$\begin{aligned}(\rho_{\mathcal{A}})_{\mp} &= \int_{J^-[\Sigma_t]} [\mathcal{D}\Phi_R]\,[\mathcal{D}\Phi_L]\, e^{iS_{\mathrm{QFT}}[\Phi_R]-iS_{\mathrm{QFT}}[\Phi_L]}\delta_L\left(\Phi^{\mp}_{RL,\mathcal{A}}\right)\\ \delta_L\left(\Phi^{\mp}_{RL,\mathcal{A}}\right) &\equiv \delta\left(\Phi_{R,\mathcal{A}}(t=0^-)-\Phi_-\right)\delta\left(\Phi_{L,\mathcal{A}}(t=0^+)-\Phi_+\right)\ ,\end{aligned} \tag{3.10}$$

where now the subscript L stands for the Lorentzian path integral formulation.

To compute the q^{th} Rényi entropy we need to multiply the reduced density matrix by itself q times. To do so, we use the replica method, which consists in replicate the computation of the path integral q times. Basically we just need to take q copies of the path integral and make some identifications between them in order to multiply the matrices in a proper manner. For the time reversal state we should identify the "$+$" component in the k^{th} density matrix with the "$-$" component in the $(k+1)^{\text{th}}$ matrix ($\Phi^{(k)}_{+} = \Phi^{(k+1)}_{-}$), while for the non-arbitrary time dependent state we should remember that the "$+$" and "$-$" components correspond to the L and R fields respectively. Therefore, for this situation we obtain the expression

$$(\rho_{\mathcal{A}})^q_{\mp} = \int \prod_{j=1}^{q-1} d\Phi^{(j)}_{L,+}\delta(\Phi^{(j)}_{L,+}-\Phi^{(j+1)}_{R,-}) \int \prod_{k=1}^{q}[\mathcal{D}\Phi^{(k)}]\left\{e^{-\Sigma_{k=1}^{q}S_{\mathrm{QFT}}[\Phi^{(k)}]}\delta_L(\Phi^{\mp,(k)}_{RL,\mathcal{A}})\right\} \tag{3.11}$$

We can think of each copy of $\rho_{\mathcal{A}}$ as being computed on a copy of the background spacetime, which for the Euclidean computation is $\mathcal{B}$ and for the Lorentzian one is $J^-[\Sigma_t] \subset \mathcal{B}$ glued together at the Cauchy slice. Then, the q copies of each manifold are identified with each other as explain above. Equivalently, these q copies of $\mathcal{B}$ together with the identifications can be thought as creating a new manifold $\mathcal{B}_q$.

To take the trace we now need to identify $\Phi^{(1)}_{R,-}$ with $\Phi^{(q)}_{L,+}$ and integrate over all the fields living on $\mathcal{B}_q$. Then, if we make the definition

$$\mathcal{Z}_q[\mathcal{A}] = \mathrm{Tr}({\rho_{\mathcal{A}}}^q) \equiv \mathcal{Z}[\mathcal{B}_q] \tag{3.12}$$

the q^{th} Rényi entropy yields

$$S^{(q)}_{\mathcal{A}} = \frac{1}{1-q}\log(\mathrm{Tr}({\hat{\rho}_{\mathcal{A}}}^q)) = \frac{1}{1-q}\log\left(\frac{\mathcal{Z}_q[\mathcal{A}]}{\mathcal{Z}_1[\mathcal{A}]^q}\right) \equiv \frac{1}{1-q}\log\left(\frac{\mathcal{Z}[\mathcal{B}_q]}{\mathcal{Z}[\mathcal{B}]^q}\right)\ , \tag{3.13}$$

where $\hat{\rho} = \frac{\rho}{Tr[\rho]}$ is the properly normalized density matrix.

To finally obtain the entanglement entropy we should take the limit of the Rényi entropies when $q \to 1$. However, our expression depends on integer values of q and nothing assures us that we can analytically continue it to real values. By means of Carlson's theorem, if the function we want to analytically continue has a sub-exponential growth at imaginary infinity, then the replica trick used above is granted to yield a well-defined entanglement entropy. In this section we assume that this is the case, but if one encounters a state that yields a non-well-behaved Rényi entropies, one should consider consider that there is some interesting physical phenomena that should be understood. It is outside of the scoop of this thesis to discuss these cases.

3.3 Properties of Entanglement Entropy

The entanglement entropy as defined above is UV divergent. This can be understood by relating it to the short distance divergence of the 2-point correlation function. Since the definition of $\rho_{\mathcal{A}}$ implies a partition of the system, we should expect the divergence of the entropy to be proportional to the number of entangled pairs that are "separated" by the entangling surface $\partial\mathcal{A}$. Therefore, we expect (and we will see in next sections when it the will be computed explicitly) the entanglement entropy to diverge proportionally to the area of the entangling surface. It is shown that the leading divergent term of the von Neumann entropy for $d > 2$ is

$$S_{\mathcal{A}} = \gamma \frac{\text{Area}(\partial\mathcal{A})}{\epsilon^{d-2}} + \dots \ , \tag{3.14}$$

where the ellipses stand for less divergent terms.

For the case where $d = 2$ the divergence is only logarithmic ($\mathcal{O}(\log \epsilon^{-1})$) and doesn't follow an area law. This is the case because in 2 dimensions $\partial\mathcal{A}$ is not a surface but two disconnected points (that is why we don't observe an area law). One can heuristically think of this logarithmic divergence as arising from the limit $d \to 2$ in the above expression [27].

Apart of the UV divergence, it is known that the von Neumann entropy satisfies different inequalities often called "quantum inequalities". Imagine we divide a system in different regions labeled as $\mathcal{A}_i$ in such a way that $\mathcal{A} = \cup_i \mathcal{A}_i$. With this setup, the system's Hilbert space will also be partitioned as $\mathcal{H} = \otimes_i \mathcal{H}_{\mathcal{A}_i}$. As a short-hand notation, and following the notation in [27], we will introduce $\mathcal{A}_i\mathcal{A}_j = \mathcal{A}_i \cup \mathcal{A}_j$. Therefore, $\rho_{\mathcal{A}_i\mathcal{A}_j}$ will be an operator acting on $\mathcal{H}_{\mathcal{A}_i} \otimes \mathcal{H}_{\mathcal{A}_j}$ and its corresponding entropy will be $S_{\mathcal{A}_i\mathcal{A}_j}$. With all of this taken into account, the inequalities satisfied by the entanglement entropy can be written as follows.

- The **subadditivity** inequality states that for a bipartition $\mathcal{H}_{\mathcal{A}_1} \otimes \mathcal{H}_{\mathcal{A}_2}$ the entropy satisfies

$$S_{\mathcal{A}_1} + S_{\mathcal{A}_2} \geq S_{\mathcal{A}_1\mathcal{A}_2} \ . \tag{3.15}$$

- The **Araki-Lieb** inequality states that, for bi-partitioned systems, the entropies satisfy

$$|S_{\mathcal{A}_1} - S_{\mathcal{A}_2}| \leq S_{\mathcal{A}_1\mathcal{A}_2} \ . \tag{3.16}$$

  If $\mathcal{A}_1\mathcal{A}_2$ is the entire (pure) system then $\mathcal{A}_2 = \mathcal{A}_1^c$ and we obtain the known result $S_{\mathcal{A}} = S_{\mathcal{A}^c}$. One can combine equations (3.15) and(3.16) to obtainthe expression

$$|S_{\mathcal{A}_1} - S_{\mathcal{A}_2}| \leq S_{\mathcal{A}_1\mathcal{A}_2} \leq S_{\mathcal{A}_1} + S_{\mathcal{A}_2} \ . \tag{3.17}$$

  From this last expression, one can infer that $S_{\mathcal{A}_1\mathcal{A}_2} \geq \max\{S_{\mathcal{A}_1}, S_{\mathcal{A}_2}\}$.

- The **strong subadditivity** inequality for a tripartite system can be expressed as

$$S_{\mathcal{A}_1\mathcal{A}_2} + S_{\mathcal{A}_2\mathcal{A}_3} \geq S_{\mathcal{A}_1\mathcal{A}_2\mathcal{A}_3} + S_{\mathcal{A}_3} \ , \tag{3.18a}$$

$$S_{\mathcal{A}_1\mathcal{A}_2} + S_{\mathcal{A}_2\mathcal{A}_3} \geq S_{\mathcal{A}_1} + S_{\mathcal{A}_2} \ . \tag{3.18b}$$

  These inequalities are only valid if the inner product between states of the Hilbert space is positive and, therefore, it implies that the QFT must be unitary.

Although one can attempt to compute the entanglement entropy by integrating the fields of a certain QFT as explained above, it is (in general) extremely tough to do so and only a few limited results are know by proceeding this way. The most common way of computing the entanglement entropy is using holography. In the next chapter I will review the very basics of the holographic correspondence and in chapter 6 I will present the techniques on how to actually compute the entanglement entropy using holography (what it is commonly known as computing the *holographic entanglement entropy*).

4. Basic concepts of the AdS/CFT Correspondence

As mentioned above, in this section I will briefly introduce the holographic correspondence (also known as the AdS/CFT, gravity-gauge correspondence or just holography) in order to later on compute the entanglement entropy. To do so, first I will introduce the main ingredients of this correspondence, i.e. the Anti-de Sitter (AdS) spacetime and the conformal field theory (CFT), paying special attention to the $\mathcal{N} = 4$ Super-Yang-Mills (SYM) theory. With all of these ingredients, I will finally give a glance on the correspondence itself.

4.1 The Anti-de Sitter (AdS) spacetime

The AdS/CFT correspondence relates $(d+1)$-dimensional AdS gravity with d-dimensional field theories with no gravity. Therefore, anticipating the use in the rest of the thesis, I am going to present the discussion about the AdS spacetime assuming $d+1$ dimensions.

The AdS_{d+1} spacetime is defined by embedding an hyperboloid given by

$$-X_0^2 + \sum_{i=1}^{d} X_i^2 - X_{d+1}^2 = -L^2 \tag{4.1}$$

in $\mathbb{R}^{2,d}$, where L is the curvature radius of the AdS spacetime. Notice that the hypersurface given by equation (4.1) is invariant under $O(2,d)$ transformations acting on $\mathbb{R}^{2,d}$ and, since $O(2,d)$ has $(d+1)(d+2)/2$ Killing vectors, that means that AdS is a maximally symmetric spacetime.

We can now introduce the so-called *global coordinates* of the Anti-de Sitter spacetime given by

$$\begin{aligned} X_0 &= L\cosh\rho\cos\tau \\ X_{d+1} &= L\cosh\rho\sin\tau \\ X_i &= L\sinh\rho\ \Omega_i\ , \end{aligned} \tag{4.2}$$

where Ω_i are the angular coordinates that parametrize a S^{d-1}, $\rho \in \mathbb{R}_+$ and $\tau \in [0, 2\pi)$ yielding a metric for the AdS_{d+1} of the form

$$ds^2 = L^2\left(-\cosh^2(\rho)d\tau^2 + d\rho^2 + \sinh^2(\rho)d\Omega_{d-1}^2\right)\ . \tag{4.3}$$

Notice that the periodicity of τ implies the possible existence of closed timelike curves and give rise to causality problems. However, this is not a property of the spacetime itself but a consequence of how we derived the metric from this embedding. We can always consider a covering space of this manifold which is given by the metric (4.3) in which we allow τ to run from $-\infty$ to ∞. Since this spacetime would have no closed timelike curves, we are going to take it as the definition of the *global AdS* spacetime.

Another useful parametrization of the hyperboloid is given by the coordinates $t \in \mathbb{R}$, $x^i \in \mathbb{R}^{d-1}$ and $r \in \mathbb{R}_+$ such that

$$\begin{aligned} X_0 &= \frac{L}{2r}\left(1 + \frac{r^2}{L^4}\left(x_i x^i - t^2 + L^2\right)\right) \\ X_d &= \frac{L^2}{2r}\left(1 + \frac{r^2}{L^4}\left(x_i x^i - t^2 - L^2\right)\right) \\ X_i &= \frac{r x_i}{L} \quad \text{and} \quad X_{d+1} = \frac{rt}{L} \ , \end{aligned} \tag{4.4}$$

yielding the metric

$$ds^2 = \frac{L^2}{r^2} dr^2 + \frac{r^2}{L^2}\left(\eta_{\mu\nu} dx^\mu dx^\nu\right) \ , \tag{4.5}$$

where $\eta_{\mu\nu} = \text{diag}(-1, +1, \ldots, +1)$ is the d-dimensional Minkowski metric. Notice that, since $r \in \mathbb{R}_+$ we only cover one half of the AdS_{d+1} spacetime and we will refer to it as the *Poincaré patch*. Notice that the metric (4.5) is a solution of the Einstein equations with negative cosmological constant

$$\Lambda = -\frac{(d-1)(d-2)}{2L^2} \ . \tag{4.6}$$

In future sections of this thesis we are going to need metrics that describe an asymptotically AdS black hole, i.e. a black hole metric that reduces to AdS when we take the limit $r \to \infty$. Considering a non-rotating and non-charged with the Poincaré coordinates we obtain the Schwarzschild-AdS_{d+1} black hole space time, given by

$$ds^2 = -f(r) dt^2 + f(r)^{-1} dr^2 + \frac{r^2}{L^2} dx_i dx^i \quad \text{with} \quad f(r) = \frac{r^2}{L^2} - \frac{r_h^d}{r^{d-2} L^2} \ , \tag{4.7}$$

where r_h is the location of the event horizon.

Lastly, an even more convenient parametrization to make holographic computations is given by the coordinate transformation $z = L^2/r$. With this reparametrization, we finally obtain the Schwarzschild-AdS_{d+1} metric in the form that we are going to be using from now on:

$$ds^2 = \frac{L^2}{z^2}\left(-f(z) dt^2 + f(z)^{-1} dz^2 + dx_i dx^i\right) \quad \text{with} \quad f(z) = 1 - \frac{z^d}{z_h^d} \ , \tag{4.8}$$

where, following the computations described in Appendix A, we see that the temperature of the black hole and the event horizon location are related by [29]

$$T = \frac{d}{4\pi z_h} = \frac{d r_h}{4\pi L^2} \ . \tag{4.9}$$

It will be useful later in the thesis to write the metric in the "Eddington-Finkelstein" coordinates, i.e. in null coordinates, which are defined by

$$dv = dt - \frac{1}{f(z)}dz \ . \tag{4.10}$$

Then, by performing this changes of variables, the metric is written

$$ds^2 = \frac{L^2}{z^2}\left(-f(z)dv^2 - 2dvdz + dx_i dx^i\right) \tag{4.11}$$

4.2 The conformal field theory (CFT)

In this section we are going to pay attention to the second ingredient of the correspondence: the conformal field theory (CFT). This theory deals with quantum field theories having a conformal symmetry, i.e. QFTs that are invariant under general coordinate transformations that present the angles between any given vectors. That means that the conformal group is the group of transformations such that leave the metric invariant up to an overall scaling factor:

$$x^\mu \to x'^\mu \quad \Longrightarrow \quad g_{\mu\nu}(x) \to g'_{\mu\nu}(x') = \Omega^2(x) g_{\mu\nu}(x) \tag{4.12}$$

and whose elements are the Poincaré transformations, the scaling transformations and the special conformal transformations

$$x^\mu \to x'^\mu = \frac{x^\mu + a^\mu x^2}{1 + 2x^\nu a_\nu + a^2 x^2} \ . \tag{4.13}$$

If we denote the generators of the Lorentz transformations, translations, scalings and special conformal transformations by $M_{\mu\nu}$, P_μ, D and K_μ respectively we can see that they satisfy the so called conformal algebra

$$\begin{aligned}
[M_{\mu\nu}, P_\rho] &= -i\left(\eta_{\mu\rho}P_\nu - \eta_{\nu\rho}P_\mu\right) & [M_{\mu\nu}, M_{\rho\sigma}] &= -i\left(\eta_{\mu\rho}M_{\nu\sigma} - (\mu \leftrightarrow \nu)\right) - (\rho \leftrightarrow \sigma) \\
[D, K_\mu] &= iK_\mu & [M_{\mu\nu}, K_\rho] &= -i(\eta_{\mu\rho}K_\nu - \eta_{\nu\rho}K_\mu) \\
[D, P_\mu] &= -iP_\mu & [P_\mu, K_\nu] &= 2i(M_{\mu\nu} - \eta_{\mu\nu}D) \ ,
\end{aligned} \tag{4.14}$$

with the rest of the commutators vanishing. This algebra is isomorphic to $S = (2, d)$, just like AdS_{d+1}.

Let us now focus on the fields living in a CFT. More precisely, we look at field that are eigenfunctions of the D operator with eigenvalue $-i\Delta$. In other words, we look at the fields that, under scaling transformations, transform as

$$\phi(x) \to \phi'(x') = \lambda^{-\Delta}\phi(x) \ . \tag{4.15}$$

By applying the relations (4.14) we see that P_μ increases the scaling dimension Δ and K_μ decreases it. However, in an unitary CFT the value of Δ has a lower bound [29] and therefore there must exists a field with the lowest possible scaling dimension that is annihilated by K_μ. These fields are called *primary field*, and the rest of them (the *secondary fields*) can be expressed as a linear combination of derivatives of primary fields.

We can now define the *operator product expansion* (OPE), which is a statement about what happens when two local operators living in a CFT approach each other. The idea

here is that the correlation function of two operators acting at nearby spacetime points can be written as a sum of operators acting at one of those points:

$$\mathcal{O}_i(x)\mathcal{O}_j(y) = \sum_n c_{ij}^n(x-y)\mathcal{O}_n(y) \ . \tag{4.16}$$

This OPE is a key piece since in a CFT there exists a one-to-one map between states and local operators. This state-operator map is only true in CFT where we can map a cylinder to a plane. Then, considering that the timelike coordinate in the cylinder corresponds to the radial coordinate in the plane with origin in the past infinity, a local operator inserted at the origin of $\mathbb{R}^d$ is mapped to a state at the infinite past.

An important example of CFT that is crucial to understand the AdS/CFT correspondence is the $\mathcal{N}=4$ super-Yang Mills theory, which is a super-conformal field theory (a CFT that includes $\mathcal{N}=4$ global supersymmetry)[1].

4.3 The AdS/CFT correspondence

Motivated by the Bekenstein bound, which states that the the maximum entropy stored in a $(d+1)$-dimensional volume V_{d+1} is given by the area of that volume A_d measured in Planck units, $S = A_d/(4G)$, the *holographic principle* states that in a gravitational theory, the number of degrees of freedom in a given volume scales as the surface area of that volume. The AdS/CFT correspondence is an important realization of the holographic principle and it relates gravity theories on asymptotically AdS spacetimes with CFTs of one less dimension living on the boundary of the gravity theory.

Although, the correspondence can be motivated in a very intuitive way by looking at the renormalization group flow of QFTs, the original and most common way to introduce the idea of an AdS/CFT duality is by studying a stack of N coincidental D3-branes in a flat spacetime.[2] Dp-branes are dynamical objects in string theory that occupy a p-dimensional subspace and where close strings can break and open strings end. In this case, the stack of branes extends in the spacetime directions x^0,x^1,x^2 and x^3 and it is transversal to the directions x^4 to x^9. Without losing generality, we can locate the branes sitting in the position $x^4 = \ldots = x^9 = 0$. The key point here is to realize that the system can be studied from the point of view of both open and closed strings, each of them giving a different perspective of the same physics. Notice that, since we are talking about D3-branes, the string theory that we are going to talk about is the type IIB superstring theory [30].[3]

4.3.1 N D3-branes from open strings perspective

To begin, let's simplify the problem to the case where we have only one Dp-brane extending in the $(x^0,\ldots,x^p)$ directions and perpendicular to the $(x^{p+1},\ldots,x^9)$ where an open string ends. Then, after quantization, we obtain the spectrum of the open string,

[1] A discussion on supersymmetry and superstring theory is not include in this thesis because it is out of the scope and it would be very long. A review on it can be found in [29, 30]

[2] In this section I will present a brief summary of the main ideas of this approach to the AdS/CFT correspondence to keep it short and understandable. If one is interested in a deep discussion of all the details, a good starting point is [29].

[3] Type IIA superstring theory includes Dp-branes with p even, while in type IIB superstring theory p is odd.

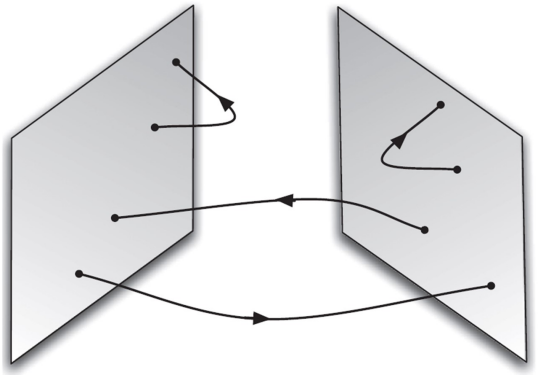

Figure 4.1: Representation of the four different types of open strings ending in two Dp-branes [31]. The strings are orientable, so a string starting at brane 1 and ending on brane 2 is different than a brane starting at 2 and ending at 1.

which consists of an massless Abelian gauge field $A_\mu(x)$ with $\mu = 0, \ldots, p$, $9-p$ massless scalar fields $\phi^i(x)$ (and their superpartners) and an infinite tower of massive excitations.

More interesting phenomena happen when we consider two Dp-branes separated by a distance r. In this case we would have four different types of open string, depending on which brane do they lie (see figure 4.1). The strings lying with both ends in the same brane give rise to two massless gauge fields $(A_\mu)^1{}_1$ and $(A_\mu)^2{}_2$, where the upper (lower) index stand for the brane where the string starts (ends) respectively. The two strings whose endpoints lie in different branes give rise to two massive gauge fields $(A_\mu)^1{}_2$ and $(A_\mu)^2{}_1$ with mass given by $m = r/2\pi\alpha$ where α is the tension of the string. We are interested in the case when the two branes are coincidental, i.e. $r = 0$, because then the four gauge fields are massless, which is precisely the number of gauge fields of a non-Abelian $U(2)$ gauge group. In the same way, the massless scalars fields become 2×2 matrices $\phi^i(x)^a{}_b$, with $a, b = 1, 2$, that transform in the adjoint representation of the $U(2)$ gauge group. In the case that we are interested in, N coincidental branes, we will find that the scalar fields transform in the adjoint representation of the $U(N)$ group and the gauge fields correspond to the non-Abelian $U(N)$ gauge field multiplet. Therefore, for low energy, i.e. if we integrate out the massive excitations, the dynamics of an open string is described by a non-Abelian gauge theory [29].

Considering N coincidental D3-branes the massless spectrum of the open string excitations consists in a gauge field A_μ, six scalars fields ϕ^i and four Weyl fermions [29], all of which transform in the adjoint representation of $U(N)$ and can be written as $N \times N$ matrices. The effective low energy energy action (up to second derivative level) corresponds to the action of a $\mathcal{N} = 4$ super-Yang Mills theory in $(3+1)$ dimensions with coupling constant $g^2_{\mathrm{YM}} = 4\pi g_s$, where g_s is the string coupling.

The full system contains closed strings too propagating in the bulk of the ten-dimensional spacetime as well as interactions between closed and open strings, but these vanish in the low energy limit. Then, in that limit, we conclude that we find two decoupled effective theories: $\mathcal{N} = 4$ super-Yang Mills theory in $(3+1)$ dimensions and type IIB supergravity on $\mathbb{R}^{9,1}$.

4.3.2 N D3-branes from closed strings perspective

Dp-branes have mass and, in a theory of gravity, all masses gravitate. The spacetime metric surrounding N Dp-branes, where the closed strings propagate, can be found by solving the equations of motion of supergravity. In our case, the supergravity solution of N D3-branes is given by

$$ds^2 = H(r)^{-1/2}\left(-dt^2 + dx_1^2 + dx_2^2 + dx_3^2\right) + H(r)^{1/2}\left(dr^2 + r^2 d\Omega_5^2\right) \ , \tag{4.17}$$

where the metric inside the parenthesis in the second term is just the metric in the directions transverse to the D3-branes written in spherical coordinates, with $r^2 = \Sigma_{i=4}^{9} x_i^2$, and

$$H(r) = 1 + \frac{L^4}{r^4} \tag{4.18}$$

where $L^4 = 4\pi g_s N l_s^4$, being l_s the string length.

In the limit when $r \gg L$ the metric reduces to that of a flat spacetime with a correction $\frac{L^4}{r^4} \sim \frac{GM}{r^4}$, which can be thought of potential created by a object of mass M in six spatial dimensions [31].

In the limit $r \ll L$ the metric reduces to

$$ds^2 = ds^2_{\mathrm{AdS}_5} + L^2 d\Omega_5^2 \tag{4.19}$$

where

$$ds^2_{\mathrm{AdS}_5} = \frac{r^2}{L^2}\left(-dt^2 + dx_1^2 + dx_2^2 + dx_3^2\right) + \frac{L^2}{r^2} dr^2 \tag{4.20}$$

which is the metric of a 5-dimensional anti-de Sitter spacetime written in Poincaré coordinates, given by equation (4.5). Therefore, we notice that, in the regime with strong gravitational interaction, the ten dimensional metric reduces to $\mathrm{AdS}_5 \times S^5$.

Just like in the previous section, in the low energy limit, we encounter two effective theories: type IIB supergravity on $\mathrm{AdS}_5 \times S^5$ and type IIB supergravity on $\mathbb{R}^{9,1}$.

4.3.3 The correspondence

The two perspectives presented above should be equivalent descriptions of the same physics and, since type IIB supergravity on $\mathbb{R}^{9,1}$ is present in both, it is natural to conjecture that $\mathcal{N} = 4$ super-Yang Mills in 4 dimensions is equivalent to type IIB supergravity on $\mathrm{AdS}_5 \times S^5$. This correspondence was first conjectured by Maldacena in [3].

Given the nature of the supergravity and CFT theories, the natural objects to relate both sides of the AdS/CFT correspondence are the fields and operators respectively. The key point to relate them is that, given a field configuration on the AdS boundary, this can be uniquely extended to the bulk spacetime. This was done originally by Witten in [32], who concluded that the generating function of the connected correlated functions in the CFT side and the partition function in the string theory side of the correspondence are related by the so called *Witten prescription*:

$$\mathcal{Z}[\phi_{(0)}] \equiv \left\langle \exp\left(\int d^d x \phi_{(0)}(x)\mathcal{O}(x)\right)\right\rangle_{CFT} = \mathcal{Z}_{\mathrm{string}}[\phi_{\mathrm{bdy}}(x)] \ , \tag{4.21}$$

where $\phi_{(0)}(x) = \lim_{z\to 0} z^{d-\Delta}\phi(x,z)$ plays the role of a source of the operator $\mathcal{O}$ of dimension Δ and $\phi_{\text{bdy}}(x) = \phi(x,z)|_{z=0}$ is a bulk field evaluated at the AdS boundary. This corresponds to the strongest form of the AdS/CFT correspondence. However, there is a "weak" form of the correspondence which states that the string partition function can be approximated by the *saddle point approximation*

$$\mathcal{Z}_{\text{string}}[\phi_{\text{bdy}}(x)] \approx e^{-S_{\text{class}}[\phi_{\text{bdy}}(x)]} \ , \tag{4.22}$$

where $S_{\text{class}}[\phi(x)]$ is the classical on-shell supergravity action. This approximation is valid in the limit when $N \to \infty$ [29], when the bulk theory reduces to the classical gravity theory.

All the discussion above relates string theory with $\mathcal{N} = 4$ super-Yang Mills theory at zero temperature. However, the correspondence can be generalized to temperature $T \neq 0$ by exciting the degrees of freedom on the D3-branes to that temperature. The final effect of this procedure is to modify the AdS metric into the Schwarzschild-AdS black brane (or black hole) metric (4.7).

4.4 Stress-energy tensor in the AdS/CFT correspondence

Given that one side of the correspondence is a (super)gravity theory, it is normal to try to understand what is the role of the graviton (or metric perturbation)$h^{\mu\nu}$ in this duality. This AdS metric fluctuations are mapped to the energy-momentum tensor T_{ab} of the field theory [29] via the source-operator term in the generating function (4.21) [33], i.e.

$$\int d^d x h^{ab} T_{ab} \ , \tag{4.23}$$

where a, b label the spacetime directions in the boundary field theory.

However, instead of relating the metric perturbations one can find a more straightforward relation between the stress-energy tensor in the field theory T_{ab} and the "boundary" stress tensor of the gravity theory τ_{ab} (note that τ_{ab} is computed at the boundary but it is actually the one corresponding to the AdS spacetime). The mentioned relation was first derived in [33] and comes from considering the Einstein-Hilbert action including a boundary term

$$S = \frac{1}{16\pi G_D}\int_{\mathcal{M}} d^D x\sqrt{-g}(R - 2\Lambda) - \frac{1}{8\pi G_D}\oint_{\partial\mathcal{M}} d^d x\sqrt{-\gamma}\Theta + S_{\text{matter}} \ , \tag{4.24}$$

where $g_{\mu\nu}$ is the metric of the gravity side of the correspondence defined on the manifold $\mathcal{M}$, $\gamma_{\mu\nu} = g_{\mu\nu} - n_\mu n_\nu$ (with n_μ normal to $\partial\mathcal{M}$ and pointing outwards) is the boundary metric of the gravity theory and $\Theta_{\mu\nu} = -\gamma_\mu{}^\rho \nabla_\rho n_\nu$ is the extrinsic curvature tensor on $\partial\mathcal{M}$ [33]. From here, one can derive the boundary stress-energy tensor as

$$\tau^{ab} \equiv \frac{2}{\sqrt{-\gamma}}\frac{\delta S}{\delta\gamma_{ab}} = \frac{1}{8\pi G_D}\left(\Theta^{ab} - \gamma^{ab}\Theta^c{}_c\right) \ . \tag{4.25}$$

Since we are interested in an AdS/CFT setup where the field theory "lives" in a boundary which is an asymptotic surface laying at $r \to \infty$, we have the problem o both the action (4.24) and the surface stress-energy tensor (4.25) diverging. To avoid this problem one can subtract the contribution of a reference background geometry with

metric $g^0_{\mu\nu}$ that matches the original spacetime asymptotically, i.e. the boundary is embedded in a reference background that satisfies $\gamma^0_{\mu\nu} = \gamma_{\mu\nu}$ [33]. Then, by proceeding like this, the result yields a finite action $\hat{S} = S[g] - S^0[g^0]$ and , therefore, also a finite surface stress-energy tensor

$$\hat{\tau}^{ab} \equiv \frac{2}{\sqrt{-\gamma}} \frac{\delta \hat{S}}{\delta \gamma_{ab}} = \tau^{ab} - (\tau^0)^{ab} \ . \tag{4.26}$$

The final key step needed to arrive to the relation between stress-energy tensors in both sides of the correspondence was given in [34] when they proved that, considering a spacetime with an asymptotically timelike Killing vector ξ^μ that satisfies $\xi_a \xi^a = -1$ and which is also an isometry of the boundary, i.e. $\mathcal{D}_{(a}\xi_{b)} = 0$, the energy is given by

$$E(\xi) = \oint_B d^{D-2}x \sqrt{-\gamma} \xi^a \hat{\tau}_{ab} \xi^b \ , \tag{4.27}$$

where B is a hypersurface at $\partial\mathcal{M}$ orthogonal to ξ^μ. This expression is finite by construction of the tensor $\hat{\tau}_{ab}$ but the measure $\sqrt{-\gamma}$ diverges as $r \to \infty$.

Then, the last considerations to take into account are that, in AdS/CFT correspondence, the metric of the CFT side is related to the asymptotic boundary geometry by a conformal transformation that, just like $\sqrt{-g}$, diverges asymptotically and that the total energy measured in the CFT should match the (super)gravity energy. Therefore, using equation (4.27), one can see that the conformal transformation, e.g. $h_{ab} = \lim_{r\to\infty} \frac{L^2}{r^2} \gamma_{ab}$, can be expressed by writing the stress-energy tensor in the field theory as [35]

$$\sqrt{-h} h^{ab} \langle T_{ab} \rangle = \lim_{r\to\infty} \sqrt{-\gamma} \gamma^{ab} \hat{\tau}_{ab} \ . \tag{4.28}$$

5. Gauss-Bonnet gravity

One of the aims of this thesis is to understand how the QNEC inequality behaves in field theories that are not dual to Einstein-Hilbert gravity, but to the minimal extension of it: the *Gauss-Bonnet* (GB) gravity.

In this section I will discuss the Gauss-Bonnet gravity and its solutions. To do so, first we need to understand what the so-called *Lovelock* gravity is and how the Gauss-Bonnet gravity is related to it. Then, I will present the solutions relevant for our case: the vacuum GB-AdS and the GB-AdS black brane solutions.

5.1 Lovelock and Gauss-Bonnet gravity

Einstein theory of general relativity is not the most general gravity theory that yields second order equations of motion. Instead, in 1971, Einstein's gravity was generalized to a gravity theory that included the most general terms yielding second order equations of motion for any arbitrary number of dimensions. This new theory is known as the Lovelock gravity [36] and its action is

$$S = \frac{1}{16\pi G_N^{d+1}} \int d^{d+1}x\sqrt{-g} \sum_{p=1}^{[\frac{d}{2}]} \alpha_p \mathcal{L}_p \tag{5.1}$$

where $[\frac{d}{2}]$ is the integer part of $\frac{d}{2}$, α_p are the Lovelock coefficients and $\mathcal{L}_p$ is the Euler density of a $2p$-dimensional manifold given by

$$\mathcal{L}_p = \frac{1}{2^p} \delta^{a_1 b_1 \cdots a_p b_p}_{c_1 d_1 \cdots c_p d_p} \prod_{i=1}^{p} R^{c_i d_i}{}_{a_i b_i} \tag{5.2}$$

with $\mathcal{L}_0$ being just the cosmological constant and $\mathcal{L}_1$ yielding the Einstein-Hilbert action. Therefore, since the Lovelock action only include terms up to $p = [\frac{d}{2}]$, for $D \equiv d+1 = 4$, the Lovelock gravity reduces to Einstein's theory. For $D \geq 5$ the Lovelock action includes higher derivative terms of the Riemann tensor. Therefore, Lovelock gravity is the most general "higher derivative gravity theory" that yields second order equations of motion.

In this thesis we will focus basically on theories with $d = 4$ and restrict our gravity action to $p \leq 2$, which is known as Gauss-Bonnet gravity. Therefore, the action we are

interested in is give by

$$S = \frac{1}{16\pi G_N^{d+1}} \int d^{d+1}x\sqrt{-g}\left(R - 2\Lambda + \alpha\left(R_{\mu\nu\gamma\delta}R^{\mu\nu\gamma\delta} - 4R_{\mu\nu}R^{\mu\nu} + R^2\right)\right) \tag{5.3}$$

where R is the Ricci scalar, α is the Gauss-Bonnet coupling, the negative cosmological constant can be rewritten as $\Lambda = -\frac{(D-1)(D-2)}{2L^2}$ the term in the last parenthesis corresponds to the $p = 2$ Euler density $\mathcal{L}_2$

$$\mathcal{L}_2 = R_{\mu\nu\gamma\delta}R^{\mu\nu\gamma\delta} - 4R_{\mu\nu}R^{\mu\nu} + R^2 \tag{5.4}$$

5.2 AdS-type solutions of Gauss-Bonnet gravity

5.2.1 AdS black branes in Gauss-Bonnet gravity

The equations of motion of the action (5.3) are given by

$$R_{\mu\nu} - \frac{1}{2}g_{\mu\nu}R + g_{\mu\nu}\Lambda = \alpha\left(\frac{1}{2}g_{\mu\nu}\mathcal{L}_2 + 4R_{\gamma\delta}R^{\gamma}{}_{\mu}{}^{\delta}{}_{\nu} + 4R_{\mu\gamma}R^{\gamma}{}_{\nu} - 2RR_{\mu\nu} - 2R_{\mu\gamma\delta\lambda}R_{\nu}{}^{\gamma\delta\lambda}\right) . \tag{5.5}$$

Since we are interested in static and spherically symmetric metrics, we can assume that the solution of the equations of motion is a metric of the type

$$ds^2 = -e^{2\nu}dt^2 + e^{2\lambda}dr^2 + \frac{r^2}{L^2}h_{ij}dx^i dx^j \ , \tag{5.6}$$

where ν and λ are functions of r and $h_{ij}dx^i dx^j$ is the metric of a $(D-2)$-dimensional surface of curvature $(D-2)(D-3)k$. In our case, we are interested a metric that is asymptotically flat AdS, and that means keeping $k = 0$. In reference [37] Cai showed that, by plugging the ansatz into the action (5.3) one finds that

$$F(r) \equiv e^{2\nu} = e^{-2\lambda} = \frac{r^2}{2\tilde{\alpha}}\left(1 - \sqrt{1 - \frac{4\tilde{\alpha}}{L^2}\left(1 - \frac{r_h^d}{r^d}\right)}\right) \ , \tag{5.7}$$

where $\tilde{\alpha} = (D-3)(D-4)\alpha$ and r_h is the location of the event horizon. Therefore, the metric is finally given by

$$ds^2 = -F(r)dt^2 + \frac{dr^2}{F(r)} + \frac{r^2}{L^2}dx_i dx^i \ , \tag{5.8}$$

where $i = 1, \ldots, d-1$.

Just like in section 4.1, we can rewrite the metric in terms of a $z = \frac{L^2}{r}$ component. By doing so, the metric becomes

$$ds^2 = \frac{L^2}{z^2}\left(-F(z)dt^2 + \frac{dz^2}{F(z)} + dx_i dx^i\right) \tag{5.9}$$

with

$$F(z) = \frac{L^2}{2\tilde{\alpha}}\left(1 - \sqrt{1 - \frac{4\tilde{\alpha}}{L^2}\left(1 - \frac{z^d}{z_h^d}\right)}\right) \ . \tag{5.10}$$

With this metric, following the computations of Appendix A, we find that the Hawking temperature of this black brane is given by

$$T = \frac{d}{4\pi z_h} = \frac{dr_h}{4\pi L^2} \ . \tag{5.11}$$

By comparing with the temperature for the black brane in Einstein-Hilbert gravity given by equation (4.9), we see that both in Einstein-Hilbert and Gauss-Bonnet gravity the black brane has the same temperature (and thermodynamic properties). However, this is only true for $k = 0$ [37].

Just like mentioned in section 4.1, we are going to be interested in using the metric in the Eddington-Finkelstein coordinates which, by using equation (4.10), is given by

$$ds^2 = \frac{L^2}{z^2}\left(-F(z)dv^2 - 2dvdz + dx_i dx^i\right) \tag{5.12}$$

5.2.2 AdS vacuum in Gauss-Bonnet gravity

Once we have the black brane solution for the action (5.3) it is straight forward to find the vacuum AdS solution just by imposing the horizon of the black hole to be point-like (or to set the mass of it to vanish). Therefore, by setting $r_h \to 0$, one can write the metric (5.8) as

$$ds^2 = \frac{r^2}{L_{\text{eff}}^2}\left(-dt^2 + d\tilde{x}_i d\tilde{x}^i\right) + \frac{L_{\text{eff}}^2}{r^2}dr^2 \ , \tag{5.13}$$

where L_{eff} is the effective AdS length scale for this solution and is given by

$$L_{\text{eff}}^2 \equiv \frac{r^2 L^2}{F(r)|_{r_h=0}} = L^2 \frac{1+\sqrt{1-\frac{4\tilde{\alpha}}{L^2}}}{2} \tag{5.14}$$

and the space coordinates have been rescaled as

$$\tilde{x}^i = \frac{L_{\text{eff}}}{L} x^i \ . \tag{5.15}$$

Of course, we can, again, rewrite the metric by making the change of variables $z = \frac{L_{\text{eff}}^2}{r}$ as

$$ds^2 = \frac{L_{\text{eff}}^2}{z^2}\left(-dt^2 + d\tilde{x}_i d\tilde{x}^i + dz^2\right) \ . \tag{5.16}$$

Notice that we obtain these same solutions if we set $r \to \infty$ (or $z \to 0$) in the black brane metrics. That means that, as we expected, the black brane solution described above is asymptotically AdS.

5.3 Holographic constrains on the Gauss-Bonnet coupling constant

By demanding $F(r)$ to be real, one finds that $\tilde{\alpha}$ is bounded by $\tilde{\alpha} \leq L^2/4$, which is known as the Chern-Simons limit. However, if we consider the Gauss-Bonnet gravity to be dual to a certain CFT, this is not the only bound of $\tilde{\alpha}$.

In [38] it is shown that $\tilde{\alpha}$ is upper and lower bounded by some values depending on the dimensions of the gravity theory. There, Buchel et.al. first generalized the results found by Hofman and Maldacena in [39], where they computed the energy flux measured at null infinity for an initial state created by the insertion of the stress-energy tensor in $d = 4$, to an arbitrary number of dimensions and then compared this result to the one obtained by computing the energy flux holographically for a CFT dual to Gauss-Bonnet gravity. In the non-holographic computation , the result yields:

$$\begin{aligned}\langle \mathcal{E}(\vec{n})\rangle &= \frac{\langle 0|\,\mathcal{O}^\dagger \mathcal{E}(\vec{n})\mathcal{O}\,|0\rangle}{\langle 0|\,\mathcal{O}^\dagger\mathcal{O}\,|0\rangle} \\ &= \frac{E}{\Omega_{d-2}}\left[1 + t_2\left(\frac{\varepsilon^*_{ij}\varepsilon_{il}n^j n^l}{\varepsilon^*_{ij}\varepsilon_{ij}} - \frac{1}{d-1}\right) + t_4\left(\frac{\left|\varepsilon_{ij}n^i n^j\right|^2}{\varepsilon^*_{ij}\varepsilon_{ij}} - \frac{2}{d^2-1}\right)\right] ,\end{aligned} \tag{5.17}$$

where $\mathcal{O} \sim \varepsilon_{ij}T^{ij}(x)$, the tensor $\varepsilon_{ij} \propto e^{-iEt}$ only carries spatial indices, Ω_{d-2} is the area of a unit $(d-2)$-dimensional sphere, n^i indicates the direction in which the flux is measured and E is the total energy. To do the computation by means of holography they followed the same procedures explained in [35] and concluded that the energy flux for a CFT dual to Gauss-Bonnet is given by

$$\langle \mathcal{E}(\vec{n})\rangle = \frac{E}{\Omega_{d-2}}\left[1 + t_2\left(\frac{n_1^2 + n_2^2}{2} - \frac{1}{d-1}\right)\right] \tag{5.18}$$

with

$$t_2 = \frac{4\,F(r)|_{r_h=0}\,\tilde{\alpha}}{1 - 2\,F(r)|_{r_h=0}\,\tilde{\alpha}}\frac{(D-1)(D-2)}{(D-3)(D-4)} . \tag{5.19}$$

Then, the constraints arise from the fact that t_2 and t_4 cannot be too large in order to keep equation (5.17) positive. To study them, first we fix the normal vector to $n^i = (1, 0, 0, \ldots)$ and then we classify the tensors ε_{ij} according to their rotational properties under the $SO(d-2)$ groups that leaves n^i invariant [38]. By doing that they encountered three different constrains which, by using $t_4 = 0$ (as deduced from equation (5.18)) and rewriting t_2 using equation (5.19), can be expressed as:

- Spin 2, e.g. $\varepsilon_{23} = \varepsilon_{32} = a$ and all other component vanishing:

$$\tilde{\alpha} \leq \frac{(D-3)(D-4)(D^2-3D+8)}{4(D^2-5D+10)^2} , \tag{5.20}$$

- Spin 1, e.g. $\varepsilon_{12} = \varepsilon_{21} = a$ and all other components vanishing:

$$\tilde{\alpha} \geq -\frac{(D+1)(D-3)}{16} , \tag{5.21}$$

- Spin 0, e.g. $\varepsilon_{ij} = a \times \mathrm{diag}(-(d-2), 1, 1, \ldots)$:

$$\tilde{\alpha} \geq -\frac{(3D-1)(D-3)}{4(D+1)^2} . \tag{5.22}$$

It is straightforward to see that the two most restrictive constraints are the ones corresponding to the spin 2 and spin 1 channels. Therefore, to ensure that the CFT has no negative energy fluxes, i.e. it does not have causality issues, we must bound $\tilde{\alpha}$ by

$$-\frac{(3D-1)(D-3)}{4(D+1)^2} \leq \tilde{\alpha} \leq \frac{(D-3)(D-4)(D^2-3D+8)}{4(D^2-5D+10)^2} . \tag{5.23}$$

6. Holographic Entanglement Entropy

As mention in chapter 3, in general, the entanglement entropy using only QFT techniques is extremely though, since it involves computing path integrals with the replica trick. However, if we attempt to do this computations using the AdS/CFT correspondence explained in chapter 4, what it is known as computing the *holographic entanglement entropy*, things become much more easy.

There are two different prescriptions to compute the entanglement entropy depending on the characteristics of the CFT state that we want to study. The *Ryu-Takayanagi* (RT) prescription is valid when we have a state that is dual to Einstein-Hilbert gravity and has a time reversal symmetry while the *Hubeny-Rangamani-Takayanagi* (HRT) prescription is valid for a general state without time-reversal symmetry. This last one reduces to the RT prescription naturally if the state is time-reversal symmetric. Both of them can be generalized to the case in which we are interested in a CFT state dual to a higher derivative gravity such as Gauss-Bonnet gravity.

Since in this thesis we are more interested in studying the QNEC for different geometries of the entangling surface instead of for different states we are only going to be making computations for the vacuum and thermal plasma state. Therefore, since both states are time-reversal, only the RT prescription and its generalizations to higher derivatives are going to be of our interest. However, in this chapter I will review both the proofs for the RT and the HRT prescription.

6.1 Derivation of the Ryu-Takayanagi (RT) prescription

In 2006,Ryu and Takayanagi [2] proposed a formula, based on the Bekenstein-Hawking entropy formula, to compute the holographic entanglement entropy of a spatial region $\mathcal{A}$ given by

$$S_{\mathcal{A}} = \frac{\text{Area}(\mathcal{E}_{\mathcal{A}})}{4G_N^{(D)}} \ , \tag{6.1}$$

where $\mathcal{E}_{\mathcal{A}}$ is the surface of minimal area in the bulk geometry that coincides with the entangling surface in the boundary $\lim_{z\to 0} \mathcal{E}_{\mathcal{A}} = \partial\mathcal{A}$ (see figure 6.1). This formula was proven in 2016 [27] and it is only valid for states with time-reversal symmetry. Here I will present a review on the proof.

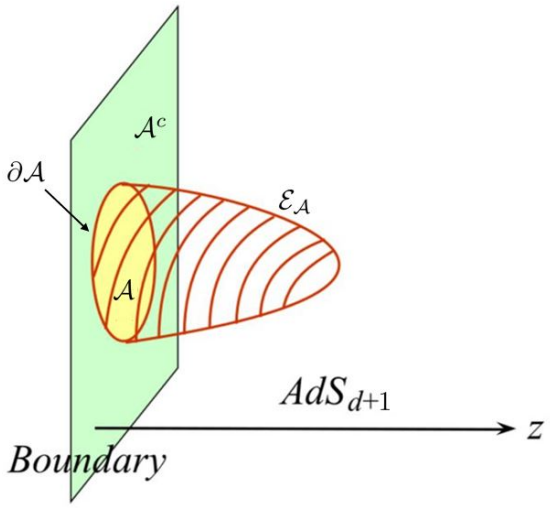

Figure 6.1: Schematic representation of the construction needed to compute the holographic entanglement entropy by means of the RT prescription. $\mathcal{E}_\mathcal{A}$ is the minimal area in the bulk geometry that coincides with $\partial\mathcal{A}$ at the boundary.

Since we are interested in states that have time-reversal symmetry, we know that $\mathcal{B}$ and $\mathcal{B}_q$ have a timelike Killing vector ∂_{t_E} and this is very useful since it allows for the analytical continuation of the bulk path integral from Lorentzian to Euclidean signature. Then, by making use of the relation (4.21), we can write the qth Rényi entropy (3.13) as

$$\begin{aligned} S^{(q)} &= \frac{1}{1-q}\log\left(\frac{\mathrm{Tr}(\rho_\mathcal{A}{}^q)}{(\mathrm{Tr}\rho_\mathcal{A})^q}\right) \\ &= \frac{1}{1-q}\log\left(\frac{\mathcal{Z}[\mathcal{B}_q]}{\mathcal{Z}[\mathcal{B}]^q}\right) \\ &= \frac{1}{1-q}\log\left(\frac{\mathcal{Z}_{\mathrm{string}}[\mathcal{M}_q]}{\mathcal{Z}_{\mathrm{string}}[\mathcal{M}_1]^q}\right) \\ &= \frac{1}{1-q}\left(\log\mathcal{Z}_{\mathrm{string}}[\mathcal{M}_q] - q\log\mathcal{Z}_{\mathrm{string}}[\mathcal{M}_1]\right), \end{aligned} \tag{6.2}$$

where, working in the $N \gg 1$ limit, we can use the saddle point approximation for the bulk partition function and write

$$\mathcal{Z}_{\mathrm{string}} = \int [\mathcal{D}\Phi] e^{-S[\Phi]} \approx e^{-S_{\mathrm{class}}[\mathcal{M}_q]} \tag{6.3}$$

with

$$S_{\mathrm{class}}[\mathcal{M}] = \frac{1}{16\pi G_N^D}\int_\mathcal{M} d^D x\sqrt{-g}\,(R - 2\Lambda) \ . \tag{6.4}$$

To find the entanglement entropy, we need to analytically continue q to non-integer values. This was argued in [40], where Maldacena and Lewkowycz showed that this continuation was easier in the gravitational setup. Their arguments can be separated into two pieces [27]:

- a kinematic part that tells us how to analytically continue q,
- a dynamical part that ensures that our ansatz satisfies Einstein's equation.

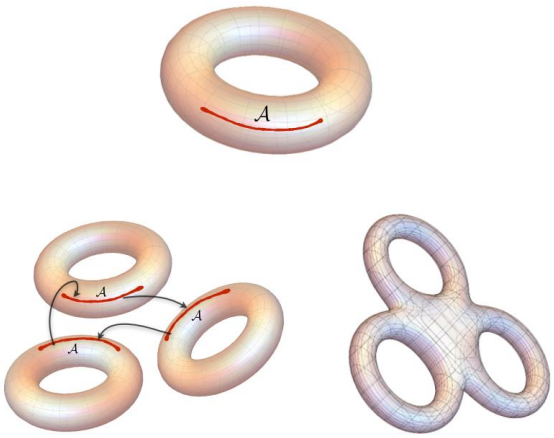

Figure 6.2: Example of the construction of a $\mathcal{B}_q$ geometry involved in computing the qth Rényi entropy.$\mathcal{B}$ is a torus and the final results $\mathcal{B}_3$ (bottom right) is a genus-3 surface made from cyclically sewing 3 copies of $\mathcal{B}$ across the region $\mathcal{A}$ [27].

6.1.1 Kinematic part

When constructing the replica manifold $\mathcal{B}_q$ as explained in chapter 3 one also gets a replica symmetry $\mathbb{Z}_q$ due to the cyclicity of the trace, which basically shuffles the copies of $\mathcal{B}$ in $\mathcal{B}_q$. Note that the quotient space $\mathcal{B}_q/\mathbb{Z}_q$ is topologically equivalent to $\mathcal{B}$, as can be seen in figure 6.2.

The key point made in [40] is to assume that one can extend the $\mathbb{Z}_q$ symmetry into the bulk geometry. That means that, since the spacetime $\mathcal{M}_q$ has to be derived from the field equations, we are interested only in spacetimes that admit a $\mathbb{Z}_q$ action, where the symmetry does not need to act smoothly. Therefore, if we consider the quotient space $\hat{\mathcal{M}}_q = \mathcal{M}_q/\mathbb{Z}_q$ this will, in general, contain some fixed $\mathbb{Z}_q$ points, which are singularities. A crucial point here is to assume that the singular locus in $\hat{\mathcal{M}}_q$, which we call e_q, is codimension-2 in the spacetime

As mention in chapter 3, the spacetime manifold is branched over $\partial\mathcal{A}$, which is a codimension-2 surface in $\mathcal{B}$. Then, since the $\mathbb{Z}_q$ action has to be given by the boundary conditions, one concludes that the bulk action has to extend $\partial\mathcal{A}$ into the bulk. Therefore, one concludes that e_q is the "continuation" of $\partial\mathcal{A}$ into the bulk geometry. This argument is local and, therefore, is only valid near the boundary. However, in [41] it is shown that the argument is generalizable to a global statement if one has a family of geometries with replica symmetry parametrized by some q that are smooth for $q \in \mathbb{Z}_+$. Therefore, in the rest of the work in [27], they assume that this is the case and also claim that the locus e_q can be treated as a source of energy-momentum which backreacts on $\mathcal{M}$ to deform it into $\hat{\mathcal{M}}_q$. Therefore, since we are taking an orbifold of a $(d+1)$-dimensional spacetime to get codimension-2 singular locus, this should be treated as a cosmic brane with tension

$$T_q = \frac{1}{4G_N^D}\frac{q-1}{q} \tag{6.5}$$

where the prefactor is the needed for a source of energy density localized in a codimension-2 surface. Then one can simply solve Einstein's equation, with the stress-energy tensor arising from the cosmic brane tension, to obtain the spacetime $\mathcal{M}$ and, therefore, $\mathcal{M}_q$ and $\hat{\mathcal{M}}_q$.

This way of reasoning turns out to be very convenient since the parameter q only appears in the tension of the brane and, therefore, this suggests that we can compute Rényi entropies for non-integer values of q, making possible to compute also the entanglement entropy. Not only that, it also allow us to separate the deformation of the geometry into a tangential and a normal to the brane. Setting the coordinates that parametrize the brane to be y^i with $i = 1, 2, \ldots, d-1$ and the coordinates normal to the brane to be t_E and x (note that the subscript E stands for the Euclidean signature) the metric in the neighborhood of the brane can be expressed as

$$ds_E^2 = dx^2 + dt_E^2 + \left(\gamma_{ij} + 2K_{ij}^x x + 2K_{ij}^t t_E\right) dy^i dy^j + \ldots, \tag{6.6}$$

where only leading terms in the Taylor expansion around $x = t_E = 0$ have been kept.

6.1.2 Dynamical part

Before setting the boundary conditions that will lead us to solve for the bulk geometry notice that, while the quotient space $\hat{\mathcal{M}}_q$ has a defect angle of $\delta = \frac{2\pi}{q}$, the spacetime $\mathcal{M}_q$ is smooth. Having said that, we can now study the locus e_q in polar coordinates, such that $x \pm t_E = re^{\pm i\tau}$ (see figure 6.3). The $\mathbb{Z}_q$ symmetry implies that the bulk action is invariant under the reparametrization $\tau \to \tau + 2\pi$. However, since we have q copies of the manifold M, as we approach e_q, the coordinate τ has to cross through all of these copies before getting back to the starting point. Because of that, it should be identified under $\tau \sim \tau + 2\pi q$.

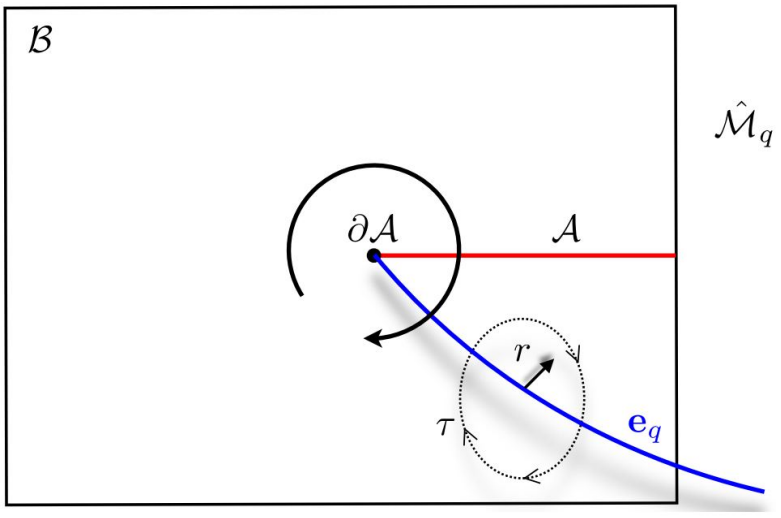

Figure 6.3: Representation of the geometry in the neighborhood of the locus e_q which is anchored in $\partial\mathcal{A}$ at the boundary. The coordinates we use to study the spacetime near e_q are r for the radial and τ for the angular one that circulates around the codimension-2 surface [27].

Then, using the fact that $\mathcal{M}_q$ is smooth, one concludes that the spacetime in the neighborhood of e_q in $\mathcal{M}_q$ is given by

$$ds^2 = \left(q^2 dr^2 + r^2 d\tau^2\right) + \left(\gamma_{ij} + 2K_{ij}^x r^q \cos\tau + 2K_{ij}^t r^q \sin\tau\right) dy^i dy^j + \ldots\ , \tag{6.7}$$

where, as said above, we only kept up to the leading order of the Taylor expansion.

Finally, now that we have the expression (6.7), one should only compute the Einstein's equations to see when they are going to be satisfied or violated. By doing so, one

can see that the curvatures for the geometry (6.7) has divergent terms proportional to $(q-1)\, r^{-1} K^a_{ij}\gamma^{ij}$ and that these cannot be compensate by higher terms contributions [27]. Then, the only way that the geometry (6.7) can satisfy Einstein's equations is by demanding that $K^a_{ij}\gamma^{ij} = 0$ in the normal directions. This, together with the fact that we are considering states with time-reversal symmetry $t \to -t$, i.e. $K^t_{ij}\gamma^{ij} = 0$, implies the minimal surface condition [2]

$$\lim_{q\to 1} e_q = \mathcal{E}_{\mathcal{A}} \ , \quad \mathcal{E}_{\mathcal{A}} \in \mathcal{M} \text{ with } t = 0,\, K^x = 0 \ , \tag{6.8}$$

where $K^x \equiv K^x_{ij}\gamma^{ij}$.

6.1.3 Evaluation of the action

Now that we know that the entanglement entropy involves a minimal surface one could attempt to evaluate the on-shell action to see that the result is actually given by the expression (6.1). However, while evaluating the action directly means that we should integrate it over the entire manifold $\hat{\mathcal{M}}_q$, one can take a easier path and evaluate the quantity $\partial_q S_{\text{class}}[\hat{\mathcal{M}}_q]$, which localizes on a codimension-2 surface. This leads us to compute not the Rényi entropy but the modular entropy $\tilde{S}^{(q)}_{\mathcal{A}}$ instead, which is related to the former one by

$$\tilde{S}^{(q)}_{\mathcal{A}} = \frac{1}{q^2}\partial_q\left(\frac{q-1}{q} S^{(q)}_{\mathcal{A}}\right) = \frac{1}{q^2}\partial_q\left(\frac{1}{q}(\log \mathcal{Z}_{\text{string}}[\mathcal{M}_q] - q \log \mathcal{Z}_{\text{string}}[\mathcal{M}_1])\right) \ . \tag{6.9}$$

Then the idea is to interpret the derivative as a change in the bulk solution. Therefore, one should study the variation of the action, which we know that can be written as the sum of the equations of motion plus some boundary terms

$$\delta[\hat{\mathcal{M}}_q] = \int_{\mathcal{M}_q} \left(E^{AB}\delta(g_q)_{AB} + d\Theta\left((g_q)_{AB}, \partial_q(g_q)_{AB}\right)\right) \ , \tag{6.10}$$

where E^{AB} are the terms that give rise to the equations of motion. If wee take $\delta g_{AB} = \partial_q g_{AB}$ then the variation satisfies that the boundary condition is changed near the locus e_q and not at the boundary, i.e. $\partial_q(g_q)_{AB}|_{\mathcal{B}_q} = 0$ and $\partial_q(g_q)_{AB}|_{e_q} \neq 0$. Therefore, we do not get any contribution from the asymptotic boundary and, instead, the variation is localized at the locus e_q.

We can evaluate the derivative by regulating the singularity at e_q considering a tubular surface of radius ϵ surrounding the locus. Thus, we can write

$$\partial_q S_{\text{class}}[\hat{\mathcal{M}}_q] = \int_{e_q(\epsilon)} \Theta\left((g_q)_{AB}, \partial_q(g_q)_{AB}\right) \ , \tag{6.11}$$

where $e_q(\epsilon)$ is the codimension-1 tubular surface around e_q.

In [27] they argue that it is possible to evaluate this integral given the symmetries but that it is much easier to evaluate the boundary term S_{bdy}, which is related to expression (6.11) by

$$\partial_q S_{\text{class}}[\hat{\mathcal{M}}_q] = -\partial_q S_{\text{bdy}}[\hat{\mathcal{M}}_q] \ , \tag{6.12}$$

and is given by the boundary term that makes sure that the action in (6.4) gives the correct equations of motion. This term, thus, is given by [27]

$$S_{\text{bdy}}[\mathcal{M}_q] = \frac{1}{8\pi G_N^{(D)}} \int_{e_q(\epsilon)} \mathcal{K}_\epsilon \ , \tag{6.13}$$

where $\mathcal{K}_\epsilon = \frac{1}{q\epsilon}$ is the trace of the extrinsic curvature of the surface $e_q(\epsilon)$. Therefore, we find that the modular entropy is given by

$$\tilde{S}^{(q)} = \partial_q S_{\text{class}}[\hat{\mathcal{M}}_q] = \frac{\text{Area}(e_q)}{4q^2 G_N^{(D)}} \ , \tag{6.14}$$

which taking the limit $q \to 1$ finally yields the RT formula

$$S = \frac{\text{Area}(\mathcal{E}_\mathcal{A})}{4G_N^{(D)}} \ . \tag{6.15}$$

6.2 The Hubeny-Rangamani-Takayanagi (HRT) prescription

In the case of dealing with time-depending states that do not have a time-reversal symmetry we cannot transform the path integral into one with an Euclidean signature since that would lead to a complex manifold. Because of that, in section 3.2 we introduced the "replica trick" using the Schwinger-Keldysh formalism. The question is then how to extend this replica construction to an holographic context.

In section 3.2 e explained that in order to compute the path integral we should evolve the initial state defined at $t_0 = -\infty$ up until the moment of interest, labeled by t, and then, instead of evolving to the future, evolve back to the far past. The idea to compute this in an holographic setup is to consider a Cauchy slice in the bulk $\tilde{\Sigma}_t$ that is analogous to one discussed above in the boundary, $\Sigma_t = \mathcal{A} \cup \mathcal{A}^c$, with the extra that, analogously to what happens in the boundary theory, the evolution in the bulk will take place only in the past of $\tilde{\Sigma}_t$, i.e. in $\tilde{J}^-[\tilde{\Sigma}_t]$, evolving from $t_0 = -\infty$ to t and back (see figure 6.4). However, notice that a Cauchy slice Σ_t on the boundary does not uniquely determine $\tilde{\Sigma}_t$. Instead, one can choose any Cauchy surface in the bulk as long as each point on it remains spacelike separated from each other. We refer to the region of the bulk conformed by all possible Cauchy slices as the FRW wedge.

Once we have set the Schwinger-Keldysh construction in the bulk we use it to construct the $\mathcal{M}_q$ manifold by gluing together $2q$ copies of the "original" bulk spacetime. Then, following the reasoning explained above, one can construct the quotient space $\hat{\mathcal{M}}_q = \mathcal{M}_q/\mathbb{Z}_q$ with a singular locus e_q. Then the whole problem reduces to understand how this locus affects to the bulk equations of motion. Since we cannot make the continuation to the Euclidean signature, the geometry near e_q will be the Lorentzian analog of (6.7)

$$\begin{aligned} ds^2 = &\left(q^2 dr^2 - r^2 d\tau^2\right) + \left(\gamma_{ij} + 2K^x_{ij} r^q \cosh\tau + 2K^t_{ij} r^q \sinh\tau\right) dy^i dy^j \\ &+ \left(r^{f_q(q-1)} - 1\right) \delta g_{\mu\nu} dx^\mu dx^\nu + \dots \ , \end{aligned} \tag{6.16}$$

with f_q being the normalizing factor that satisfies $f_q(q-1) \in 2\mathbb{Z}_+$ for $q \in \mathbb{Z}_+$.

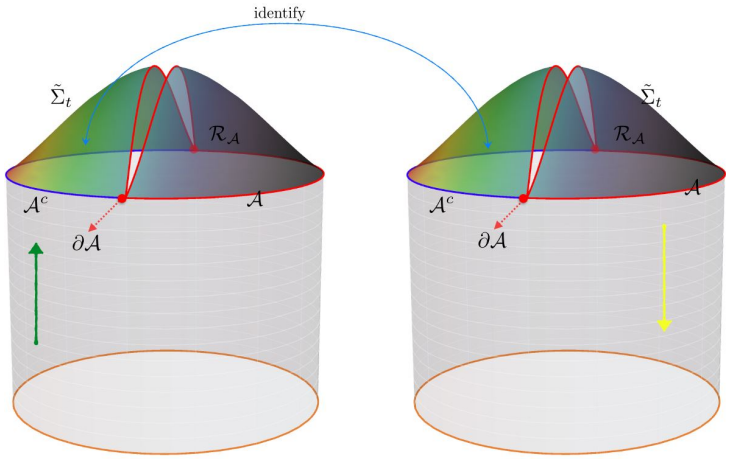

Figure 6.4: The Schwinger-Keldysh construction for the bulk geometry (left evolving from past to "present" and right evolving from "present" to past) involves two copies of the manifold that are glued together across the part of the bulk geometry that is dual to $\mathcal{A}^c$ [27].

Just like in the RT case, the extrinsic curvature terms in (6.16) lead to a singularity at $r = 0$ that cannot be cancel out by higher terms in the expansion. Therefore, similar to before, one concludes that the trace of the extrinsic curvature in the normal directions must vanish, i.e. $K^t = K^x = 0$ (with $K^a = K^a_{ij}\gamma^{ij}$). Finally, by defining $x^\pm = \frac{1}{\sqrt{2}}(x^0 \pm x^1)$, one has the extremal surface condition:

$$\begin{aligned} K^{0,1} = 0 \implies \theta^\pm &= \frac{1}{\sqrt{2}}\left(K^0 \pm K^1\right) = 0 \\ &\implies \lim_{q\to 1} e_q = \mathcal{E}_\mathcal{A}, \quad \mathcal{E}_\mathcal{A} \in \mathcal{M} \text{ is extremal.} \end{aligned} \tag{6.17}$$

Now that e know that $\mathcal{E}_\mathcal{A}$ is extremal, we can study what Cauchy slice of all the available in the FRW wedge is the suitable for our case. These surface $\tilde{\Sigma}_t$ has to satisfy two conditions, namely being anchored at the boundary at the boundary Cauchy slice, i.e. $\partial\tilde{\Sigma}_t = \Sigma_t$, and include the extremal surface, i.e. $\mathcal{E}_\mathcal{A} \in \tilde{\Sigma}_t$.

Just like before, the last step in the derivation is to evaluate the on-shell action of the gravity theory. However, in this case the computations is way harder since one has to evaluate the path integral in the Lorentzian signature directly. As done above in equation (6.12), one can simplify its computations by evaluating the boundary terms. Here I just present the final result, which yields

$$\partial_q S_{\text{class}}[\tilde{\mathcal{M}}_q] = \frac{1}{8\pi G_N^{(D)}}\partial_q \int_{e_q(\epsilon)} \mathcal{K}_\epsilon = i\frac{\text{Area}(e_q)}{4q^2 G_N^{(D)}} , \tag{6.18}$$

which in the limit $q \to 1$ implies

$$S_A = \frac{\text{Area}(\mathcal{E}_\mathcal{A})}{4G_N^{(D)}} . \tag{6.19}$$

It is worth mentioning again, that the difference between the RT and HRT prescriptions is that the former deals with time-reversal situations and implies a bulk surface of minimal area while the latter is valid for a general case and states that the bulk surface is extremal

but does not need to be of minimal area. A more easy interpretation of this latter case is given by the *maximin* construction [42], which is a reformulation of the HRT prescription. This construction tells us that the surface $\mathcal{E}_{\mathcal{A}}$ can be found by proceeding as follows: considering a boundary region $\mathcal{A}$, one chooses a bulk Cauchy slice $(\tilde{\Sigma}_t)_{\text{guess}}$ that is anchored at Σ_t at the boundary. Then one find a minimal area surface on that slice in the same way as in the RT case. Then, we should vary our Cauchy slice and repeat the process until we have picked all possible Cauchy slices in the FRW wedge. Doing that, we end up with an infinite family of minimal area surfaces. From all of them, one is instructed to pick that surface with maximum area. From that perspective it is clear to see that, in the case of considering a time-independent situation, the HRT prescription converges into the RT one.

6.3 Generalization to higher derivative gravity

We now turn our attention to the case when we have a state which is dual to a gravity theory given by the lagrangian

$$\mathcal{L} = R - 2\Lambda + \sum_i \alpha_k \mathcal{D}^{2k} R + \mathcal{L}_{\text{matter}} \ , \tag{6.20}$$

where the third term includes higher derivative terms and it is non-zero. Then one should proceed as explained above to derive the formula for th entanglement entropy, with the difference that now the equations of motion has changed.

We will not present here a full review again on how to derive the holographic entanglement entropy formula for higher derivate theories, instead one can find the fill discussion in [43] where Dong derives the final generic formula for the entanglement entropy in higher derivative gravity

$$\begin{aligned} S = \frac{1}{8G_N^{(D)}} \int d^d x \sqrt{g} \Bigg\{ -\frac{\delta \mathcal{L}}{\delta R_{\mu\rho\nu\sigma}} \varepsilon_{\mu\rho} \varepsilon_{\nu\sigma} + \sum_\alpha \left(\frac{\delta^2 \mathcal{L}}{\delta R_{\mu_1\nu_1\rho_1\sigma_1} \delta R_{\mu_2\nu_2\rho_2\sigma_2}} \right)_\alpha \frac{2 K_{\lambda_1\rho_1\sigma_1} K_{\lambda_2\rho_2\sigma_2}}{q_\alpha + 1} \\ \times \Big[(n_{\mu_1\mu_2} n_{\nu_1\nu_2} - \varepsilon_{\mu_1\mu_2} \varepsilon_{\nu_1\nu_2}) n^{\lambda_1\lambda_2} + (n_{\mu_1\mu_2} \varepsilon_{\nu_1\nu_2} + \varepsilon_{\mu_1\mu_2} n_{\nu_1\nu_2}) \varepsilon^{\lambda_1\lambda_2} \Big] \Bigg\} \ , \end{aligned} \tag{6.21}$$

where $n_{\mu_1\mu_2} \equiv n_\mu^{(a)} n_\nu^{(b)} g_{ab}$ projects to the induced metric $g_{\mu\nu}$ onto the normal directions, $\varepsilon_{\mu_1\mu_2} \equiv n_\mu^{(a)} n_\nu^{(b)} \varepsilon_{ab}$ (being ε_{ab} the Levi-Civita symbols) and $K_{\lambda\mu\nu} = n_\lambda m_\mu^{(i)} m_\nu^{(j)} K_{ij}$ being K_{ij} the extrinsic curvature tensor and $m_\mu^{(i)}$ a set of d orthogonal unit vectors.

Notice that the first term above is the so-called "Ward functional", which computes the entropy of a black hole in a theory given by the lagrangian (6.20). In the case of considering a state dual to Gauss-Bonnet gravity, the entropy functional becomes

$$S = \frac{1}{4G_N^{(D)}} \int_{\mathcal{E}_{\mathcal{A}}} d^{d-1} x \sqrt{\gamma} \left(1 + 2\alpha L^2 R_{\mathcal{E}_{\mathcal{A}}} \right) \ , \tag{6.22}$$

where α is the Gauss-Bonnet coupling and $R_{\mathcal{E}_{\mathcal{A}}}$ is the Ricci scalar of the entanglement surface $\mathcal{E}_{\mathcal{A}}$, which is found by extremizing the functional (6.22).

6.4 Determination of the bulk extremal surface

Both the RT and HRT prescriptions require to find the bulk extremal surfaces. In the case of the RT prescription this extremal surface will also be the one with minimal area. In this section I will briefly comment how can one find such surfaces since it is going to be of importance later on in this thesis.

Given the bulk metric expressed as

$$ds^2 = g_{\mu\nu}dx^\mu dx^\nu \ , \tag{6.23}$$

the induced metric on the bulk extremal surface $\mathcal{E}_\mathcal{A}$ is given by the pullback of the metric 6.23 such that

$$ds^2\big|_{\mathcal{E}_\mathcal{A}} = g_{\mu\nu}\frac{\partial x^\mu}{\partial\zeta^a}\frac{\partial x^\nu}{\partial\zeta^b}d\zeta^a d\zeta^b \equiv \tilde{\gamma}_{ab}d\zeta^a d\zeta^b \ . \tag{6.24}$$

Then, the area of this surface is nothing more than the integral of the square root of the determinant of the metric and, therefore, the entropy will be given by

$$S = \frac{1}{4G_N^{(D)}}\int d^{d-1}\zeta\sqrt{\det\left(g_{\mu\nu}\frac{\partial x^\mu}{\partial\zeta^a}\frac{\partial x^\nu}{\partial\zeta^b}\right)} = \frac{1}{4G_N^{(D)}}\int d^{d-1}\zeta\sqrt{\det\left(\hat{\gamma}_{ab}\right)} \equiv \frac{1}{4G_N^{(D)}}\int d^{d-1}\zeta\mathcal{L} \ . \tag{6.25}$$

Then, to find the extremal surface one can just solve the Euler-Lagrange equations of motion of the Lagrangian $\mathcal{L}$. However, this equations of motion will vary depending if $\mathcal{L}$ depends on terms going as $\dot{q}$, $\ddot{q}$ or even higher derivatives, where q is just a generic variable and the dot stands for derivative with respect to ζ. In the case of studying situations where the bulk theory is given by Einstein-Hilbert gravity, then both the RT and the HRT prescriptions will give rise to a Lagrangian with only dependence on q_i and $\dot{q}_i$. However, when moving to Gauss-Bonnet gravity theory, since the entanglement entropy (6.22) implies computing the Ricci scalar on the surface $\mathcal{E}_\mathcal{A}$, the Lagrangian will actually depend also on $\ddot{q}_i$. Therefore in this case we will need to use the suitable Euler-Lagrange equations which are given by

$$\frac{\partial\mathcal{L}}{\partial q_i} - \frac{d}{d\zeta}\left(\frac{\partial\mathcal{L}}{\partial\dot{q}_i}\right) + \frac{d^2}{d\zeta^2}\left(\frac{\partial\mathcal{L}}{\partial\ddot{q}_i}\right) = 0 \ . \tag{6.26}$$

However, one can argue that this procedure is not a well defined variational problem since, in order to obtain the equation (6.26) from the variation of an action S, we have to impose that $\delta(\dot{q}_i) = 0$ at the boundaries of the integration interval. In [44], the authors proposed a way around this difficulty. The key point here is to modify the prescription (6.22) by adding a boundary term which, when varying th action, will cancel the conflictive term. This new prescription for the holographic entanglement entropy of a Gauss-Bonnet holographic dual that they propose is

$$S = \frac{1}{4G_N^{(D)}}\int_{\mathcal{E}_\mathcal{A}} d^{d-1}x\sqrt{\gamma}(1+2\alpha L^2 R_{\mathcal{E}_\mathcal{A}}) + \frac{1}{2G_N^{(D)}}\int_{\partial\mathcal{E}_\mathcal{A}} d^{d-2}x\sqrt{\gamma}2\alpha L^2\mathcal{K} \ , \tag{6.27}$$

where the lat term is the Gibbons-Hawking boundary term, $\partial\mathcal{E}_\mathcal{A}$ is the boundary of $\mathcal{E}_\mathcal{A}$, i.e. the slice of $\mathcal{E}_\mathcal{A}$ at $z = z_{\text{cut}}$ and $\mathcal{K}$ is the trace of the extrinsic curvature tensor of $\partial\mathcal{E}_\mathcal{A}$. When varying this entropy functional one obtains the Euler-Lagrange equation (6.26) without the second order term.

In the ideal case where can extend the minimal surface up to the boundary ($z = 0$) both entropy functionals should yield the same results. This is because at the boundary $\delta q^i = 0$ and, since the metric diverges at $z = 0$, $\delta \dot{q}^i = 0$. However, in the real life we have to introduce the cutoff z_{cut} to regularize the divergences. This implies that, at $z = z_{\text{cut}}$, $\delta \dot{q}^i \neq 0$ and, therefore, we must include the Gibbons-Hawking boundary term in order to have a well defined variational principle.

6.5 Numerical computation of the holographic entanglement entropy

As mention in the introduction, the goal of this thesis is to explicitly compute the QNEC inequality in different situations to study its behavior and properties. More precisely, we are interested in situations where we are dealing with strip-like and spherical entangling regions defined by $\{y \in (-l/2, l/2) \text{ and } (x_1, x_2) \in \mathbb{R}^2\}$ and $\{\xi = R \text{ and } (\theta, \phi) \in S^2\}$ respectively. However, computing the holographic entanglement entropy is in general an extremely hard task to do analytically. Because of that in the next chapters most of the computations will be performed numerically using Mathematica[1], with the exception of sections 7.2.1 and 7.2.2 where also an analytical approximation is computed. To properly understand the reasoning explained in this section, take into account that the integral (6.25) and the expression (6.27) can be reduced to a one dimensional problem since, for both cases, the lagrangian $\mathcal{L}$ will only depend on either y or ξ. This, however, will be proven in the following chapters. In what follows, we use the notation $\dot{z}$ to express $\frac{dz}{dy}$ and z' for $\frac{dz}{d\xi}$.

Starting for the case in which we are interested in computing the holographic entanglement entropy in the dual of Einstein-Hilbert gravity, we start by writing the effective lagrangian as defined in (6.25) and then solve its equations of motion to find the minimal area surface. To do so, one can specify the boundary conditions ($\partial\mathcal{E}_{\mathcal{A}} = \partial\mathcal{A}$) and find the extremal surface using a relaxation method or one can specify the position z and "velocity" $\dot{z}$ (z' for the sphere) at a given point and solve using a shooting method. We chose the second method because, unlike in a relaxation method, one does not need an initial ansatz and the initial conditions are very natural to impose. These initial conditions are

$$z(0) = z_* \qquad \text{and} \qquad \dot{z}(0) = 0 \tag{6.28}$$

for the strips while for the spheres they are

$$z(0) = z_* \qquad \text{and} \qquad z'(0) = 0 \ . \tag{6.29}$$

Then one can find the minimal area surface (as a function of z_*) by solving the corresponding Euler-Lagrange equation and obtain $z(y; z_*)$ and $z(\xi, z_*)$. We do this by using the function "ParametricNDSolve" already implemented in Mathematica.

The way we proceed once we obtained the equations that parametrize $\mathcal{E}_{\mathcal{A}}$ is by numerically integrate the effective lagrangian in order to compute the entropy for each value of z_*. This is done both for the vacuum and the thermal state. Since the bulk metric diverges at $z \to 0$ we introduce a cutoff at $z_{\text{cut}} = 0.005$ [2] to regulate these divergences.

[1] Of course one can use any language or program to do this computations. We use Mathematica because its built-in functions and routines will be very useful.

[2] Smaller cutoffs introduced too much numerical noise. This is the smallest value we could consider where we have the numerical noise under control. See appendix B for a more extended explanation on how the parameters of our numerical methods affect the results.

Because of this, the effective one-dimensional entropy integral ranges from 0 to $\frac{l}{2}-\omega$ for the strip (where l is the width of the strip) and from 0 to $R-\omega$, being R the radius of the entangling region for the spherical case. To numerically find the endpoints of the integrals one only needs to find the value of y or ξ where the minimal area surface crosses the surface $z=z_{\text{cut}}$, i.e. one should find the root of the equation

$$z(y;z_*)|_{y=y_{\text{end}}}=z_{\text{cut}}\ , \tag{6.30}$$

where $y_{\text{end}}=\frac{l}{2}-\omega$ is the endpoint of the integral for the strips (the same works for the spheres if one sets $y\to\xi$). Setting the precision of the Mathematica "FindRoot" function to 25 digits is more than enough to minimize the possible numerical error without taking too much computation time. The numerical integral is done using the function "NIntegrate" setting the final result to be precise up to 20 digits.

As mentioned before, we must integrate the effective lagrangian $\mathcal{L}\left[\xi,z(\xi),\dot{z}(\xi);z_*\right]$ for each value of z_*. By doing so, and by pairing each integral result with its corresponding integration endpoint y_{end} or ξ_{end}, we obtain a list of values $S_{\text{tab}}(R)$, where the subscript "tab" means that we are considering a table of numerical values. However, we cannot compare the vacuum and the thermal results since the minimal surfaces, and therefore the integrals, depend on z_* in a different way in each case. The final step is then to interpolate a function to the values of $S_{\text{tab}}(R)$ and obtain $S(R)$. Finally, this function can be treated as an analytical function, and thus we will be able to compare the functions for both the vacuum and thermal states and to compute the QNEC by calculating the corresponding formulas. However, this method only allow us to differentiate the entropy with respect to the variable y in case of the strips and ξ in case of the spheres. That means that we will not be able to consider all possible variations of the strip-like regions and only the ones that leave the entangling surface, and therefore also the minimal surface, lying in a constant t Cauchy slice will be allowed. We refer the reader to figure 7.5(b) to understand what kind of variations work for this numerical methods.

The general method used to compute the holographic entanglement entropy in Gauss-Bonnet holography is very similar to the one explained above, with the difference that we now have to take care of the new parameter α. In this new case, the lagrangian depend on α in a non-trivial way (see chapter 8) and finding the equations of motion that one has to solve to find the extremal surfaces is not possible. Because of this, we expand the effective lagrangian in powers of α (up to linear or second order, depending on the situation explained later) and find the results of the equations of the minimal surface and the entropy integral corresponding to this "expanded" lagrangian for some fixed values of α that will range from the most negative to the most positive possible.

In this case, since we have to take into account the α parameter, we run the ParametricNDSolve function inside a loop in order to find the functions $z_\alpha(\xi;z_*)$ for each fixed value of α. Then, we just compute the numerical integral in a very similar way as before (but running it inside a loop) in order to obtain a table of 2 indices as a final result, i.e. a table of tables. The first index of that table will stand for the value of α and the second for each pair of values inside $S_{\text{tab},\alpha}(R)$. In other words, we obtain a table $S[i,j]$, where i run for each value of α and j for all the pairs $\{S,\xi_{\text{end}}\}$, such that $S[i]=S_{\text{tab},\alpha_i}(R)$. Lastly, just like before, we only need to interpolate function for each $S_{\text{tab},\alpha}(R)$ table and obtain the final result $S_\alpha(R)$.

The computation time scales very fast when we increase the order of α which we are considering. Because of this and the fact that α is small, it is not worth to go to orders higher than two.

7. The QNEC

7.1 Review of the proof of the QNEC

As explained in section 2.3, the QNEC involves computing the second derivative of the entanglement entropy of a region $\mathcal{A}$ when varying the entangling surface $\partial\mathcal{A}$ in a null direction parametrized by the null vector k^μ. This inequality comes from considering the QFC and, while this last one is just a conjecture, one can proof the QNEC to be true by other means. In this section I will review the holographic proof given in [45] by Koeller and Leichenauer.

The starting point of the proof is the fact that *for any two boundary regions* $\mathcal{A}_1$ *and* $\mathcal{A}_2$ *with domain of dependence* $D(\mathcal{A}_1)$ *and* $D(\mathcal{A}_2)$ *such that* $D(\mathcal{A}_1) \subset D(\mathcal{A}_2)$, $\mathcal{E}_{\mathcal{A}_1}$ *is spacelike- or null-separated from* $\mathcal{E}_{\mathcal{A}_2}$ [42,45]. This relies in the null curvature condition in the bulk gravity theory. With that taken into account, let's consider a general entangling region $\mathcal{A}$ bounded by the entangling surface $\partial\mathcal{A}$. Then we can consider deformations on $\partial\mathcal{A}$ by varying them along null geodesics generated by k^μ and obtain a whole family of entangling surfaces $\partial\mathcal{A}(\lambda)$, where λ is the affine parameter along the null geodesic. By doing so, we will also obtain a family of bulk extremal surfaces $\mathcal{E}_\mathcal{A}(\lambda)$ and, thus, also a whole family of entanglement entropies. Then, demanding that the domain of dependence of $\mathcal{A}$ is either shrinking or growing as a function of λ, we can see that the union of all the $\mathcal{E}_\mathcal{A}(\lambda)$, that we denote as $\mathcal{M}$ is an achronal surface in the bulk (see figure 7.1 for a representation of it). That means that all the tangent vectors to $\mathcal{M}$, which

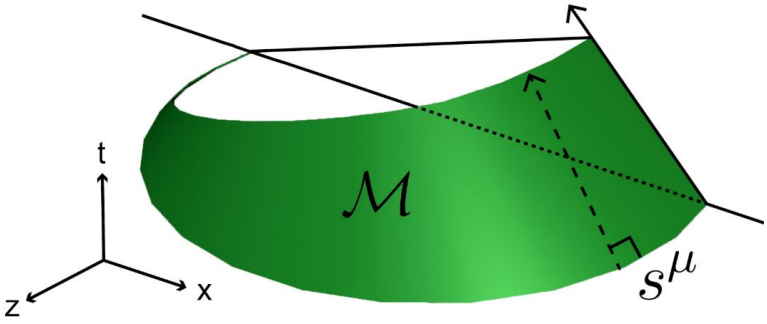

Figure 7.1: Schematic representation of the hypersurface $\mathcal{M}$ generated by the union of infinite minimal surfaces $\mathcal{E}_\mathcal{A}(\lambda)$. The solid line represents the null vector k^μ at the boundary while the dashed line represents the vector field s^μ that parametrizes the changes in $\mathcal{E}_\mathcal{A}(\lambda)$. The QNEC arises from the fact that $g_{\mu\nu}s^\mu s^\nu \geq 0$ [45].

we denote as s^μ, are either null or spacelike. In other words, we have that $g_{\mu\nu}s^\mu s^\nu \geq 0$ which, written in a proper way, gives rise to the QNEC (2.17).

To express this inequality in the form of the QNEC that we know from above, let's first take the basis $\partial_a X^\mu$, $\partial_z X^\mu$ and $\partial_\lambda X^\mu$ (being X^μ the embedding functions for the extremal surface $\mathcal{E}_\mathcal{A}$), where the first two vectors are tangent to each extremal surface $\mathcal{E}_\mathcal{A}(\lambda)$ and the latter points in the direction of the variation. Then, we can just choose s^μ to be normal the extremal surface and, therefore, to be the normal part of $\partial_\lambda X^\mu$.

In order to perform the computations it is simpler to consider the basis form by the vectors normal to the extremal surface at any λ and then write s^μ as a linear combination of them. Start by considering the null vectors at the boundary k^μ and l^μ which are orthogonal to $\partial\mathcal{A}$. Here k^μ is the vector that generates the variation of $\partial\mathcal{A}$ and l^μ is the other linearly independent null vector at the boundary, which is normalized so that $l^\mu k_\mu = 1$. Then, we can define two null vectors in the bulk K^μ and L^μ which are orthogonal to $\mathcal{E}_\mathcal{A}(\lambda)$ and limit with k^μ and l^μ respectively at the boundary. Then, as said before, we write the vector that parametrizes the variation in the bulk extremal surface s^μ as the linear combination

$$s^\mu = \alpha K^\mu + \beta L^\mu \ , \tag{7.1}$$

where α and β are determined by demanding s^μ to be tangent to $\mathcal{M}$. If we do so, we find that the coefficients are given by

$$\alpha = g_{\mu\nu}L^\mu \partial_\lambda X^\mu, \quad \beta = g_{\mu\nu}K^\mu \partial_\lambda X^\mu \tag{7.2}$$

and the inequality $g_{\mu\nu}s^\mu s^\nu \geq 0$ becomes

$$\alpha\beta \geq 0 \ . \tag{7.3}$$

One can derive the QNEC by writing a perturbative expansion for the field K^μ and compute β. This requires knowledge of the asymptotic expansion of the bulk embedding functions for the extremal surface X^μ and the metric $g_{\mu\nu}$ up to order z^d which are given in [45]. Writing the trace of the extrinsic curvature tensor of $\partial\mathcal{A}$ as $\mathcal{K}^\mu$ one can eliminate the divergences of the entropy by assuming $k_\mu \mathcal{K}^\mu = 0$. . By doing that one finally obtains that the asymptotic expansion of X^μ is given by [45]

$$X^\mu(z,y) = x^\mu(i) + B(y,z)k^i(y) + \frac{1}{d}V^i(y)z^d + \mathcal{O}(z^d) \ , \tag{7.4}$$

where $B(x,y)$ vanishes at $z=0$ and contains powers of z less than d, x^i are the embedding functions of $\partial\mathcal{A}$ and we have used the superscript i to specify that we we are talking about objects leave in the boundary. Then, to construct the expansion for K^μ one can use the ansatz

$$K^\mu(y,z) = \delta^\mu_z k^z(y,z) + \delta^\mu_i \left(k^i(y) + z^d \Delta k^i(y)\right) \tag{7.5}$$

with

$$(k^z)^2 + \left(\frac{16\pi G_N}{dL^{d-1}}T_{kk} + 2k_i \Delta k^i\right) z^d = \mathcal{O}(z^d) \ , \tag{7.6}$$

which ensures that K^μ is null. Now we can take the inner product of K^μ wit $\partial_\lambda X^\mu$ and obtain the expression

$$g_{\mu\nu}K^\mu\partial_\lambda X^\mu = \left(k_i\Delta k^i + \frac{1}{d}k_i\partial_\lambda V^i + \frac{16\pi G_N}{dL^{d-1}}T_{kk}\right)z^d + \mathcal{O}(z^d)\ . \tag{7.7}$$

Then, demanding that K^μ is orthogonal to both $\mathcal{E}_\mathcal{A}$ one write Δk^i in terms of T_{kk} and V^i and visceversa. Using that and equation (7.7) we find that the expression (7.3) becomes

$$\frac{8\pi G_N}{L^{d-1}}T_{kk} \geq -k_i\partial_\lambda V^i \tag{7.8}$$

for $d > 2$ and

$$\frac{8\pi G_N}{L^{d-1}}T_{kk} \geq -k_i\partial_\lambda V^i + (k_iV^i)^2 \tag{7.9}$$

for$d = 2$.

Then, one can relate the right hand side of these equations with the variation of the area of the extremal surface $\mathcal{E}_\mathcal{A}$ which, at the same time, is related to the entanglement entropy by

$$S = \frac{\text{Area}(\mathcal{E}_\mathcal{A})}{4G_N^{(D)}}\ . \tag{7.10}$$

The relation between V^i and the area of $\mathcal{E}_\mathcal{A}$ is derived in [45] and is given by

$$\frac{\delta\text{Area}(\mathcal{E}_\mathcal{A})}{\delta X^i(y)} = C(y,\epsilon)k_i(y) - L^{d-1}\sqrt{h(y)}V_i(y)\ , \tag{7.11}$$

where $C(y,\epsilon)k(y)_i$ is a function of only the local geometric data of $\partial\mathcal{A}$ and $h(y)$ is the induced metric of $\partial\mathcal{A}$.

Applying all of these together to the inequalities above one finds that for $d > z2$

$$T_{kk} \geq \frac{1}{2\pi\sqrt{h}}k^i\frac{D}{D\lambda}\frac{\delta S}{\delta X^i} \tag{7.12}$$

and for $d = 2$

$$T_{kk} \geq \frac{1}{2\pi\sqrt{h}}\left[k^i\frac{D}{D\lambda}\frac{\delta S}{\delta X^i} + \frac{4G_N^{(D)}}{L}\left(k^i\frac{\delta S}{\delta X^i}\right)^2\right]\ , \tag{7.13}$$

where $D/D\lambda$ is the derivative with respect to λ and takes into account the case when we vary the whole surface $\partial\mathcal{A}$ in a null direction. When we restrict the variation only to an infinitesimal neighborhood of the point y we have the relation

$$k^i(y)\frac{D}{D\lambda}\frac{\delta S}{\delta X^i(y)} \to \frac{d^2S(y)}{d\lambda^2} \tag{7.14}$$

and, therefore, in this case we find that the QNEC is given by

$$T_{kk} \geq \frac{1}{2\pi\sqrt{h}}\frac{d^2S}{d\lambda^2} \tag{7.15}$$

for $d > 2$ and

$$T_{kk} \geq \frac{1}{2\pi\sqrt{h}}\left[\frac{d^2S}{d\lambda^2} + \frac{6}{c}\left(\frac{dS}{d\lambda}\right)^2\right]\ . \tag{7.16}$$

7.1.1 The "conformal QNEC"

In [45] the authors also derived the expression of the QNEC in the case when we are interested in CFTs in $d > 2$. Consider the Weyl transformation $\eta_{ij} \to \hat{g}_{ij} = e^{2\Upsilon}\eta_{ij}$. We are interested in studying how equation (7.15) transforms we we work in this new conformal frame. To do so, we just need to see how T_{kk} and S transform when applied the Weyl transformation.

In the case of d odd T_{ij} transforms covariantly with weight $d-2$ while for even dimensions we have that the stress-energy tensor is shifted by an anomaly $\mathcal{A}_{ij}^{(T)}$ which depends on Υ as

$$T_{ij} = e^{(d-2)\Upsilon}\left(\hat{T}_{ij} - \mathcal{A}_{ij}^{(T)}\right). \tag{7.17}$$

On the other hand, for the entropy, the Weyl transformation is completely determined by the cutoff dependence of the divergent terms. This is because a Weyl transformation on the boundary is just a coordinate transformation in the bulk and, therefore, the extremal surface $\mathcal{E}_{\mathcal{A}}$ does not change. However, the divergent parts of S all transform with different weights and anomalous shifts [46] and that makes determining the transformation of the whole S difficult. Notice, though, that the QNEC isolates the finite part of the entropy S_{fin} and, thus, we only need to understand how this part transforms. This was studied in [46] where they proved that S_{fin} is invariant when d is odd and has an anomalous shift in even d

$$S_{\text{fin}} = \hat{S}_{\text{fin}} - \mathcal{A}^{S}\ , \tag{7.18}$$

where $\mathcal{A}^{(S)}$ depends on $\partial\mathcal{A}$ and Υ. Then, working the derivatives with respect to λ and taking into account that the null vector at the boundary transforms as $\hat{k}^i = e^{-2\Upsilon}k^i$ we can finally write the expression for the "conformal QNEC"

$$T_{kk} - \mathcal{A}_{kk}^{(T)} \geq \frac{1}{2\pi\sqrt{h}}\left[\frac{d^2\left(S_{\text{fin}} - \mathcal{A}^{(S)}\right)}{d\lambda^2} + \frac{2}{d-2}\theta\frac{d\left(S_{\text{fin}} - \mathcal{A}^{(S)}\right)}{d\lambda}\right]\ , \tag{7.19}$$

where $\theta = (d-2)\,\hat{k}^i\partial_i\Upsilon$ is the expansion in the $\hat{k}^i$ direction.

7.2 Case of study: the thermal plasma

To analyze the QNEC I centered myself in studying the case of a thermal plasma state in CFT_4 with different geometries of the entangling region. In the first section, I study the computations performed by Ecker et al. in [4] for the case of the thermal plasma state with entangling region of strip-like geometry. While studying this computations I realized that not all possible variations of the entangling surface were taking into account and, by simply looking at the symmetries of the problem, I expanded this computations in the next section to cover all possible variations. Lastly, I also studied the case in which we are dealing with a spherically symmetric entangling surface. This case is interesting mainly for three things: unlike strip-like regions, a spherical entangling region is finite, it has a great degree of symmetry and its entanglement entropy diverges.

7.2.1 QNEC in a strip-like entangling region (I)

In this section I will review part of the computations performed by Ecker, Grumiller, van der Schee and Stanzer in 2018 in [4]. In this paper, they presented the first series of explicit computations of the QNEC inequality (2.17) for vacuum, thermal plasma

in equilibrium, a homogeneous far-from-equilibrium quench and a shock-wave collision system where the NEC is violated. All this computations are done for the case of strip-like entangling regions since it is the most appropriate choice for the shock-wave system. Here I will discuss the case of the thermal plasma in equilibrium.

As mentioned in section 4.3 a thermal state of the boundary CFT_d is dual to a Schwarzschild-AdS_{d+1} black brane spacetime with metric

$$ds^2 = \frac{L^2}{z^2}\left(-f(z)dt^2 + d\mathbf{x}_{d-1}^2 + \frac{dz^2}{f(z)}\right), \quad f(z) = 1 - \frac{z^d}{z_h^d} \tag{7.20}$$

where z_h is the location of the black brane horizon and, from now on, we will set $L = 1$.

Recall that the temperature of the black brane, and therefore the temperature of the thermal state at the boundary, is related to the horizon by

$$T = \frac{d}{4\pi z_h} \ . \tag{7.21}$$

In our case now, since we are treating a strip-like entangling region which is infinite in 2 spatial directions and finite in the remaining one, we can decompose the 3 spatial directions of the boundary in $\mathbf{x}_{d-1} = (\mathbf{x}_{d-2}, y)$. Therefore, our entangling region is defined by $\mathcal{A}_{\parallel} = \left\{\mathbf{x}_{d-1} \in \mathbb{R}^{d-1} \mid y \in (-l/2, l/2) \text{ and } \mathbf{x}_{d-2} \in \mathbb{R}^{d-2}\right\}$ (see figure 7.2) and the metric (7.20) can be rewritten as

$$ds^2 = \frac{1}{z^2}\left(-f(z)dt^2 + \frac{dz^2}{f(z)} + dy^2 + d\mathbf{x}_{d-2}^2\right) \tag{7.22}$$

Once the geometry of the problem is set, we can compute both the left and right hand side of the expression (2.17) and see if it is violated, saturated or just obeyed. To compute the left hand side of the QNEC, the averaged value of the projection of the stress-energy tensor, it was proved in [47] and used in [4] that for five-dimensional metrics of the form

$$ds^2 = 2dt\left(Fdy - \frac{dz}{z^2}\right) - Adt^2 + R^2\left(e^B dx_1^2 + e^B dx_2^2 + e^{-B}dy^2\right) \tag{7.23}$$

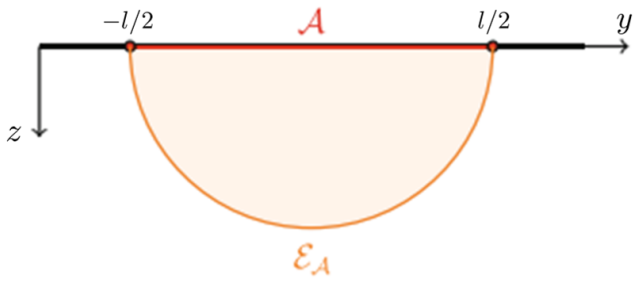

Figure 7.2: Sketch of the geometry of the entangling region $\mathcal{A}_{\parallel}$ and the extremal surface $\mathcal{E}_{\mathcal{A}_{\parallel}}$. The dimensions x_1 and x_2 has been suppressed in the figure.

with A,B,F, and R depending on the boundary coordinates y and t and on the bulk coordinate z and expanded near the AdS_5 boundary as

$$A = z^{-2} + a_4(t,y)z^2 + \mathcal{O}(z^3) \tag{7.24a}$$
$$B = b_4(t,y)z^4 + \mathcal{O}(z^5) \tag{7.24b}$$
$$F = f_4(t,y)z^2 + \mathcal{O}(z^3) \tag{7.24c}$$
$$R = z^{-1} + \mathcal{O}(z^4)\ . \tag{7.24d}$$

the projection of the stress-energy tensor can be determined as

$$\frac{1}{N^2}\left\langle T^{\pm}_{kk}\right\rangle = \frac{1}{2\pi^2}\left(-a_4 - 2b_a \pm 2f_4\right) \tag{7.25}$$

where the $\pm$ sign stands for the two light-like directions, i.e. $k^\mu_\pm = \delta^\mu_t \pm \delta^\mu_y$.

In our case, it is straight forward to see that if we consider only the case of AdS_5 and write the metric (7.22) in the form of (7.23) then the expressions we obtain for the functions A,B,F and R are:

$$A = z^{-2} - (\pi T)^4 z^2 \tag{7.26a}$$
$$R = z^{-1} \tag{7.26b}$$
$$B = F = 0\ . \tag{7.26c}$$

Therefore, for the thermal plasma in ths geometry, the averaged value of the null projection of the energy momentum tensor is

$$\frac{1}{N}\left\langle T^{\pm}_{kk}\right\rangle = \frac{\pi^2}{2}T^4 \approx 0.0507\pi^4 T^4\ . \tag{7.27}$$

In this case the two projections are the same for both $k^\mu_\pm$ directions because of the parity symmetry.

To compute the right hand side of QNEC as it is expressed in equation (2.17), i.e. the second derivative of the entanglement entropy with respect to null deformations of the entangling region $\mathcal{A}_\parallel$, we first need to clarify how we parametrize these deformations. In Eckel et al. work, they took into account deformations of the entangling surface where only one side of the $\mathcal{A}_\parallel$ boundary is deformed. That means that the deformation can be parametrize by $(t_-, y_-) = (0, -l/2)$ and $(t_+, y_+) = (\lambda, l/2 + \lambda)$, where λ is the deformation parameter and the subscripts "+" and "−" stand for the each of the boundaries of the entangling region, one at $y > 0$ and the other at $y < 0$ respectively (see figure 7.2) Note that, since the thermal state is symmetric under time reversal transformations, the bulk geometry must also be invariant under such transformation. Therefore, one can easily see that the deformation of $\mathcal{A}_\parallel$ proposed is equivalent to a deformation where we deform not just one side of the entangling region but both in such a way that $(t_\pm, y_\pm) = (\pm\lambda/2, \pm(l+\lambda)/2)$. As one can check, the total variation in the temporal and the spacial direction are both λ, just like before. The two kind of variations are sketched in figure 7.3.

Due to the fact that the geometry in the bulk is invariant under time reversal transformations, they used the RT prescription to compute the entanglement entropy. Recall that, following this prescription, the entanglement entropy in the boundary CFT_d is

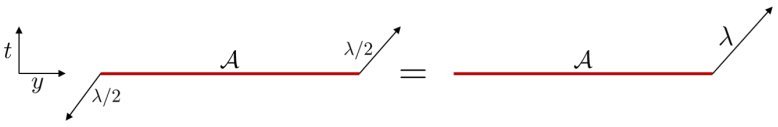

Figure 7.3: Varying one end by λ in an outgoing null direction is equivalent to vary both ends by $\lambda/2$ in the outgoing null direction and opposite time direction. The same holds for the inwards direction. Since the CFT is time-reversal symmetric, the reasoning holds for both future and past directed variations.

computed as equation (6.1). In this case the induced metric $\tilde{\gamma}_{\mu\nu}$ on the bulk extremal surface $\mathcal{E}_{\mathcal{A}_\parallel}$ is computed from equation (6.24) and it gives the result

$$ds^2\big|_{\mathcal{E}_{\mathcal{A}_\parallel}} = \frac{1}{z^2}\left(-f(z)\dot{t}^2 + \frac{\dot{z}^2}{f(z)} + 1\right)dy^2 + \frac{1}{z^2}d\mathbf{x}_{d-2}^2 \tag{7.28}$$

where the dots mean total derivatives with respect to y.

Then, the area functional of $\mathcal{E}_{\mathcal{A}_\parallel}$ is given by

$$\begin{aligned}\text{Area}(\mathcal{E}_{\mathcal{A}_\parallel}) &= \int_{-\infty}^{+\infty} dx^{d-2}\int_{-\frac{l+\lambda}{2}+\omega}^{\frac{l+\lambda}{2}-\omega} dy\frac{1}{z^3}\sqrt{1+\frac{\dot{z}^2}{f(z)} - \dot{t}^2 f(z)} \\ &= D^{d-2}\int_0^{\frac{l+\lambda}{2}-\omega} dy\frac{2}{z^3}\sqrt{1+\frac{\dot{z}^2}{f(z)} - \dot{t}^2 f(z)} \\ &\equiv D^{d-2}\int_0^{\frac{l+\lambda}{2}-\omega} dy\mathcal{L}(z,\dot{z},\dot{t};y)\end{aligned} \tag{7.29}$$

where D^{d-2} is an infrared regulator of the translationally invariant directions $\mathbf{x}_{d-2}$ of the strip, y is the direction in which the deformation is performed, l is the width of the strip and ω is a cut-off in the y coordinate, such that is relates to the holographic coordinate cut-off as $z(l/2-\omega) = z_{\text{cut}} \ll 1$. In the second line we use the fact that the integral is symmetric in the y coordinate and we rewrote the expression in terms of an effective lagrangian in the last line.

Since we want to revisit the computations in [4], from now on we are going to restrain ourselves to $d = 4$. To make sure we are computing the area of the minimal surface we should first solve the equations of movement for this effective lagrangian. This is not a trivial problem. First, realize that the lagrangian is explicitly independent on y. Hence, we have an associated Noether charge

$$\mathcal{Q}_1 = L - \dot{z}\frac{\partial\mathcal{L}}{\partial z} - \dot{t}\frac{\partial\mathcal{L}}{\partial t} = \frac{2}{z^3\sqrt{1+\dot{z}^2 f(z)^{-1} - \dot{t}^2 f(z)}} \equiv \frac{2}{z_*^3 N_*} \tag{7.30}$$

where $N_* = \sqrt{1-\dot{t}^2\, f(z)|_{z=z_*}}$ and z_* is the z coordinate at the tip of the surface $\mathcal{E}_{\mathcal{A}_\parallel}$, i.e. $z_* = z(y\to 0)$ and $\dot{z}(z_*) = 0$. From the fact that $\mathcal{L}$ does not depend on t, we have a second conserved charge:

$$\partial_y\frac{\partial\mathcal{L}}{\partial\dot{t}} = 0 \implies \mathcal{Q}_2 = \frac{\partial\mathcal{L}}{\partial\dot{t}} = \frac{-2\dot{t}f(z)}{z^3\sqrt{1+\dot{z}^2 f(z)^{-1} - \dot{t}^2 f(z)}} = -\dot{t}f(z)\mathcal{Q}_1 \equiv \Lambda\mathcal{Q}_1\ . \tag{7.31}$$

Therefore, from the last equality, we can define a new constant of motion $\Lambda = \dot{t}f(z)$. Then using equation (7.31) in equation (7.30) and solving for $\dot{z}$ we get the expression

$$\dot{z} = -\sqrt{\left(\frac{N_*^2 z_*^6}{z^6} - 1\right) f(z) + \Lambda^2} \ . \tag{7.32}$$

Using equation 7.32 we can write the expression

$$\frac{l+\lambda}{2} = \int_0^{\frac{l+\lambda}{2}} dy = \int_{z_*}^0 \left(\frac{dz}{dy}\right)^{-1} dz = -\int_{z_*}^0 \frac{dz}{\sqrt{\left(\frac{N_*^2 z_*^6}{z^6} - 1\right) f(z) + \Lambda^2}} \ . \tag{7.33}$$

Then introducing the dimensionless coordinate $x = z/z_*$ we get

$$\frac{l+\lambda}{2} = z_* \int_0^1 \frac{x^3 dx}{R(x)} \tag{7.34}$$

where $R(x) = \sqrt{(N_*^2 - x^6)\left(1 - \pi T z_* x^4\right) + \Lambda^2 x^6}$

Then we can do something similar with the expression for Λ. In this case, since $\Lambda = \dot{t}f(z) = \frac{dt}{dz}\dot{z}f(z)$, we can write

$$\frac{\lambda}{2} = \int_{z_*}^0 \frac{\Lambda dz}{\dot{z} f(x z_*)} = \Lambda z_* \int_0^1 \frac{x^3 dx}{R(x) f(x z_*)} \ . \tag{7.35}$$

By combining both equations (7.34) and (7.35) it is easy to see that we get an expression that determines Λ as

$$\Lambda = \frac{\lambda}{l + \lambda + 2 z_* I_\Delta} \tag{7.36}$$

with

$$I_\Delta \equiv \int_0^1 dx \frac{x^3}{R(x)} \left(\frac{1}{f(x z_*)} - 1\right) \ . \tag{7.37}$$

Notice that equations (7.36) and (7.37) are only valid in the small l regime. If l is small, then $f(x z_*) \to 1$ and therefore the integral is finite, while for large l $f(x z_*) \to 0$ and, therefore, the integral diverges. We will look at this case later.

Now, by writing the area integral (7.29) as an integral in z and by combining equations (7.34) and (7.35) we see that

$$\tilde{A} \equiv \int_{z_*}^{z_{\text{cut}}} dz \frac{\mathcal{L}}{\dot{z}} = z_* \int_0^1 \frac{x^3 \mathcal{L}(x)}{R(x)} dx = \frac{2}{z_*^2} \int_0^1 \frac{N_*}{x^3 R(x)} dx \tag{7.38}$$

where one should take into account in the second equality that $z_{\text{cut}} \to 0$. Although, we have written the expression for the area functional in a nice way, this integral is still divergent. The good news are that we can write down the area as the sum of a divergent term plus a finite expansion on z_{cut}. Begin by adding and subtracting 1 to the integrand:

$$\tilde{A} = \frac{2}{z_*^2} \int_0^1 dx \left(\frac{N_*}{x^3 R(x)} - \frac{1}{x^3} + \frac{1}{x^3}\right) \ . \tag{7.39}$$

Then, since the integral for x^{-3} term is

$$\frac{2}{z_*^2}\int_0^1 \frac{dx}{x^3} = \frac{1}{z_{\text{cut}}^2} - \frac{1}{z_*^2} + \mathcal{O}(z_{\text{cut}}^2) \tag{7.40}$$

we finally obtain that the area functional for the minimal surface $\mathcal{E}_{\mathcal{A}_\parallel}$ is

$$\tilde{A} = \frac{1}{z_{\text{cut}}^2} + \frac{2}{z_*^2}\left(I^\lambda_{\mathcal{E}_{\mathcal{A}_\parallel}} - \frac{1}{2}\right) + \mathcal{O}(z_{\text{cut}}^2)\ . \tag{7.41}$$

Where we wrote the area functional in terms of $I^\lambda_{\mathcal{E}_{\mathcal{A}_\parallel}}$, which is an integral of finite contribution:

$$I^\lambda_{\mathcal{E}_{\mathcal{A}_\parallel}} = \int_0^1 dx \frac{1}{x^3}\left(\frac{N_*}{R(x)} - 1\right)\ . \tag{7.42}$$

Since the solution for equation (7.41) is not trivial, in order to obtain an analytical result, Eckel et al. considered the limits of small and large widths expansions ,$Tl \ll 1$ and $Tl \gg 1$ respectively.

Small width approximation

In the case of the small width approximation ($0 < \lambda/l \ll Tl \ll 1$) we can determine z_* and Λ by expanding equations (7.34) and (7.35) in powers of of λ/l respectively. We only need to expand up to, and including, $\mathcal{O}(\lambda^2/l^2)$ since this is going to be the leading term for the QNEC, due to the contribution of $\frac{d^2S}{d\lambda^2}$. The expression for the expansion of Λ and z_* can be found in the appendix of [4]. I am not showing them here for shortness and because they do not give us a better physical intuition of the problem.

Finally, by plugging the results for Λ and z_* in equation (7.41) and expanding up to order λ^2/l^2 we obtain the expression

$$\begin{aligned}\tilde{A} = &\frac{1}{z_{\text{cut}}^2} - \frac{1}{2c_0^3 l^3} + (\pi T)^4 l^2 \frac{\pi c_0^3}{5\sqrt{3}} + (\pi T)^8 l^6\left(\frac{c_0^6}{12} - \frac{2c_0^9\pi^2}{225}\right)\\ &+ \frac{\lambda}{l}\left(\frac{1}{c_0^3 l^2} + (\pi T)^4 l^2 \frac{2\pi c_0^3}{5\sqrt{3}} + (\pi T)^8 l^6\left(\frac{c_0^6}{2} - \frac{4c_0^9\pi^2}{75}\right)\right)\\ &+ \frac{\lambda^2}{l^2}\left(-\frac{2}{c_0^3 l^2} + (\pi T)^4 l^2 \frac{2\pi c_0^3}{15\sqrt{3}} + (\pi T)^8 l^6\left(\frac{4c_0^6}{3} - \frac{88c_0^9\pi^2}{675}\right)\right)\\ &+ \mathcal{O}(z_{\text{cut}}^2) + \mathcal{O}(T^{12}l^{10}) + \mathcal{O}(\lambda^3/l^3)\end{aligned} \tag{7.43}$$

where the result has been expressed in terms of c_0, and this is

$$c_0 = \frac{3\Gamma\left[1/3\right]^3}{2^{1/3}(2\pi)^2} \approx 1.159595 \tag{7.44}$$

Therefore, we can compute the right hand side of the QNEC (equation (2.17)) by taking the second of the area with respect to λ evaluated at $\lambda = 0$. This yields the result for the second derivative of the entropy per transverse area

$$\frac{1}{2\pi}\frac{d^2\tilde{S}_\parallel}{d\lambda^2} = \frac{1}{4\pi^2}\frac{d^2\tilde{A}}{d\lambda^2} = -\frac{1}{\pi^2 c_0^3 l^4} + \frac{(\pi T)^4 c_0^3}{15\sqrt{3}\pi} - (\pi T)^8 l^4\left(\frac{44c_0^9}{675} - \frac{2c_0^6}{3\pi^2}\right) + \mathcal{O}(T^{12}l^8)\ . \tag{7.45}$$

It is worth noting that the vacuum entanglement entropy for a strip is known analytically [27]

$$\tilde{A} = \left(\frac{1}{z_{\text{cut}}^2} - \frac{1}{2c_0^3 \tilde{L}^2} \right) \tag{7.46}$$

where $\tilde{L} = \sqrt{(l \pm \lambda)^2 + \lambda^2}$ is the length of the strip. Hence, the vacuum contribution to the QNEC can be computed analytically as

$$\frac{1}{2\pi} \frac{d^2 \tilde{S}_{\|}}{d\lambda^2} = -\frac{1}{\pi^2 c_0^3 l^4} \simeq -\frac{0.06498}{l^{-4}} \ . \tag{7.47}$$

Notice that, for small widths of the entangling region, the thermal QNEC reduces to the vacuum case. This was expected since for small l the turning point z_* of the minimal surface $\mathcal{E}_{\mathcal{A}_{\|}}$ is far away from the black brane horizon ($z_* \ll z_h$) and, therefore, $\mathcal{E}_{\mathcal{A}_{\|}}$ does not "feel" the presence of the horizon. This is clearly shown in figure 7.4(a).

Large width approximation

In the case of the large width approximation ($Tl \gg 1$) the turning point z_* approaches the horizon z_h and, therefore, we can write

$$z_* = \frac{1-\epsilon}{\pi T} \qquad 0 < \epsilon \ll 1 \ . \tag{7.48}$$

Hence, we can again do perturbative analysis with respect to the parameter ϵ. However, as I mentioned before, the integral (7.42) diverges at the upper integration boundary $x = 1$.

The strategy to follow in this case is the same as for the small width approximation. By introducing the integrals

$$I_1 \left[h(x)\right] = \int_0^1 \frac{h(x) dx}{\sqrt{1-x}\,(1-x+\epsilon x)^{3/2}} = \frac{2h(1)}{\epsilon} + \mathcal{O}(\ln \epsilon) \tag{7.49a}$$

$$\begin{aligned} I_2 \left[h(x)\right] &= \int_0^1 \frac{h(x) dx}{\sqrt{(1-x)\,(1-x+\epsilon x)}} \\ &= -h(1) \ln \frac{\epsilon}{4} + \int_0^1 dx \frac{h(x) - h(1)}{1-x} - \big(h(1) + h'(1)\big) \frac{\epsilon}{2} \ln \frac{\epsilon}{4} + \mathcal{O}(\epsilon) \end{aligned} \tag{7.49b}$$

where $h(x)$ is a function that can be Taylor-expanded around $x = 1$, we can rewrite equations (7.34) and (7.35) respectively as

$$\frac{\lambda}{2} = \Lambda z_* I_1 \left[h_\Lambda(x)\right] \tag{7.50}$$

and

$$\frac{l+\lambda}{2z_*} \simeq I_2 \left[h_z(x)\right] + \lambda^2 (\pi T)^2 \epsilon I_1 \left[h_\lambda(x)\right] \tag{7.51}$$

where $h_\Lambda(1) = 1/(8\sqrt{6}) + \mathcal{O}(\epsilon)$ and $h_z(1) = 2h_\lambda(1) = 1/(2\sqrt{6}) + \mathcal{O}(\epsilon)$. With all of this, equation (7.50) yields

$$\Lambda \simeq 2\sqrt{6} \epsilon \lambda (\pi T) + \mathcal{O}(\lambda \epsilon^2 \ln \epsilon) \ . \tag{7.52}$$

On the other hand, by expanding the result of equation (7.51) we obtain

$$\frac{l+\lambda}{2z_*} \simeq -h_z(1)\ln\frac{\epsilon}{4} + h_z^0 + 2\lambda^2 h_\lambda(1) + \mathcal{O}(\epsilon\ln\epsilon) \tag{7.53}$$

with $h_z^0 \equiv \int_0^1 dx\,[h_z(x) - h_z(1)]/(1-x) \approx -0.25032$. From this result, we can determine ϵ as a function of l and λ, which is going to be useful later, as

$$\epsilon \simeq \epsilon_0 \exp\left[-\sqrt{6}(l+\lambda)\pi T + \lambda^2(\pi T)^2\right] + ... \tag{7.54}$$

where "..." stand for terms that decay exponentially faster than the one written down and the numerical value for the constant is $\epsilon_0 = 4\exp\left[h_z^0/h_z(1)\right] \approx 1.173487$.

Finally, we can write the integral (7.41) as

$$\begin{aligned} I^\lambda_{\hat{\mathcal{E}}_{\mathcal{A}_\parallel}} &\simeq I_2\left[h_z(x) + \epsilon k_z(x)\right]\lambda^2(\pi T)^2\epsilon I_1\left[h_\lambda(x) + \epsilon k_\lambda(x)\right] \\ &\simeq \frac{l+\lambda}{2z_*} + \epsilon(I_2\left[k_z(x)\right] + \lambda^2(\pi T)^2\epsilon I_1\left[k_\lambda(x)\right]) \end{aligned} \tag{7.55}$$

where $k_z(1) = -1/2$ and $k_\lambda(1) = -\sqrt{6}/4$. The reason to divide the integrals in h and k terms is due to the fact that, for the large width case, the holographic entanglement entropy grows linearly with l.

Finally, the area of the extremal surface $\mathcal{E}_{\mathcal{A}_\parallel}$ is expressed as

$$\tilde{A} \simeq \frac{1}{z_{\text{cut}}^2} + \frac{l+\lambda}{z_*^3} + \frac{1}{z_*^2}(b_0 + b_1\epsilon + b_{\log}\epsilon\ln\epsilon) + \lambda^2(\pi T)^4 b_2\epsilon + \mathcal{O}(z_{\text{cut}}^2) + \mathcal{O}(\epsilon^2\ln\epsilon) \tag{7.56}$$

where $b_0 \approx -0.66589$, $b_1 \approx -0.08889$, $b_2 = -\sqrt{6}$ and $b_{\log} = \sqrt{6}/2$. By introducing the result (7.54) and taking the second derivative of the area with respect to λ evaluated at $\lambda = 0$, we find the result for the right hand side of QNEC as expressed in equation (2.17) to be

$$\frac{1}{2\pi}\frac{d^2\tilde{S}_\parallel}{d\lambda^2} = \frac{1}{4\pi^2}\frac{d^2\tilde{A}}{d\lambda^2} = -\frac{5\sqrt{6}\epsilon_0}{4\pi^2}(\pi T)^4 e^{-\sqrt{6}(\pi T)l} + ... \tag{7.57}$$

where the "..." stand for terms of the order $l\exp\left(-2\sqrt{6}\pi T l\right)$, and they are neglected since they decay faster at large l.

In figure 7.4(b) we can see that the QNEC for the thermal state behaves like in the vacuum state for small l while for larger l it approaches to zero exponentially. Since the Computations always yield results that are negative, the QNEC is trivially satisfied.

7.2.2 QNEC in a strip-like entangling region (II)

In the above section I reviewed the computations made by Ecker et al. in [4] for the thermal plasma in strip-like entangling region. However, their computations do not take into account all possible ways in which we can vary the entangling region in order to compute the QNEC. The null variations that they parametrized are sketched in figure 7.5(a), while in figure 7.5(b) I sketched the other possible variations that we could study. Therefore, in this section I generalize their computations to the missing cases.

Following the reasoning explained above, the new null deformations can be parametrized as a function of the affine parameter λ as $(t_\pm, y_\pm) = (\lambda, \pm(l/2+\lambda))$. In figure 7.5(b) one

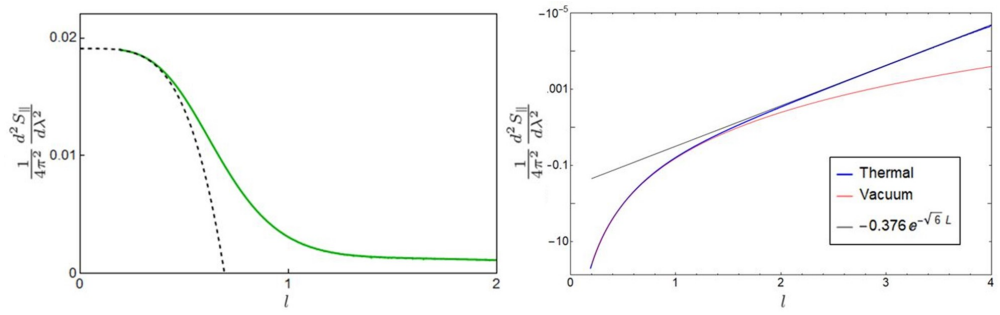

Figure 7.4: **(a)** In green, numerical computation of the right hand side of the QNEC (equation (2.17)) for the thermal state after subtraction of the vacuum contribution ("Thermal−Vacuum"). For small l we can see that it fits the small width expansion (7.45). **(b)** Right hand side of the QNEC for the thermal state only (in blue). For small widths, it follows the vacuum behavior (in red) while for large widths approaches zero exponentially (in gray). We can clearly see that the QNEC is trivially satisfied [4].

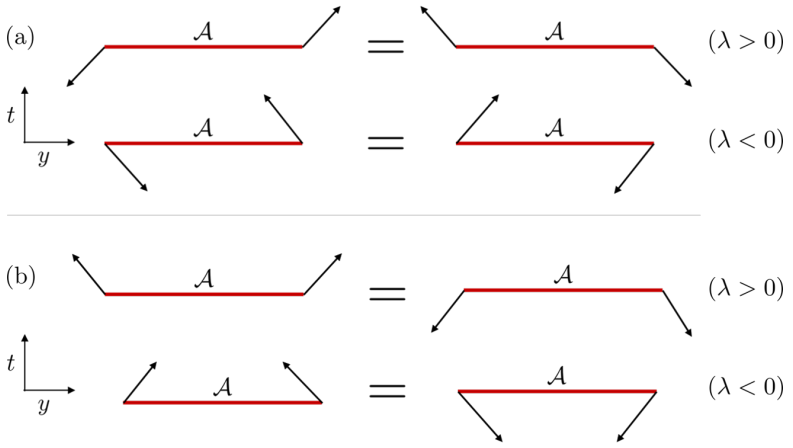

Figure 7.5: **(a)** Representation of all variations taken into account in the work of Eckel et al. in [4]. The dependence on the sign of λ as parametrized in the above section is also indicated and the equal sings stand for the fact that the CFT is symmetric under time-reversal transformations. **(b)** Sketches of the missing variations. These are the ones I am going to address in this section. Again, the equal sign stand for the time-reversal invariance of the field theory and the dependence on the sing of λ, as parametrized in this section, is shown.

can see how deformations depend on the sign of λ. Notice that in this case we cannot write the deformation in both boundaries of the entangling region as the variation of only one of the boundaries as we shown in figure 7.3. Therefore, we must vary each boundary in the null direction by λ and not by $\lambda/2$ as before.

Small width approximation

With this setup, one can easily see that, since the strip moves forward or backwards in time as a whole, equation (7.35) reduces to

$$0 = \int_{z_*}^{0} \frac{\Lambda dz}{\dot{z} f(xz_*)} = \Lambda z_* \int_0^1 \frac{x^3 dx}{R(x) f(xz_*)} \ , \tag{7.58}$$

from where we can infer that $\Lambda = 0$. Another way of justifying this result is by realizing that, since the entangling region $\mathcal{A}_\parallel$ will move uniformly forward or backwards in time,

the extremal surface will lay on a Cauchy slice of constant t ($\dot{t} = 0$). Therefore, from the definition (7.31) one can see that this corresponds to $\Lambda = 0$. This means that the deformation of the entangling surface is effectively only in the spatial direction y.

Defining $L = l + 2\lambda$, equation (7.34) will become

$$\frac{l}{2} + \lambda = \frac{L}{2} = z_* \int_0^1 \frac{x^3 dx}{R(x)} \tag{7.59}$$

and therefore, the equations are all explicitly λ independent. Following the computations done in the above section, one can show that the final result for the area will be nothing more than the result computed previously setting $\lambda \to 0$ and $l \to L$ in equation (7.45). Then, to take the derivative over λ that enters the QNEC one only needs to do the replacement $L \to l + 2\lambda$ and derive. Hence, after the taking the derivative at $\lambda = 0$, the right hand side of the QNEC results in

$$\frac{1}{2\pi}\frac{d^2\tilde{S}_{\parallel}}{d\lambda^2} = \frac{1}{4\pi^2}\frac{d^2\tilde{A}}{d\lambda^2} = -\frac{3}{\pi^2 c_0^3 l^4} + \frac{2c_0^3}{5\sqrt{3}\pi} + \left(\frac{5c_0^6}{2\pi^2} - \frac{4c_0^9}{15}\right) l^4 + \mathcal{O}\left(T^{12} l^8\right) \tag{7.60}$$

where c_0 is defined in (7.44). Numerically, the expression reads

$$\frac{1}{2\pi}\frac{d^2\tilde{S}_{\parallel}}{d\lambda^2} \simeq -\frac{0.194941}{l^4} + 0.114622 - 0.395087 l^4 \ . \tag{7.61}$$

Like before, the l^{-4} term corresponds to the vacuum contribution to the QNEC. In figure 7.6(a) I plot the thermal-vacuum contribution to the QNEC and see that it behaves as predicted by the expansion (7.61).

Large width approximation

The same reasoning as for the small width approximation works here. In this case, the integral (7.50) reduces to

$$0 = \Lambda z_* I_1 \left[h_\Lambda(x)\right] \tag{7.62}$$

and, after performing the substitution $L \to l + 2\lambda$ and the deformation of the entangling region is characterized by λ and not by $\lambda/2$ as in the previous case, the integral (7.51) becomes

$$\frac{L}{2z_*} = I_2 \left[h_z(x)\right] \ , \tag{7.63}$$

As it was expected, equation (7.62) implies that $\Lambda = 0$.

As before, the problem reduces to a λ independent situation and, therefore, equation (7.56) becomes

$$\tilde{A} = \frac{1}{z_{\text{cut}}^2} + \frac{L}{z_*^3} + \frac{1}{z_*^2}(b_0 + b_1\epsilon + b_{\log}\epsilon \ln \epsilon) + \mathcal{O}(\epsilon^2 \ln \epsilon) \tag{7.64}$$

where, in this case, ϵ also does not depend on λ and reduces to the expression

$$\epsilon = \epsilon_0 \exp\left[-\sqrt{6} L \pi T\right] + \dots \ . \tag{7.65}$$

Then, by plugging equations (7.65) and (7.48) in expression (7.64) and taking the derivative over λ at $\lambda = 0$ we find the right hand side of the QNEC (2.17) to be

$$\frac{1}{2\pi}\frac{d^2\tilde{S}_{\parallel}}{d\lambda^2} = \frac{1}{4\pi^2}\frac{d^2\tilde{A}}{d\lambda^2} = \frac{6}{\pi^2}(\pi T)^4\epsilon_0 e^{-\sqrt{6}\pi T l}(2b_0 + b_1 + b_{\log}\ln\epsilon_0) \ . \tag{7.66}$$

By plugging the numerical values of all the parameters, we find that the expressions yields

$$\frac{1}{2\pi}\frac{d^2\tilde{S}_{\parallel}}{d\lambda^2} \simeq -0.87372 e^{-\sqrt{6}l^4} \ . \tag{7.67}$$

In figure 7.6(b) we can clearly see how the QNEC for the thermal state transitions from a "vacuum behavior" to an exponentially approach to zero. Like in the previous case, since the second derivative of the entanglement entropy of the thermal state is negative for all l, it satisfies the QNEC in a trivial way.

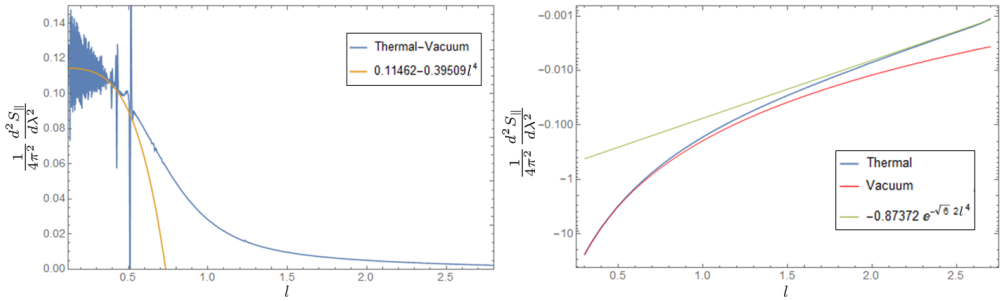

Figure 7.6: **(a)** In blue, numerical computation of the right hand side of the QNEC (equation (2.17)) for the thermal state after subtraction of the vacuum contribution ("Thermal−Vacuum"). For small l, the numerical computations are very noisy but we can see that it fits the small width expansion (7.61). **(b)** Right hand side of the QNEC for the thermal state only (in blue). For small widths, it follows the vacuum behavior (in red) while for large widths approaches zero exponentially (in green). We can clearly see that the QNEC is trivially satisfied.

7.2.3 QNEC in a spherically symmetric entangling region

It is of particular interest to study the behavior of the QNEC in spherical entangling regions since the entanglement entropy for these has special properties. It is conjectured in [48] that, among all continuously connected shapes with the same entangling surface area (Area($\partial\mathcal{A}$)), spheres minimize the entanglement entropy. This led to use the entropy of a sphere as a c-function [49]. Spheres also play an important role since they should be the obvious choice to study any physical state that preserve spherical symmetry.

Since the boundary state that we are interested in is the the as in the precious section, a thermal state, the bulk metric will be again given by (7.20). In this case, however, the entangling region is given by

$$\mathcal{A}_\bullet = \left\{\mathbf{x} \in \mathbb{R}^{d-1} \mid |\mathbf{x}| \leq R\right\} = \left\{(\theta,\phi) \in S^{d-2}, \xi \in \mathbb{R} \mid 0 < \xi \leq R\right\} \tag{7.68}$$

where in the second equality I have rewritten x_i in spherical coordinates, which will be more convenient for the following computations since the symmetry is shown explicitly.

Since, as we did in the previous section, we are interested in computing the QNEC integrated along all the entangling surface, we will need to vary each point at the boundary of the entangling region in the null direction. Hence, since $\partial\mathcal{A}_\bullet$ is continuously

connected, the whole region will expand (or contract) uniformly and move forward (or backward) as a whole. If one point of the entangling surface was varied radially outwards and another inwards, that would mean that some points in between those two should move in a non-null direction (and at least one would not even move in the spatial direction). The same applies for the time direction and, therefore, we can conclude that the only variations possible are those that expand or contract the sphere uniformly and that leave $\mathcal{A}_\bullet$ laying at a constant t surface. With that in mind we use equation (6.24) to determine the induced metric on $\mathcal{E}_{\mathcal{A}_\bullet}$, taking into account that ζ^α are the variables that parametrize the sphere and that, by symmetry, the holographic coordinate can only depend on the radial variable ξ. The result is then

$$ds^2|_{\mathcal{E}_{\mathcal{A}_\bullet}} = \frac{1}{z^2}\left(1+\frac{z'^2}{f(z)}\right)d\xi^2 + \frac{\xi^2}{z^2}d\Omega_{d-2}^2 \tag{7.69}$$

where the prime stands for the derivative with respect to ξ and $d\Omega_{d-2}$ contains the angular part of the metric.

Redoing the computations in the same way as we did them in the previous section, the area functional for a spherically symmetric entangling region is given by

$$\begin{aligned}\text{Area}(\mathcal{E}_{\mathcal{A}_\bullet}) &= \int d\Omega_{d-2}\int_0^{R-\delta} d\xi \frac{\xi^2}{z^3}\sqrt{1+\frac{z'^2}{f(z)}} \\ &= \Omega_{d-2}\int_0^{R-\delta} d\xi \mathcal{L}(z,z',\xi)\end{aligned} \tag{7.70}$$

where $\Omega_{d-2} = \frac{2\pi^{(d-1)/2}}{\Gamma\left(\frac{d-1}{2}\right)}$ is the area of the unit S^{d-2}, R is the radius of the entangling region $\mathcal{A}_\bullet$ and δ is the cut-off in the ξ coordinate such that it relates to the holographic coordinate cut-off as $z(R-\delta) \equiv z_{\text{cut}} \ll 1$.

Recall from section 7.1.1 that, for the case of theories that are related by a conformal transformation the QNEC inequality becomes (7.19). Naively, first of all, one would be interested in finding the expressions for $\mathcal{A}_{kk}^{(T)}$ and $\mathcal{A}^{(S)}$, but in [45] showed that, if we are interested in the integrated version of (7.19), the expression simplifies significantly. First, notice that for spheres in a flat background $\mathcal{A}_{kk}^{(T)} = 0$ and $\Upsilon = \ln(R)$, then, by considering only that the variation is uniformly and directed inward (see the bottom of figure 7.5(b)), the expansion is given by $\theta = -(d-2)/R$ and, therefore, integrating equation (7.19), we obtain

$$2\pi R^{d-2}\int d\Omega\, T_{kk}(\Omega) \geq \frac{d^2}{d\lambda^2}\left(S_{\text{fin}} - \mathcal{A}^{(S)}\right) - \frac{2}{R}\frac{d}{d\lambda}\left(S_{\text{fin}} - \mathcal{A}^{(S)}\right)\ . \tag{7.71}$$

They choose the setup with the inwards variation because it is known that, in this case, the QNEC should be saturated in the vacuum since the extremal surface corresponds to the boundary of the causal wedge and transporting the entangling surface inward in a null direction just transports the extremal surface along the wedge. Therefore for vacuum (where T_{kk}) we have the saturation of the inequality:

$$0 = \frac{d^2}{d\lambda^2}\left(S_{\text{fin,vac}} - \mathcal{A}^{(S)}\right) - \frac{2}{R}\frac{d}{d\lambda}\left(S_{\text{fin,vac}} - \mathcal{A}^{(S)}\right)\ . \tag{7.72}$$

Then, by subtracting this equation to expression (7.71) we obtain the new inequality independent of $\mathcal{A}^{(S)}$:

$$2\pi R^{d-2}\int d\Omega\; T_{kk}(\Omega) \geq \frac{d^2}{d\lambda^2}\left(S - S_{\text{vac}}\right) - \frac{2}{R}\frac{d}{d\lambda}\left(S - S_{\text{vac}}\right) \ . \tag{7.73}$$

Notice that in this expression we do not need to specify the finite part of the entropy S_{fin} or $S_{\text{fin,vac}}$ since the vacuum subtraction cancels the divergent term of the entropies.

In [45] they just discuss the case where the variation is uniformly inwards directed but we could say something more for the outward directed case. If we consider an expanding sphere, then equation (7.71) becomes

$$2\pi R^{d-2}\int d\Omega\; T_{kk}(\Omega) \geq \frac{d^2}{d\lambda^2}\left(S_{\text{fin}} - \mathcal{A}^{(S)}\right) + \frac{2}{R}\frac{d}{d\lambda}\left(S_{\text{fin}} - \mathcal{A}^{(S)}\right) \ . \tag{7.74}$$

In this case the reasoning explained above is not valid anymore since it is no longer true that expanding the spherical entangling region corresponds to transporting the extremal surface along the causal wedge. However, we do know from [27] that the analytic solution for the entanglement surface $\mathcal{E}_{\mathcal{A}_\bullet}$ is a semisphere parametrized by

$$\mathcal{E}_{\mathcal{A}_\bullet} = \left\{(\theta,\phi)\in S^{d-2}, \xi\in\mathbb{R}, z\in\mathbb{R}^+ \mid z^2+\xi^2 = R^2\right\} \ . \tag{7.75}$$

Since we are interested on varying $\partial\mathcal{A}_\bullet$ in a null direction and see how $\mathcal{E}_{\mathcal{A}_\bullet}$ varies, we can split this variation in a timelike plus a spacelike variation. Then, since $\mathcal{E}_{\mathcal{A}_\bullet}$ lies in a Cauchy slice defined by constant t, where t is precisely the boundary time, $\mathcal{E}_{\mathcal{A}_\bullet}$ will move forward (or backwards) in time together with $\mathcal{A}_\bullet$. More in particular, if the null variation of $\partial\mathcal{A}_\bullet$ is parametrized by λ (see figure 7.5(b)) then the surface $\mathcal{E}_{\mathcal{A}_\bullet}$ together with $\mathcal{A}_\bullet$ will move $\frac{\lambda}{\sqrt{2}}$ forward in time. On the other hand, if we focus on the spatial variation, the entangling surface $\partial\mathcal{A}_\bullet$ will vary $\frac{\lambda}{\sqrt{2}}$ radially inwards (outwards) and, since the minimal surface is a semisphere, that means that the spatial variation of a point lying on $\mathcal{E}_{\mathcal{A}_\bullet}$ will be parametrized by $s^i = (\mp\frac{\lambda}{\sqrt{2}}\sin(\varphi), \mp\frac{\lambda}{\sqrt{2}}\cos(\varphi), 0, 0)$, where the vector is parametrized as $s^i = (z,\xi,\theta,\phi)$, the $-$ $(+)$ sign is for variations directed radially inwards (outwards) and φ is the angle showed in figure 7.7. A schematic representation of this spatial variations is shown in figure 7.7. Therefore, putting together the temporal and the spatial part of the variation, we find that the variation of the bulk minimal surface after varying the entangling surface in a null direction is characterized by

$$s^\mu = \frac{\lambda}{\sqrt{2}}\left(1, \mp\sin(\varphi), \mp\cos(\varphi), 0, 0\right) \tag{7.76}$$

and, since $g_{\mu\nu}s^\mu s^\nu = 0$, the QNEC is saturated both for ingoing and outgoing null variations of the spherical entangling region. Thus, we can write

$$0 = \frac{d^2}{d\lambda^2}\left(S_{\text{fin,vac}} - \mathcal{A}^{(S)}\right) \mp \frac{2}{R}\frac{d}{d\lambda}\left(S_{\text{fin,vac}} - \mathcal{A}^{(S)}\right) \ . \tag{7.77}$$

Therefore, the inequality that we want to study is finally

$$2\pi R^{d-2}\int d\Omega\; T_{kk}(\Omega) \geq \frac{d^2}{d\lambda^2}\left(S - S_{\text{vac}}\right) \mp \frac{2}{R}\frac{d}{d\lambda}\left(S - S_{\text{vac}}\right) \ . \tag{7.78}$$

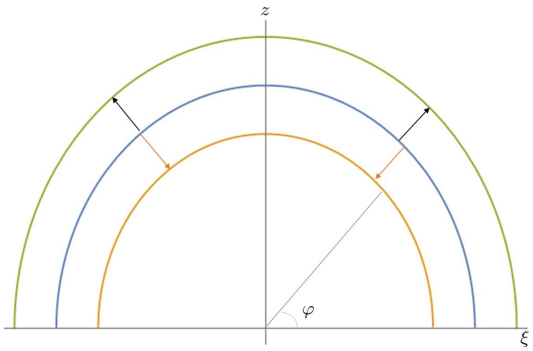

Figure 7.7: Schematic representation of the spatial variation of $\mathcal{E}_{\mathcal{A}_\bullet}$ when we vary $\mathcal{A}_\bullet$ in a null direction. When varying radially inwards, the minimal surface (blue) shrinks uniformly into a new semisphere (yellow). When varying radially outwards, the the minimal surface expands spatially into the new semisphere (green). This, combined with the movement in the timelike direction implies that the minimal surface $\mathcal{E}_{\mathcal{A}_\bullet}$ varies everywhere in a null direction no matter if we take the boundary variation to be ingoing or outgoing of $\mathcal{A}_\bullet$.

Notice that, since $\langle T_{kk}\rangle$ does not depend on any angle, after plugging equation (7.27) in (7.78) and setting $d = 4$ the inequality reduces to

$$\frac{2\pi R^2}{N}\langle T_{kk}\rangle = \frac{R^2}{2\pi^2} \geq \frac{1}{\Omega_2}\left(\frac{d^2}{d\lambda^2}(S - S_{\text{vac}}) \mp \frac{2}{R}\frac{d}{d\lambda}(S - S_{\text{vac}})\right) . \tag{7.79}$$

In figure 7.8 we show that the QNEC inequality for a thermal state is indeed satisfied in both situations, although for the case of the variation directed radially outwards of the $\mathcal{A}_\bullet$ surface it is nearly saturated. This, apart from being an interesting result itself, gives us interesting reasons to study the QNEC in Gauss-Bonnet holography since we expect to find that the QNEC is violated for certain values of the Gauss-Bonnet coupling or, on the contrary, the T_{kk} and the derivative of the entropy behave in such a way that the saturations remains or relaxes. In any case the results will be interesting to analyze.

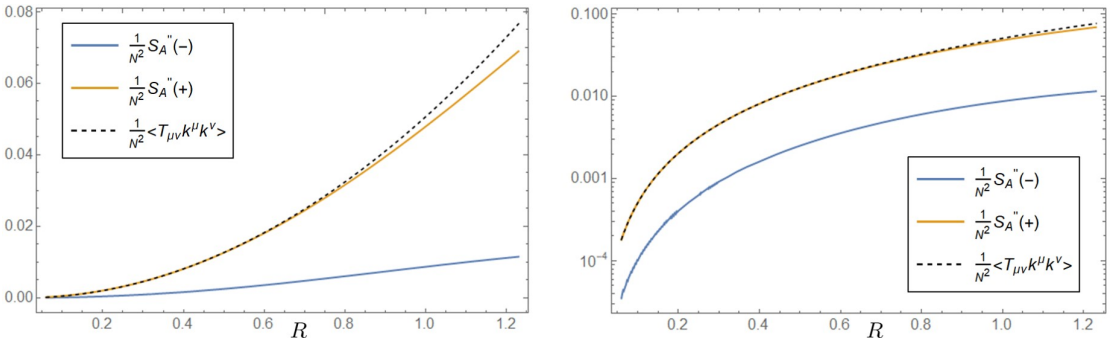

Figure 7.8: In yellow the right hand side of the inequality (7.79) for the expanding sphere while in blue is shown the same expression for a variation directed radially inwards. In both cases the QNEC is satisfied, although for the case of an expanding sphere is nearly saturated.

8. The QNEC in the holographic dual of Gauss-Bonnet gravity

In this chapter we are going to extend the study of the QNEC to a field theory dual to Gauss-Bonnet gravity, motivated by the previous results. The goal is then to explicitly compute the QNEC inequality for strip-like and spherical entangling regions as a function of the Gauss-Bonnet coupling constant. Since in [50] the authors gave a general proof of the QNEC using only QFT techniques and not referring to the AdS/CFT correspondence, one can think that the inequality holds equally true in field theories dual to Gauss-Bonnet gravity. However, this is not completely clear since it is not known what the dual field theory in this setup is and, therefore, it is not clear if [50] applies in this case. In what follows, we will assume that the same inequality holds true for Gauss-Bonnet holography. However, the results presented in this chapter will tell us that we might be wrong by making this assumption. We will discuss this in the conclusions of the thesis

First of all, recall that the bulk metric dual to a vacuum state in the boundary theory can be written like in equation (5.16), which we rewrite here for convenience

$$ds^2 = \frac{L_{\text{eff}}^2}{z^2}\left(-dt^2 + d\tilde{x}_i d\tilde{x}^i + dz^2\right) \ . \tag{8.1}$$

From here, one can see that the boundary theory lives in a Minkowski spacetime with metric

$$ds^2 = -dt^2 + d\tilde{x}_i d\tilde{x}^i \ . \tag{8.2}$$

Notice that, since the boundary theory now depend on the coordinates $\tilde{x}^i$ instead of x^i, the null variation at the boundary will be given by $k_{\pm}^{\mu} = \delta_t^{\mu} \pm \delta_X^{\mu}$, where $X = \tilde{y}$ for the strip-like situation and $X = \tilde{\xi}$ for the spheres. Because of this, it is convenient to write also the black brane metric (5.9) in terms of the tilde coordinates. By rewriting the metric (5.8) in terms of L_{eff} and substituting $r \to \frac{L_{\text{eff}}^2}{z}$ one obtains the desired expression

$$ds^2 = \frac{L_{\text{eff}}^2}{z^2}\left(-F(z)\Phi^2 dt^2 + \frac{dz^2}{F(z)\Phi^2} + d\tilde{x}_i d\tilde{x}^i\right) \ , \tag{8.3}$$

where $\Phi^2 \equiv \frac{L_{\text{eff}}^2}{L^2}$.

Now, with both expressions (8.1) and (8.3) we proceed to follow a very similar reasoning as we did above. First, we will focus on the strip-like entangling regions and later

we will pay attention to the situation where we are dealing with spherical entangling regions. In this case, however, we will only consider variations of the strip-like entangling regions where both borders of the region are varied together forward or backwards in time. This is because the numerical methods that we explained in section 6.5 only works for the cases where the entangling regions lives in a constant t Cauchy slice. That means that we are only taking into account the variations represented in figure 7.5(b).

8.1 QNEC in Gauss-Bonnet holography and strip-like entangling regions

In this section we are going to take a look at the behavior of the QNEC for entangling regions with strip-like geometries, i.e.

$$\mathcal{A}_{\parallel} = \left\{ \tilde{\mathbf{x}}_{d-1} \in \mathbb{R}^{d-1} \mid \tilde{y} \in (-l/2, l/2) \text{ and } \tilde{\mathbf{x}}_{d-2} \in \mathbb{R}^{d-2} \right\} \ . \tag{8.4}$$

Just like in the previous chapter, the first step towards studying the QNEC is to determine the metric of the minimal area surface in the bulk that is anchored at $\partial\mathcal{A}_{\parallel}$ at the boundary. Again, by using the expression (6.24), we can write down the metric of $\mathcal{E}_{\mathcal{A}}$ as

$$ds^2 = \frac{L_{\text{eff}}^2}{z^2}\left(1 + \frac{\dot{z}^2}{F(z)\Phi^2}\right) d\tilde{y}^2 + \frac{L_{\text{eff}}^2}{z^2} d\tilde{\mathbf{x}}_{d-2}^2 \ , \tag{8.5}$$

where the dot stands for a derivative with respect to $\tilde{y}$ and $\tilde{\mathbf{x}}_{d-2}$ are the spatial directions on the boundary perpendicular to $\tilde{y}$.

Now that we have set the geometry of the problem we move to compute both the left- and right-hand-side of the QNEC inequality. With respect to the former one, in 2011 Hu et.al. obtained an expression for the stress-energy tensor of the field theory dual to Gauss-Bonnet gravity in the case of this being boosted with certain velocity u^μ. We recover the expression here by convenience:

$$T_{\mu\nu} = \frac{1}{16\pi G}\left[\frac{r_h^4}{L_{\text{eff}}^3}\left(\eta_{\mu\nu} + 4u_\mu u_\nu\right) - \frac{2U^2 r_h^3}{L_{\text{eff}}^3}\sigma_{\mu\nu}\right] \ , \tag{8.6}$$

where $\eta_{\mu\nu} = \text{diag}(-1, +1, \ldots, +1)$ is the metric at the boundary, $r_h = \frac{L_{\text{eff}}^2}{z_h}$, $U = \sqrt{1 - \frac{4\tilde{\alpha}}{L^2}}$ and $\sigma_{\mu\nu}$ is the shear tensor and depends only on u_μ and $\partial_\nu u_\mu$ in such a way that if $\partial_\nu u_\mu = 0$ then $\sigma_{\mu\nu} = 0$. In our case, since we do not have a boosted metric in the bulk, we can directly substitute $u^\mu = (1, 0, \ldots, 0)$ in the expression above to finally obtain

$$T_{\mu\nu} = \frac{1}{16\pi G}\left[\frac{r_h^4}{L_{\text{eff}}^3}\left(\eta_{\mu\nu} + 4u_\mu u_\nu\right)\right] \ . \tag{8.7}$$

If we now proceed as in the previous chapter and set $d = 4$, $L = 1$ and $(4G_N^{(D)})^{-1} = \frac{N^2}{2\pi}$ we obtain that the stress tensor is given by

$$\begin{aligned} T_{t\mu} &= \frac{3\pi^2 T^4 N^2}{8L_{\text{eff}}^3}\delta_{t\mu} \\ T_{ij} &= \frac{\pi^2 T^4 N^2}{8L_{\text{eff}}^3}\delta_{ij} \ , \end{aligned} \tag{8.8}$$

which finally yields

$$\frac{1}{N^2}\langle T^{\pm}_{kk}\rangle = \frac{\pi^2 T^4}{2L^3_{\text{eff}}} = \frac{1}{2\pi^2 L^3_{\text{eff}}} \ , \tag{8.9}$$

where in the last equality we set $T = \pi^{-1}$ just like before. Once again, since the "+" and "-" results are the same, we will drop the $\pm$ superscript from now on.

With respect to the right-hand-side of the QNEC inequality, one must first derive the holographic entanglement entropy functional for the case where $\mathcal{E}_{\mathcal{A}}$ is given by the geometry (8.5). To do so, it is extremely convenient to adopt a very similar notation to the one used in [44]. To begin, notice that the metric of the minimal area surface (8.5) can be written as

$$ds^2 = ds^2_X + \sum_i e^{2F_i} ds^2_{Y_i} \ , \tag{8.10}$$

where the conformal factor F_i only depends on the coordinates of the subspace X and, in our case, the sum only runs for $i = 1$. In our case, we have that

$$ds^2_X = \frac{L^2_{\text{eff}}}{z^2}\left(1 + \frac{\dot{z}^2}{F(z)\Phi^2}\right) d\tilde{y}^2 \equiv \gamma_{\tilde{y}\tilde{y}} d\tilde{y}^2 \tag{8.11a}$$

$$e^{2F} \equiv \frac{1}{z^2} \implies F = \ln\left(\frac{1}{z}\right) \tag{8.11b}$$

$$ds^2_Y = L^2_{\text{eff}} d\tilde{\mathbf{x}}^2_{d-2} \ . \tag{8.11c}$$

With this notation in mind let's start by computing the Ricci scalar of the minimal surface $\mathcal{E}_{\mathcal{A}_\parallel}$. On [44] it is shown that for a warped geometry of the form (8.10) the Ricci scalar is given by

$$R = R_X + \sum_i \left[e^{-2F_i} R_{Y_i} - 2d_i(\nabla^2 F_i) - d_i(\partial F)^2\right] - \sum_{ij} d_i d_j (\partial F_i \cdot \partial F_j) \ , \tag{8.12}$$

where the Laplacian ∇^2 is evaluated on the subspace X, d_i are the number of dimensions of the subspace Y_i and R_X and R_{Y_i} are the Ricci scalars of the subspaces X and Y_i respectively.

Taking into account that the subspace X is one-dimensional and the subspace Y is just the $(d-2)$-dimensional plane, we find that $R_Y = R_X = 0$. Then, since i (and j) can only take the value $i = 1$ and the dimension of the subspace Y is $d_Y = d-2$, combining the two last terms of the expression we finally obtain that

$$R = -2(d-2)\nabla^2 F - (d-2)(d-1)\gamma^{\tilde{y}\tilde{y}}\dot{F}^2 \ , \tag{8.13}$$

where $\gamma^{\tilde{y}\tilde{y}} = (\gamma_{\tilde{y}\tilde{y}})^{-1}$, the dot stands for differentiation with respect to $\tilde{y}$ and, since F is a scalar, we can write

$$\nabla^2 F = \frac{1}{\sqrt{\gamma_{\tilde{y}\tilde{y}}}}\partial_{\tilde{y}}\left(\sqrt{\gamma_{\tilde{y}\tilde{y}}}\gamma^{\tilde{y}\tilde{y}}\partial_{\tilde{y}} F\right) \ . \tag{8.14}$$

The last piece we need to compute the entropy functional (6.27) is the trace of the extrinsic curvature tensor of $\partial\mathcal{E}_{\mathcal{A}_\parallel}$. Therefore, we proceed to compute

$$\mathcal{K} = \gamma^{ab}\, \nabla_a n_b|_{\partial\mathcal{E}_{\mathcal{A}}} \ , \tag{8.15}$$

where n^a is the unit vector perpendicular to the surface $\partial\mathcal{E}_\mathcal{A}$ given by

$$n_b = -\sqrt{\gamma_{\tilde{y}\tilde{y}}}\delta_{\tilde{y}b} \tag{8.16}$$

and a runs over $\tilde{y}$ and a 2-dimensional plane. With that taken into account we can rewrite $\mathcal{K}$ as

$$\mathcal{K} = \left[\gamma^{\tilde{y}\tilde{y}}\nabla_{\tilde{y}}n_{\tilde{y}} + \gamma^{ik}\nabla_i n_k\right]_{\partial\mathcal{E}_\mathcal{A}} , \tag{8.17}$$

with γ_{ik} being the metric of the $(d-2)$-dimensional plane. One can now just simply evaluate the first and second terms of this expressions and obtain

$$\gamma^{\tilde{y}\tilde{y}}\nabla_{\tilde{y}}n_{\tilde{y}} = \partial_{\tilde{y}}n_{\tilde{y}} - \Gamma^{\tilde{y}}{}_{\tilde{y}\tilde{y}}n_{\tilde{y}} = -\frac{1}{2(\gamma_{\tilde{y}\tilde{y}})^{3/2}}\partial_{\tilde{y}}\gamma_{\tilde{y}\tilde{y}} + \frac{1}{2(\gamma_{\tilde{y}\tilde{y}})^{3/2}}\partial_{\tilde{y}}\gamma_{\tilde{y}\tilde{y}} = 0 \tag{8.18a}$$

$$\gamma^{ik}\nabla_i n_k = -\gamma^{ik}\Gamma^{\tilde{y}}{}_{ik}n_{\tilde{y}} = -\frac{(d-2)}{2\sqrt{\gamma_{\tilde{y}\tilde{y}}}}\partial_{\tilde{y}}e^{2F} . \tag{8.18b}$$

Thus, in the end, one can just express the integral of the trace of the extrinsic curvature tensor of $\partial\mathcal{E}_\mathcal{A}$ as

$$\int_{\partial\mathcal{E}_\mathcal{A}}\mathcal{K} = -(d-2)L_{\text{eff}}^2 D_{d-2}\,(\gamma_{\tilde{y}\tilde{y}})^{-1/2}\partial_{\tilde{y}}e^{2F}\Big|_{\tilde{y}_{\text{cut}}} , \tag{8.19}$$

where $\tilde{y}_{\text{cut}}$ is the cutoff on $\tilde{y}$, related to the holographic coordinate cutoff as $z(\tilde{y}_{\text{cut}}) = z_{\text{cut}}$ and D_2 is the infrared regulator of the translationally invariant directions $\tilde{\mathbf{x}}_{d-2}$.

Plugging both the expressions for the Ricci scalar and the Gibbons-Hawking term, the entropy functional (6.27) becomes

$$\begin{aligned} S =& \frac{1}{4G_N^{(D)}}\int_{\mathcal{E}_\mathcal{A}} d^{d-1}x\sqrt{\gamma}\left(1 + 2\alpha L^2\left(-2(d-2)\nabla^2 F - (d-2)(d-1)\gamma^{\tilde{y}\tilde{y}}\dot{F}^2\right)\right) \\ &- (d-2)\frac{L^2\alpha}{G_N^{(D)}}L_{\text{eff}}^2 D_{d-2}\,(\gamma_{\tilde{y}\tilde{y}})^{-1/2}\partial_{\tilde{y}}e^{2F}\Big|_{\tilde{y}_{\text{cut}}} . \end{aligned} \tag{8.20}$$

This expression seems highly complicated, but writing $d^{d-1}x = d\tilde{y}d^2\tilde{\mathbf{x}}_2$, substituting $d = 4$ and integrating the first line by parts, one arrives to

$$\begin{aligned} S_{\mathcal{A}_\parallel} =& -\frac{L^2\alpha}{G_N^{(D)}}L_{\text{eff}}^2 D_2 2\,(\gamma_{\tilde{y}\tilde{y}})^{-1/2}\partial_{\tilde{y}}e^{2F}\Big|_{\tilde{y}_{\text{cut}}}^{0} \\ &+ 2\frac{D_2 L_{\text{eff}}^2}{4G_N^{(D)}}\int_0^{\tilde{y}_{\text{cut}}} d\tilde{y}\sqrt{\gamma_{\tilde{y}\tilde{y}}}e^{2F}\left(1 + 4\left(\frac{L}{L_{\text{eff}}}\right)^2\alpha L_{\text{eff}}^2\gamma^{\tilde{y}\tilde{y}}\dot{F}^2\right) \\ &- 2\frac{L^2\alpha}{G_N^{(D)}}L_{\text{eff}}^2 D_2\,(\gamma_{\tilde{y}\tilde{y}})^{-1/2}\partial_{\tilde{y}}e^{2F}\Big|_{\tilde{y}_{\text{cut}}} . \end{aligned} \tag{8.21}$$

Notice that the first term evaluated at $\tilde{y} = 0$ vanishes by symmetry, while when evaluated at $\tilde{y}_{\text{cut}}$ is cancels with the last term. Therefore, the holographic entanglement entropy for a strip-like entangling region in Gauss-Bonnet holography is finally given by

$$S_{\mathcal{A}_\parallel} = 2\frac{D_2 L_{\text{eff}}^2}{4G_N^{(D)}}\int_0^{\tilde{y}_{\text{cut}}} d\tilde{y}\sqrt{\gamma_{\tilde{y}\tilde{y}}}e^{2F}\left(1 + 4\left(\frac{L}{L_{\text{eff}}}\right)^2\alpha L_{\text{eff}}^2\gamma^{\tilde{y}\tilde{y}}\dot{F}^2\right) . \tag{8.22}$$

Writing down the equations of motion of the functional (8.22) is not easy. Because of this, we opt to expand the entropy in powers of α and compute the entanglement entropy for the case up to linear order in α:

$$S_{\parallel} \equiv S_{\mathcal{E}_{\mathcal{A}_{\parallel}}} = S^{(0)}_{\mathcal{E}_{\mathcal{A}_{\parallel}}} + \alpha S^{(1)}_{\mathcal{E}_{\mathcal{A}_{\parallel}}} + \mathcal{O}(\alpha^2) \ . \tag{8.23}$$

With this expansion, we can now determine the minimal surfaces in the bulk and compute the entanglement entropy and its second derivative with respect to the null direction. By doing so, we find that the QNEC is still trivially satisfied in Gauss-Bonnet holography, since the second derivative of the entropy is negative everywhere while the stress-energy tensor is positive (see figure 8.1). We show the results for four different values of α, two most negative and positive possible values (according to the bounds explained in section 5.3) and two more values, one positive and one negative, close to zero: $\alpha = \{-7/72, -0.01, 0.01, 9/200\}$ In figure 8.2 one can see how the second derivative of the entanglement entropy varies with respect to α.

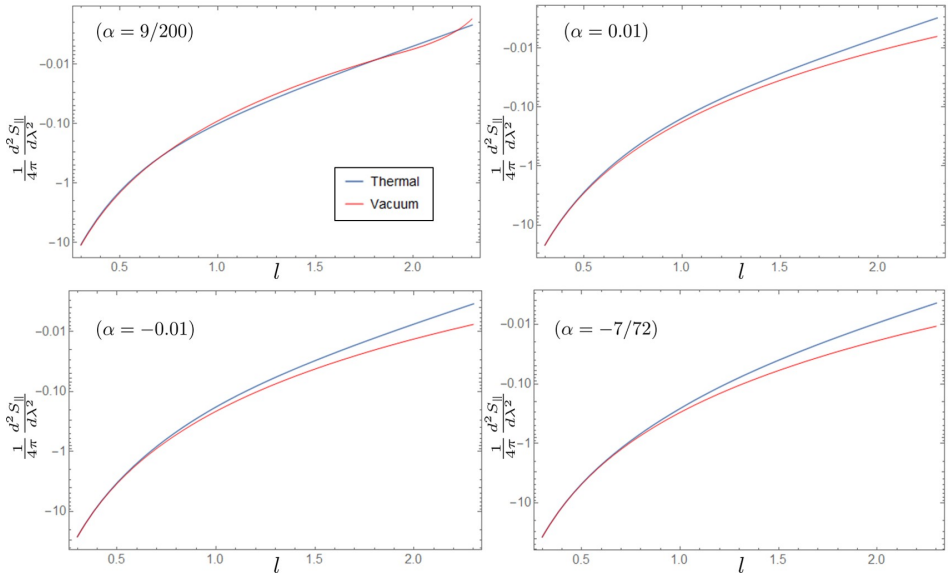

Figure 8.1: In blue the second derivative of the entanglement entropy for strip-like regions in a thermal state. In red, the same function for the vacuum state. We can see that, no matter the value of α the QNEC is always trivially satisfied, since $\frac{d^2S_{\parallel}}{d\lambda^2} < 0$ and $\langle T_{kk} \rangle > 0$.

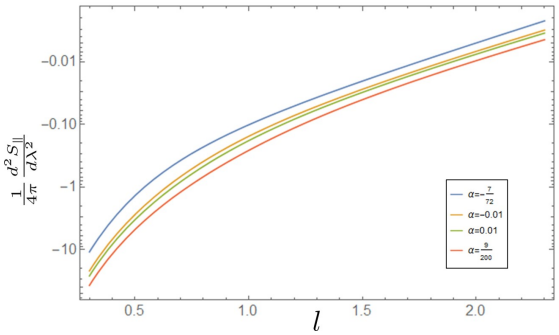

Figure 8.2: Plot of the second derivative of the entanglement entropy for strip-like regions in a thermal state for different values of α. Notice that, the more negative the α the less negative the $\frac{d^2S_{\parallel}}{d\lambda^2}$.

8.2 QNEC in Gauss-Bonnet holography and spherical regions

In order to study the QNEC of spherical entangling regions in Gauss-Bonnet holography we proceed in a very similar way as we did for the strip-like regions. Of course, since in both cases we are considering the same state living on the boundary theory, i.e. a thermal state, the energy density $\langle T_{kk} \rangle$ of the CFT will be the same as before. Thus, we only should derive the expression for the entropy functional in this case.

As explained in the previous chapter, the spherical entangling region is characterized by

$$\mathcal{A}_\bullet = \left\{ \tilde{\mathbf{x}} \in \mathbb{R}^{d-1} \mid |\tilde{\mathbf{x}}| \leq R \right\} = \left\{ (\theta, \phi) \in S^{d-2}, \tilde{\xi} \in \mathbb{R} \mid 0 < \tilde{\xi} \leq R \right\} \ , \tag{8.24}$$

where in this case we wrote it in terms of the tilde coordinates, just like for the strips. We then repeat the same process as before and use the relation (6.24) to find the geometry of the extremal surface $\mathcal{E}_{\mathcal{A}_\bullet}$ and obtain

$$ds^2 = \frac{L_{\text{eff}}^2}{z^2} \left(1 + \frac{(z')^2}{F(z)\Phi^2} \right) d\tilde{\xi}^2 + \frac{L_{\text{eff}}^2 \tilde{\xi}^2}{z^2} d\Omega_{d-2}^2 \ , \tag{8.25}$$

where the primer stands for differentiation with respect to $\tilde{\xi}$. Notice that, again, the metric can be written in terms of (8.10) if we do the following identifications:

$$ds_X^2 = \frac{L_{\text{eff}}^2}{z^2} \left(1 + \frac{(z')^2}{F(z)\Phi^2} \right) d\tilde{\xi}^2 \equiv \gamma_{\tilde{\xi}\tilde{\xi}} d\tilde{\xi}^2 \tag{8.26a}$$

$$e^{2F} \equiv \frac{\xi^2}{z^2} \implies F = \ln\left(\frac{\xi}{z} \right) \tag{8.26b}$$

$$ds_Y^2 = L_{\text{eff}}^2 d\Omega_{d-2}^2 \ . \tag{8.26c}$$

With these identifications one can, once again, use equation (8.12) to compute the Ricci scalar of the extremal surface $\mathcal{E}_{\mathcal{A}_\bullet}$ where, in this case, $R_X = 0$ since the subspace X is still one-dimensional and R_Y is the Ricci scalar of a $(d-2)$-sphere of radius L_{eff} given by

$$R_Y = \frac{(d-2)(d-3)}{L_{\text{eff}}^2} \ . \tag{8.27}$$

Then, by pugging this in equation (8.12) one finds that the Ricci scalar of $\mathcal{E}_{\mathcal{A}_\bullet}$ is given by

$$R = e^{-2F} \frac{(d-2)(d-3)}{L_{\text{eff}}^2} - 2(d-2)\nabla^2 F - (d-2)(d-1)\gamma^{\tilde{\xi}\tilde{\xi}}(F')^2 \ . \tag{8.28}$$

This time the derivatives of the Laplacian are with respect to $\tilde{\xi}$ and not with respect $\tilde{y}$, i.e.

$$\nabla^2 F = \frac{1}{\sqrt{\gamma_{\tilde{\xi}\tilde{\xi}}}} \partial_{\tilde{\xi}} \left(\sqrt{\gamma_{\tilde{\xi}\tilde{\xi}}} \gamma^{\tilde{\xi}\tilde{\xi}} \partial_{\tilde{\xi}} F \right) \ . \tag{8.29}$$

Now that we have the Ricci scalar, we proceed to compute the trace of the extrinsic curvature tensor $\mathcal{K}$ of the surface $\partial\mathcal{E}_{\mathcal{A}_\bullet}$. The normalized vector normal to the surface is now given by

$$n_b = -\sqrt{\gamma_{\tilde{\xi}\tilde{\xi}}} \delta_{\tilde{\xi} b} \tag{8.30}$$

and the index a in equation (8.15) now runs over $\tilde{\xi}$ and a $(d-2)$-dimensional sphere. It is now straightforward to show that the results given in equation (8.18b) hold true also for the sphere if we substitute $\tilde{y} \to \tilde{\xi}$ and we take into account the new definition of F. Thus, the integral of $\mathcal{K}$ yields

$$\int_{\partial \mathcal{E}_{\mathcal{A}_\bullet}} \mathcal{K} = -\frac{(d-2)}{2} L_{\text{eff}}^2 \Omega_{d-2} \left(\gamma_{\tilde{\xi}\tilde{\xi}}\right)^{-1/2} \partial_{\tilde{\xi}} e^{2F} \Big|_{\tilde{\xi}_{\text{cut}}} , \tag{8.31}$$

where Ω_{d-2} is the area of a unit S^{d-2} and $\tilde{\xi}_{\text{cut}}$ is related to the holographic cutoff by $z(\tilde{\xi}_{\text{cut}}) = z_{\text{cut}}$. Notice that in this case there is a factor 2^{-1} that did not appear before due to the fact that the integral runs from 0 to $\tilde{\xi}_{\text{cut}}$ and in the previous case the integral in $\tilde{y}$ run from $-\tilde{y}_{\text{cut}}$ to $\tilde{y}_{\text{cut}}$.

We now proceed as before: first we plug these results into the entropy functional (6.27), we set $d^{d-1}x = d\tilde{\xi} d\Omega_{d-2}^2$ with $d = 4$ and then we integrate by parts to finally find that the entropy functional is given by

$$\begin{aligned} S_{\mathcal{A}_\bullet} = &- \frac{L^2 \alpha}{G_N^{(D)}} L_{\text{eff}}^2 \Omega_2 \left(\gamma_{\tilde{\xi}\tilde{\xi}}\right)^{-1/2} \partial_{\tilde{\xi}} e^{2F} \Big|_0^{\tilde{\xi}_{\text{cut}}} \\ &+ \frac{\Omega_2 L_{\text{eff}}^2}{4 G_N^{(D)}} \int_0^{\tilde{\xi}_{\text{cut}}} d\tilde{\xi} \sqrt{\gamma_{\tilde{\xi}\tilde{\xi}}} e^{2F} \left(1 + 4 \left(\frac{L}{L_{\text{eff}}}\right)^2 \alpha \left[e^{-2F} + L_{\text{eff}}^2 \gamma^{\tilde{\xi}\tilde{\xi}} (F')^2\right]\right) \\ &- \frac{L^2 \alpha}{G_N^{(D)}} L_{\text{eff}}^2 \Omega_2 \left(\gamma_{\tilde{\xi}\tilde{\xi}}\right)^{-1/2} \partial_{\tilde{\xi}} e^{2F} \Big|_{\tilde{\xi}_{\text{cut}}} . \end{aligned} \tag{8.32}$$

Once again, just like before, the first term vanishes when evaluated at $\tilde{\xi} = 0$ and cancels with the Gibbons-Hawking term when evaluated at $\tilde{\xi} = \tilde{\xi}_{\text{cut}}$. Thus, the final expression for the holographic entanglement entropy of spherical entangling regions dual to Gauss-Bonnet gravity is given by

$$S_{\mathcal{A}_\bullet} = \frac{\Omega_2 L_{\text{eff}}^2}{4 G_N^{(D)}} \int_0^{\tilde{\xi}_{\text{cut}}} d\tilde{\xi} \sqrt{\gamma_{\tilde{\xi}\tilde{\xi}}} e^{2F} \left(1 + 4 \left(\frac{L}{L_{\text{eff}}}\right)^2 \alpha \left[e^{-2F} + L_{\text{eff}}^2 \gamma^{\tilde{\xi}\tilde{\xi}} (F')^2\right]\right) . \tag{8.33}$$

Just like before, we expand the entropy as in (8.23) to compute the extremal surfaces and the entropy functional. However, to compute the QNEC for spheres we should first look at what happens in the case where we consider the vacuum state in order to know if the reasoning we did for the holographic setup with Einstein-Hilbert gravity in the bulk is still valid for the Gauss-Bonnet situation. From the discussion made above, we know that the boundary theory has "tilde" coordinates and that means that the null variation of the $\partial\mathcal{A}$ surface is done in the tilde coordinates too. Thus, we should study what happens to the extremal surfaces in the bulk that minimize the functional (8.33) when we perform the null deformation in the boundary surface. In [44] is is shown that these extremal surfaces, when considering a vacuum state, spherical entangling regions and spatial coordinates given by the tilde coordinates, are perfect semispheres given by

$$\tilde{\xi}(\varphi) = R\cos(\varphi) \quad \text{and} \quad z(\varphi) = R\sin(\varphi) , \tag{8.34}$$

being R the radius of the spherical entangling region at the boundary. Therefore, we are left with the same situation as in Einstein-Hilbert holography, with the difference of the new definition of the spatial coordinates. Then, this just means that, in this case, we

obtain again that the variation of the extremal surfaces are null and, therefore, that the QNEC is saturated again:

$$g_{\mu\nu}\tilde{s}^{\mu}\tilde{s}^{\nu} = 0 \ . \tag{8.35}$$

With this in mind we can follow exactly the same reasoning as explained in section 7.2.3 to derive that the QNEC for spheres in Gauss-Bonnet holography can also be computed using

$$2\pi R^{d-2}\int d\Omega\ T_{kk}(\Omega) \geq \frac{d^2}{d\lambda^2}\left(S - S_{\text{vac}}\right) \mp \frac{2}{R}\frac{d}{d\lambda}\left(S - S_{\text{vac}}\right) \ , \tag{8.36}$$

or, after substituting the value of T_{kk} and rearranging the expression, using

$$\frac{2\pi R^2}{N}\langle T_{kk}\rangle = \frac{R^2}{2\pi^2 L_{\text{eff}}^3} \geq \frac{1}{\Omega_2}\left(\frac{d^2}{d\lambda^2}\left(S - S_{\text{vac}}\right) \mp \frac{2}{R}\frac{d}{d\lambda}\left(S - S_{\text{vac}}\right)\right) \ . \tag{8.37}$$

Finally, we evaluated the expression (8.37) for different values of α. In figure 8.3 we show the results for four different values of the Gauss-Bonnet constant, two most negative and positive possible values (according to the bounds explained in section 5.3) and two more values, one positive and one negative, close to zero: $\alpha = \{-7/72, -0.01, 0.01, 9/200\}$. As one can see in the figure, for positive α the QNEC is satisfied everywhere and we can say that the original saturation that we found in Einstein-Hilbert holography ($\alpha = 0$) "relaxes". However, the interesting results are those for $\alpha < 0$. For these values we see that, when expanding the spherical entangling region, the QNEC is violated. This is a very interesting result that is telling us that something is wrong with this holographic setup for $\alpha < 0$. However, before giving any premature conclusion, we should look at what happens if instead of expanding S up to linear order in α we go to higher orders.

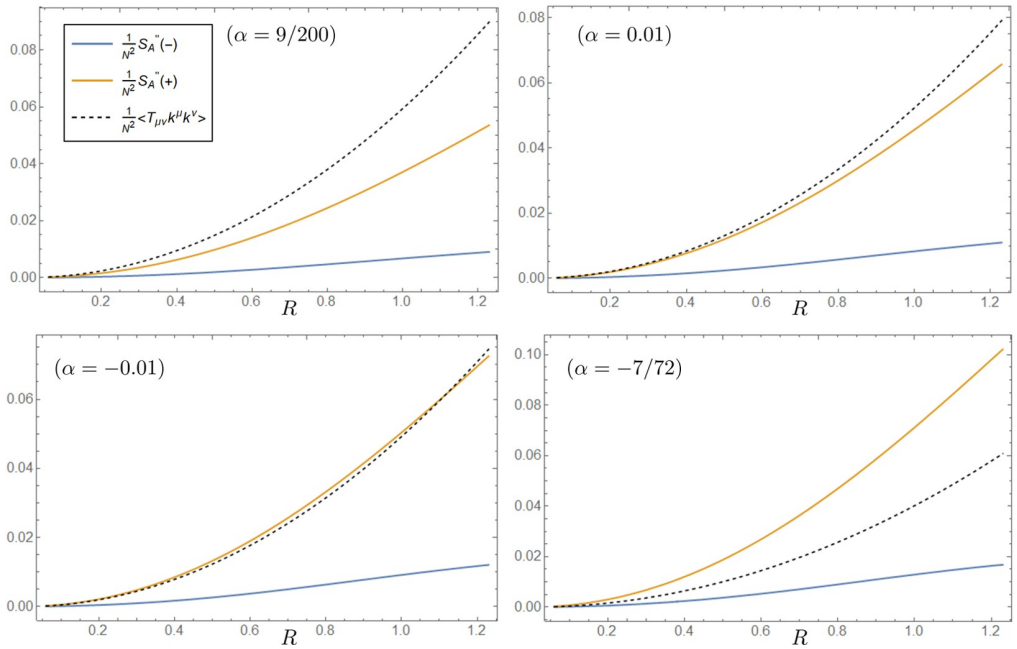

Figure 8.3: In yellow the right hand side of the inequality (8.37) for the expanding sphere while in blue is shown the same expression for a variation directed radially inwards. For positive α the QNEC is satisfied everywhere while for negative values of the Gauss-Bonnet coupling constant the QNEC is violated for expanding spheres. In the case of $\alpha = -0.01$ (bottom left) the yellow line crosses the dashed line from $R = 0.2$ to $R = 1.1$ approximately (see figure 8.6).

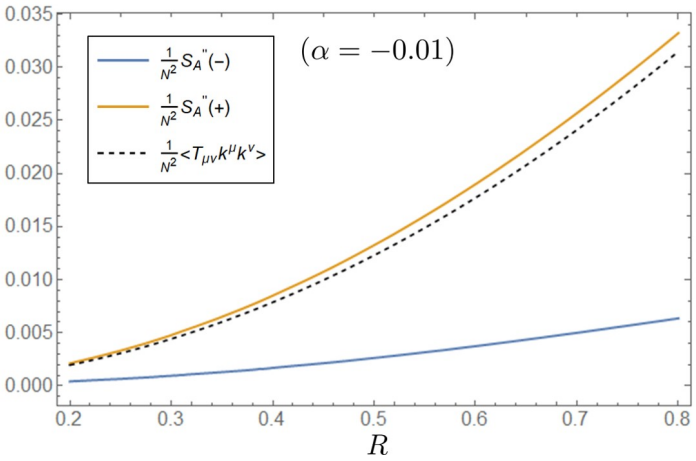

Figure 8.4: Zoomed plot for the results of the QNEC in the case of $\alpha = -0.01$. In yellow the right hand side of the inequality (8.37) for the expanding sphere, in blue is shown the same expression for a variation directed radially inwards and in dashed line the left hand side of the QNEC inequality. It is clearly shown that the QNEC is violated for the expanding situation.

In order to test this results, then, we recompute the holographic entanglement entropy and the QNEC expanding the entropy functional up to second order in the Gauss-Bonnet constant. We expect that, either the second derivative of the entropy for the case of expanding spheres (yellow lines in the pots 8.3 and 8.6) approaches the value of the left hand side of the QNEC (dashed lines) or the new results show exactly the same behavior as for the linear α expansion. If the former is true then we could argue that, for a "non-expanded" entropy functional, the QNEC would may not be violated while for the latter option we would conclude that the original expansion was enough to capture all the relevant results of the QNEC and, therefore, we could conclude that the QNEC is violated.

As seen in figure 8.5, the QNEC is still violated when we consider up to second order corrections in the entropy functional. Not only that, but we see that the results match the original first order expansion results. Thus, since $\alpha^3 \ll \alpha$, we do not expect that going to higher orders in the expansion will change the results. And therefore we finally conclude that the QNEC is violated for $\alpha < 0$ and a thermal state when we consider a null variation of the spherical boundary entangling surface pointing radially outwards.

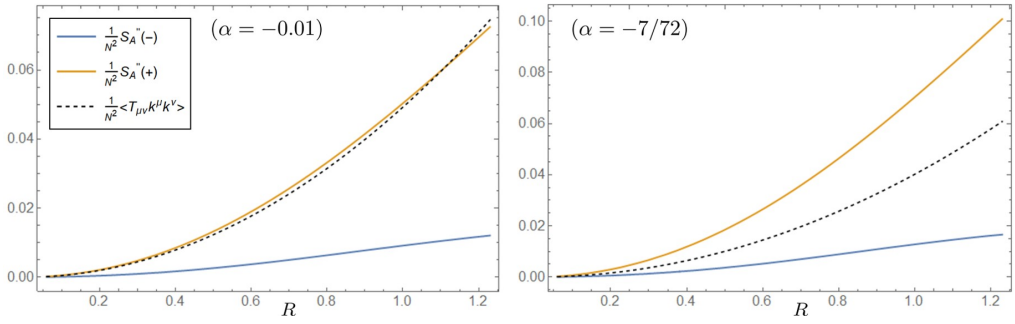

Figure 8.5: Results of the QNEC computed for a holographic entanglement entropy of the form $S = S^{(0)} + \alpha S^{(1)} + \alpha^2 S^{(2)} + \mathcal{O}(\alpha^3)$. On the left the results for $\alpha = -0.01$, on the right the results for $\alpha = -7/72$. In yellow the right hand side of the inequality (8.37) for the expanding sphere while in blue is shown the same expression for a variation directed radially inwards. We can clearly see that the results match the ones for a linear α expansion (figure 8.3).

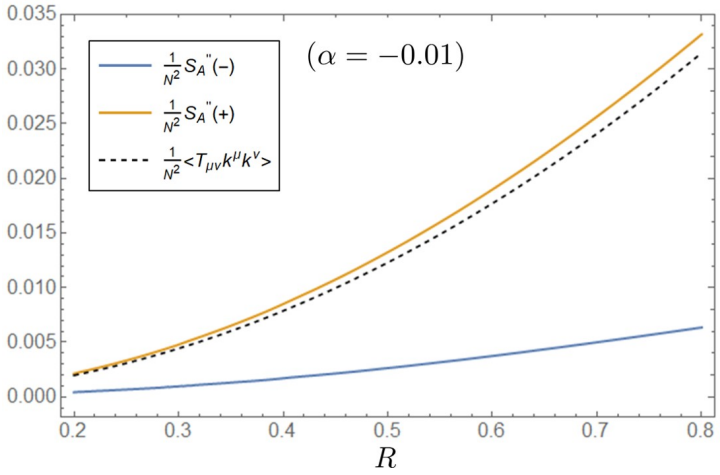

Figure 8.6: Zoomed plot for the results of the QNEC in the case of $\alpha = -0.01$. In yellow the right hand side of the inequality (8.37) for the expanding sphere, in blue is shown the same expression for a variation directed radially inwards and in dashed line the left hand side of the QNEC inequality. It is clearly shown that the QNEC is violated for the expanding situation.

9. Conclusions and Outlook

In this thesis we have presented a review on the Quantum Null Energy Condition, and all the necessary concepts to understand and study it, as well as studied its behavior in several interesting situations. Due to the nature of the entanglement entropy, which highly depends on the geometry of the entangling surface $\partial\mathcal{A}$ that we are considering, and the fact that the second derivative of the entropy diverges for non-flat entangling surfaces [45], we were interested in studying the QNEC for entangling surfaces that were flat or curved everywhere. Because of this we considered both strip-like and spherical entangling surfaces. For both of the cases, we considered variations of the whole surface instead of purely local variations. In other words, we studied the integrated version of the QNEC. All of this, we were interested in studying it for field theories holographically dual to both Einstein-Hilbert and Gauss-Bonnet gravity.

First we look at the QNEC for both geometries in an holographic setup with Einstein-Hilbert gravity as the bulk theory. For the strip-like region, since the entangling surface$\partial\mathcal{A}$ is actually two separated planar surfaces separated by a distance l, we consider all possible variations of $\partial\mathcal{A}$ allowed (see figure 7.5 for a schematic representation of all of them) and give the analytical results for both the small l and large l limits as well as the numerical computations for any value of l. In all the cases we find that the QNEC is satisfied trivially, since the second derivative of the entropy is negative everywhere and the energy density of the thermal state is positive.

On the other hand, the results for the spherical entangling surfaces are more interesting. In this case we first had to understand how to compute the QNEC, since the second derivative of the entropy diverges due to the non-planar nature of the surface. Once we had the expression for the QNEC in spherical regions, which depends on performing the null variation radially inwards or outwards, we computed it numerically and found that for both types of variations the QNEC is satisfied. However, for expanding spheres (null variation pointing outwards of the spherical surface) the QNEC is nearly saturated. This last result motivated us even more to look at the QNEC in Gauss-Bonnet holography since this last depends on a coupling constant that can take both positive and negative values and, naively, one could expect a violation of the QNEC for one of the two signs.

The last chapter of the thesis, then, is centered in computing the QNEC for Gauss-Bonnet holography. However, since the holographic entropy functional depends on the Gauss-Bonnet coupling in a non-trivial way it was impossible for us to compute it without taking the expansion of the entropy in powers of the couping. Therefore, we repeated

the same process as in the previous cases to compute the QNEC for the two geometries considering that an expansion of the entropy up to linear order in the coupling constant.

For the case of the strip-like regions, we showed that the QNEC is still trivially satisfied for any value of the coupling constant possible. Just like before, the second derivative of the entropy is is still negative, while $\langle T_{kk} \rangle$ continues being positive. Therefore, we continue not finding anything new for this geometry.

However, as expected from the previous results, the QNEC computed for spherical entangling regions in Gauss-Bonnet holography gave us a very interesting results. As expected, we find two different behaviors of the QNEC inequality depending on the sign of the Gauss-Bonnet constant. For positive values, the original saturation of the QNEC relaxes and becomes satisfied everywhere, even for expanding spheres. On the other hand, the QNEC is violated when considering negative values of the coupling constant. Of course, this result is telling us that something is wrong for this values of the constant but, do we know what it is wrong? We have some ideas on where one should look at in order to answer this question.

Since in [50] Balakrishnan et.al. proved the QNEC inequality directly using QFT techniques without referring to the AdS/CFT correspondence, we know that this should be true for any unitary field theory no matter what its holographic dual looks like. Therefore, one possible point where we can have problems is in the fact that two extremal surfaces are null separated in the Gauss-Bonnet bulk theory may not mean that the QNEC is saturated in that situation. This was implicitly assumed in order to re-derive the QNEC inequality (8.36) for spherical entangling regions dual to Gauss-Bonnet gravity. Therefore, the next step is to study the relation between the variation of the extremal surfaces in the bulk and the QNEC inequality in the case of Gauss-Bonnet holography. One can check this by proceeding in an analogous way as it was done for Einstein-Hilbert holography [45], where the authors proved the QNEC only relying on the properties of the extremal surfaces near the AdS boundary, with the advantage that both Einstein and Gauss-Bonnet AdS near the boundary are formally the same. However, the main difference that one has to take into account is that, in this case the holographic entanglement entropy is not given by the area of the minimal surface area but by the functional (6.22) computed on the bulk surface that minimizes it. This work will actually be done but for lack of time it has not been included in this thesis.

Then, if we show that the null separation between extremal surfaces in the bulk imply saturation of the QNEC, then we will conclude that the problem is somewhere in the Gauss-Bonnet holographic setup. This would not be the first result yielding this conclusion. In the thesis we already discussed that the Gauss-Bonnet coupling constant has to be bounded in order to satisfy causality of the boundary theory, but there are other authors who argued that actually Gauss-Bonnet holography is not a consistent theory no matter the value of the coupling constant. In [51] the authors considered the corrections to the graviton three-point coupling and argued that, in order to not violate causality, the higher derivative coupling constant (Gauss-Bonnet constant in our case) should be infinitesimal. Our result would then just put some more arguments in that direction.

However, even if we agree that Gauss-Bonnet holography is not well behaved, we still would not understand where the actual problem is. In one hand maybe the field theory is non-unitary or just non-physical, just like the classical field theories that do not obey the NEC are non-physical or non-unitary. On the other hand maybe the holographic

correspondence itself is wrong and the dictionary should be modified when considering higher derivative gravities in the bulk. These are questions that remain open nowadays and that we do not have clear arguments to postulate which one of the two is more plausible.

Lastly, a very nice way to extend the work done in this thesis would be to check if the QNEC violation is true in any arbitrary number of dimensions or if it just happens for some particular dimensions, namely even dimensions. This would be interesting to check in order to have even a stronger argument with respect to the holographic correspondence with Gauss-Bonnet gravity.

Appendices

A. Hawking temperature of a black brane

In this appendix we show how the Hawking radiation of a black brane (or black hole) metric is computed. Consider we have a metric of the form

$$ds^2 = a(r)\left[-f(r)dt^2 + dx_i dx^i\right] + \frac{1}{h(r)}dr^2 \ , \tag{A.1}$$

where $f(r)$ and $h(r)$ has a first order zero at the horizon $r = r_h$ while $g(r_h) \neq 0$. Let us now define a new coordinate $\tau = it$. By expressing the metric in terms of τ, this one will take the Euclidean from

$$ds^2 = a(r)\left[f(r)d\tau^2 + dx_i dx^i\right] + \frac{1}{h(r)}dr^2 \ . \tag{A.2}$$

Since know that the singularity of the metric at $r = r_h$ is just a coordinate singularity and not a physical one, we demand the metric to be regular at the horizon. Expanding the expression (A.2) near the horizon we have

$$ds^2 \approx d\rho^2 + \rho^2 d\theta^2 + a(r_h)dx_i dx^i \ , \tag{A.3}$$

with

$$\rho = 2\sqrt{\frac{r - r_h}{h'(r_h)}}, \quad \theta = \frac{\tau}{2}\sqrt{a(r_h)f'(r_h)h'(r_h)} \tag{A.4}$$

and the prime stands for derivative with respect to r.

Since the first two terms describe a plane in polar coordinates and we want to avoid the singularity at $r = r_h$ ($\rho = 0$) we must demand θ to be periodic with period 2π. Then, by relating $\beta = \tau$, we finally find that the period of θ yields that the temperature of a black brane metric is given by

$$\beta = \frac{1}{T} = \frac{4\pi}{\sqrt{a(r_h)f'(r_h)h'(r_h)}} \ . \tag{A.5}$$

B. Testing the convergence of the numeric computations

In this appendix we present how the choice of the parameters of our numerical computation method affects the results and which of them are the ones we used to obtain the plots shown in the main text. Here we present plots of the QNEC for spherical entangling regions only, but for strips works exactly the same. The small difference between then will be commented at the end of this appendix.

Our computations have basically 5 different free parameters that we can change: the precision set for the "NDSolve" function to determine the minimal area surface, the precision to find the endpoint (upper limit) R of the entanglement entropy S integral, the precision set for the numerical integral result, the cutoff z_{cut} of the holographic coordinate and the spacing between the z_* parameters in order to create the list of S-R (see section 6.5). The first parameter we chose it to be precise enough to know that we would not have problems from that side. Therefore, we set the "AccuracyGoal" of the "NDSolve" function to be of 23 digits. The rest of the parameters are discussed in the following sections.

B.1 Changing the spacing

First let us know what happens if we change the spacing between z_*. Since the max value of z_* for the thermal state is $z_* = z_h$ (in our case $z_h = 1$) while the vacuum minimal surfaces are not bounded in that sense, we cannot use the same values of z_* for both cases. For the vacuum state, we varied the z_* from 0.005 to 1.3 with a spacing Δz_*, while for the thermal state we varied from 0.005 to 0.85 by Δz_* and from 0.0852 to 0.94 with a spacing of 0.002. In figure B.1 we show how the results change for values of the spacing given by $\Delta z_* = \{0.001, 0.003, 0.005, 0.007, 0.01\}$ and a cutoff $z_{\text{cut}} = 0.005$. One can clearly see that the precision of the results are very affected by these changes. Given the results, and because we do not want to take spacing too big in order to have as many computed points as possible, we took $\Delta z_* = 0.005$ to do all the numerical computations in the thesis. Since for larger values of the spacing the numerical noise does not decrease, we conclude that there must be some other source of noise. In next section we will show that this remaining noise is not dependent on the cutoff z_{cut}.

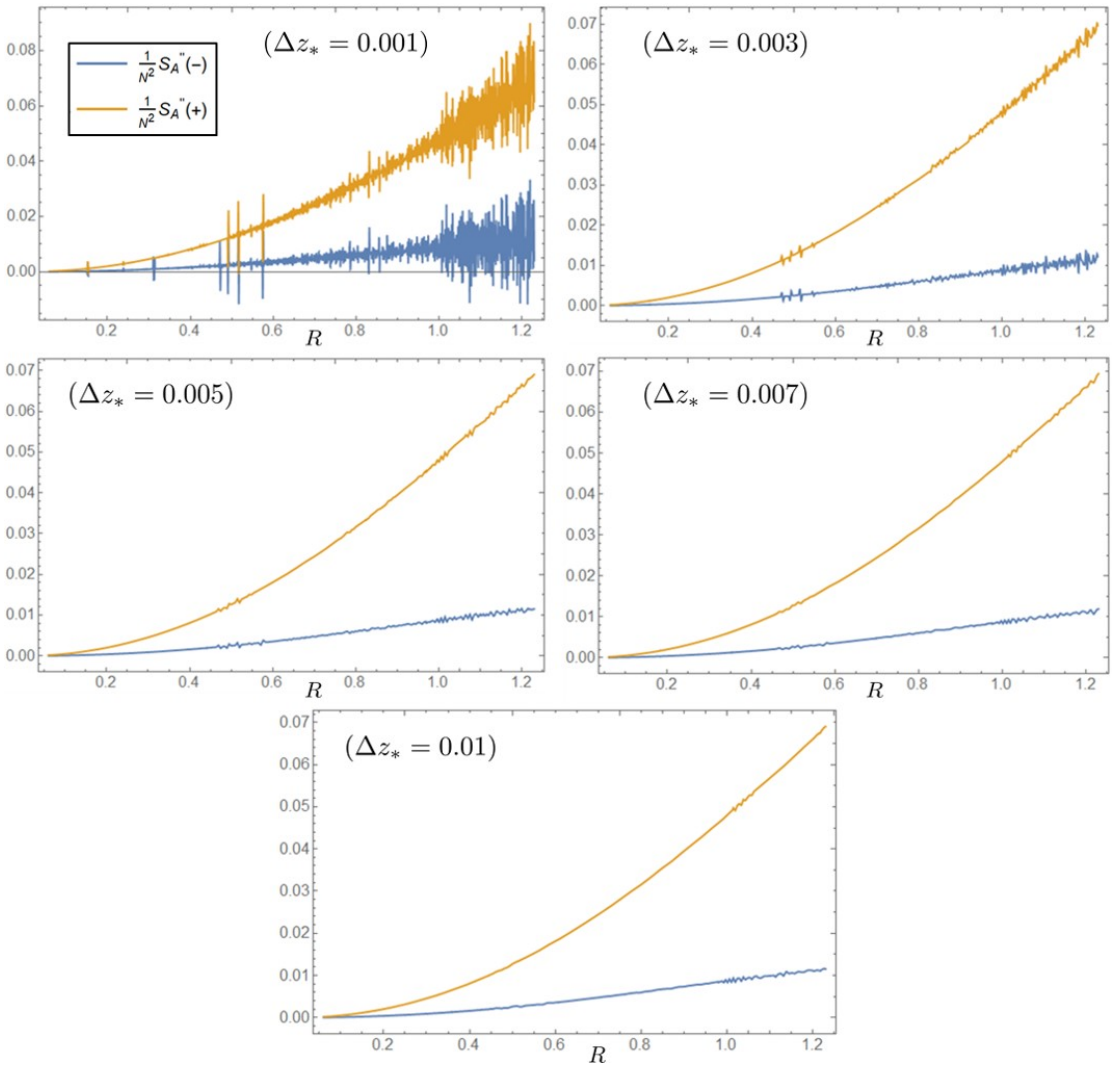

Figure B.1: Plot of the QNEC for spherical entangling regions in Einstein-Hilbert holography for different values of the spacing Δz_* and $z_{\text{cut}} = 0.005$. We used $\Delta z_* = 0.005$ to compute all the plots in the main text since it is the smallest spacing that has reasonable numerical noise.

B.2 Changing the cutoff

As seen above, for spacing parameters larger than $\Delta z_* = 0.005$ we still encounter some numerical noise that does not completely disappear by just increasing the spacing. Here we present a series of results similar to the ones above but, in this case, for different values of the cutoff. In figure B.2 we show the results of the QNEC for values of the cutoff given by $z_{\text{cut}} = \{0.001, 0.003, 0.005, 0.007, 0.01\}$ and a spacing $\Delta z_* = 0.005$. As one can see the smallest value that one can impose to the cutoff that yields well-behaved results is $z_{\text{cut}} = 0.005$. However, the numerical noise is still not completely vanished. Because of this and the fact that, by construction of the QNEC formula (7.78), we know that the results should not depend on the cutoff we decided to increase the precision of the numerical computations to values larger than the machine precision (which for Mathematica is of 16 digits).

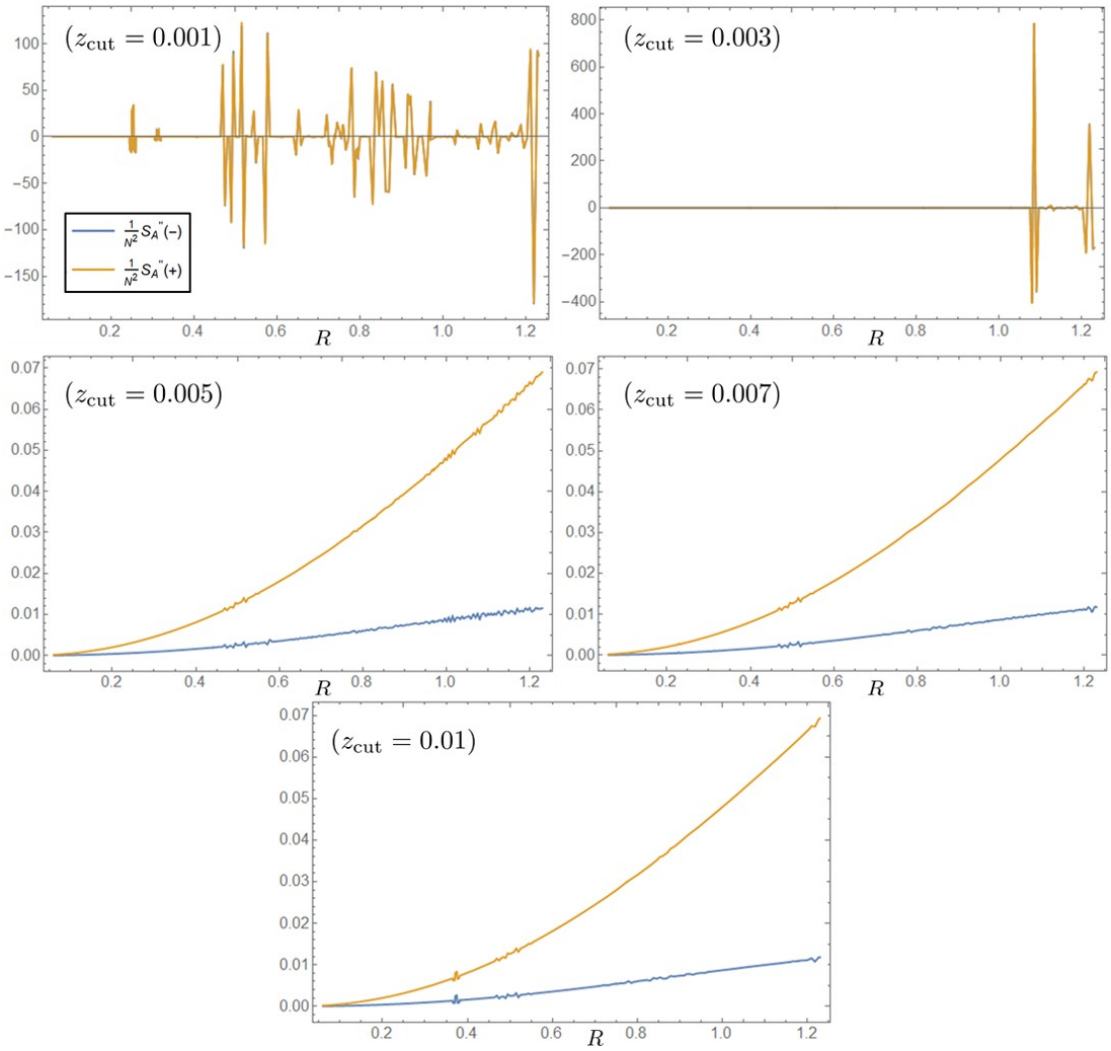

Figure B.2: Plot of the QNEC for spherical entangling regions in Einstein-Hilbert holography for different values of the spacing z_{cut} and $\Delta z_* = 0.005$.

B.3 Changing the numerical precision

In order to eliminate the numerical noise of the results for $z_{\text{cut}} \geq 0.005$ we can only change the precision of the endpoint R and the numerical integration of the entanglement entropy S. Here we present again the results of the QNEC for different values of the cutoff when demanding a precision of 20 digits to R and 25 digits to S. These are the precision values that we used to compute all the results in the main text. As seen in B.3, as we expected the general behavior of the QNEC is now the same for all values of the cutoff and the results are noise free for the values $z_{\text{cut}} \geq 0.005$. Because of this, in the main text we used the cutoff $z_{\text{cut}} = 0.005$ to derive all our results.

With respect to the strips, the values of the cutoff and accuracy of the NDSolve are the sameHowever, the precision required for those computations is much higher since, as seen in figure 7.6 and 8.1 the values that $\frac{d^2S}{d\lambda^2}$ takes are much smaller. In these cases we demanded a precision for R of 25 digits and a precision of S of 30 digits. We also demand the spacing to be the same as for the spheres. However, since the minimal surface of the thermal state cannot cross $z_h = 1$, we decrease gradually the spacing as we approach to

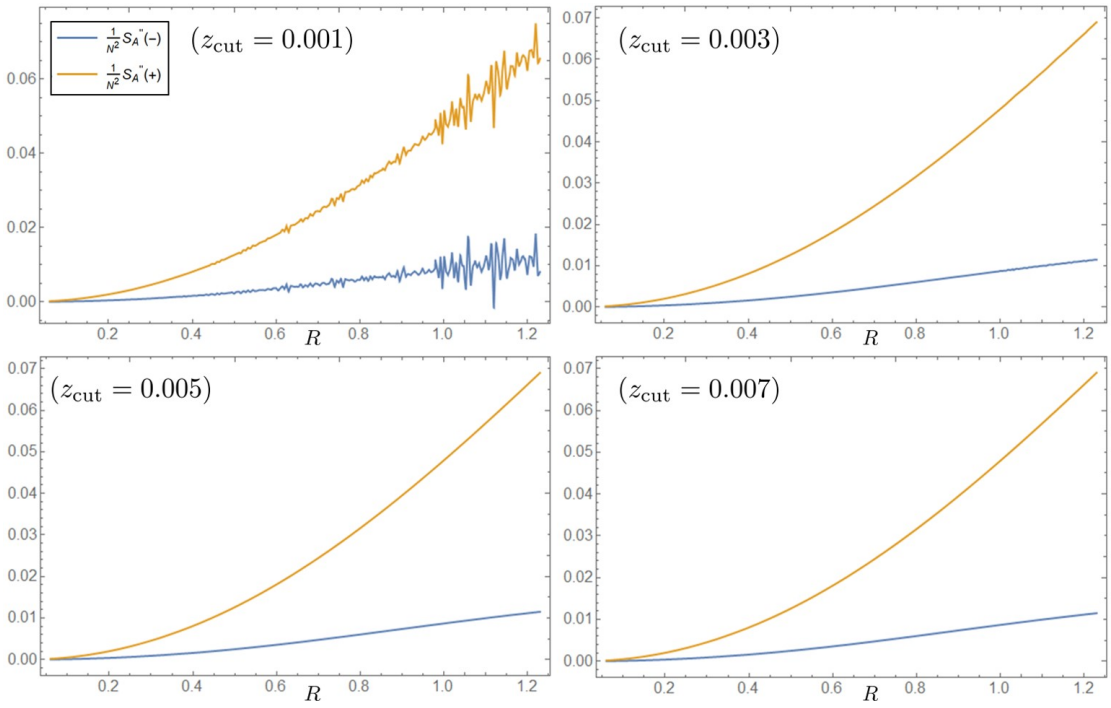

Figure B.3: Plot of the QNEC for spherical entangling regions in Einstein-Hilbert holography for different values of the spacing z_{cut}, $\Delta z_* = 0.005$, $Precision(R) = 20$ and $Precision(S) = 25$.

the horizon. In this case, we set the spacing for the thermal state to be from 0.005 to 0.85 in steps of 0.005, from 0.852 to 0.97 in steps of 0.002, from 0.971 to 0.9895 in steps of 0.0005 and from 0.99 to 0.999 in steps of 0.0001. The thermal minimal area for the strip has to approach the horizon more than the sphere in order to see the transition from vacuum behavior to an exponential decay in the figure 7.6.

Bibliography

[1] Raphael Bousso, Zachary Fisher, Stefan Leichenauer, and Aron C Wall. Quantum focusing conjecture. *Physical Review D*, 93(6):064044, 2016.

[2] Shinsei Ryu and Tadashi Takayanagi. Holographic derivation of entanglement entropy from the ads/cft correspondence. *Physical review letters*, 96(18):181602, 2006.

[3] Juan Maldacena. The large-n limit of superconformal field theories and supergravity. *International journal of theoretical physics*, 38(4):1113–1133, 1999.

[4] Christian Ecker, Daniel Grumiller, Wilke Van Der Schee, and Philipp Stanzer. Saturation of the quantum null energy condition in far-from-equilibrium systems. *Physical Review D*, 97(12):126016, 2018.

[5] Sean M Carroll. *Spacetime and geometry. An introduction to general relativity.* 2004.

[6] Sean M Carroll, Mark Hoffman, and Mark Trodden. Can the dark energy equation-of-state parameter w be less than- 1? *Physical Review D*, 68(2):023509, 2003.

[7] Eanna E Flanagan and Robert M Wald. Does back reaction enforce the averaged null energy condition in semiclassical gravity? *Physical Review D*, 54(10):6233, 1996.

[8] Roger Penrose. Gravitational collapse and space-time singularities. *Physical Review Letters*, 14(3):57, 1965.

[9] John L Friedman, Kristin Schleich, and Donald M Witt. Topological censorship. *Physical Review Letters*, 71(10):1486, 1993.

[10] Stephen W Hawking. Chronology protection conjecture. *Physical Review D*, 46(2):603, 1992.

[11] Henri Epstein, Vladimir Glaser, and Arthur Jaffe. Nonpositivity of the energy density in quantized field theories. *Il Nuovo Cimento (1955-1965)*, 36(3):1016–1022, 1965.

[12] Valerii A Rubakov. The null energy condition and its violation. *Physics-Uspekhi*, 57(2): 128, 2014.

[13] Dimitrios Krommydas. Violations of the null energy condition in qft and their implications. *arXiv preprint arXiv:1806.00107*, 2018.

[14] Noah Graham and Ken D Olum. Achronal averaged null energy condition. *Physical Review D*, 76(6):064001, 2007.

[15] Robert Wald and Ulvi Yurtsever. General proof of the averaged null energy condition for a massless scalar field in two-dimensional curved spacetime. *Phys. Rev. D*, 44:403–416, Jul 1991.

[16] William R Kelly and Aron C Wall. Holographic proof of the averaged null energy condition. *Physical Review D*, 90(10):106003, 2014.

[17] Larry H Ford and Thomas A Roman. Restrictions on negative energy density in flat spacetime. *Physical Review D*, 55(4):2082, 1997.

[18] Larry H Ford and Thomas A Roman. Averaged energy conditions and quantum inequalities. *Physical Review D*, 51(8):4277, 1995.

[19] Erik Curiel. A primer on energy conditions. In *Towards a theory of spacetime theories*, pages 43–104. Springer, 2017.

[20] Jacob D Bekenstein. Black holes and entropy. *Physical Review D*, 7(8):2333, 1973.

[21] Jacob D Bekenstein. Relativistic gravitation theory for the modified newtonian dynamics paradigm. *Physical Review D*, 70(8):083509, 2004.

[22] Stephen W Hawking. Particle creation by black holes. *Communications in mathematical physics*, 43(3):199–220, 1975.

[23] Stephen W Hawking. Black hole explosions? *Nature*, 248(5443):30, 1974.

[24] Jacob D Bekenstein. Black holes and the second law. *Lettere Al Nuovo Cimento (1971–1985)*, 4(15):737–740, 1972.

[25] Leonard Susskind and John Uglum. Black hole entropy in canonical quantum gravity and superstring theory. *Physical Review D*, 50(4):2700, 1994.

[26] Ted Jacobson. Black hole entropy and induced gravity. *arXiv preprint gr-qc/9404039*, 1994.

[27] Mukund Rangamani and Tadashi Takayanagi. *Holographic Entanglement Entropy*. Springer, 2017.

[28] Felix M Haehl, R Loganayagam, and Mukund Rangamani. Schwinger-keldysh formalism i: Brst symmetries and superspace. *arXiv preprint arXiv:1610.01940*, 2016.

[29] Martin Ammon and Johanna Erdmenger. *Gauge/Gravity Duality: Foundations and Applications*. Cambridge University Press, 2015.

[30] Ralph Blumenhagen, Dieter Lüst, and Stefan Theisen. *Basic concepts of string theory*. Springer Science & Business Media, 2012.

[31] Jorge Casalderrey-Solana, Hong Liu, David Mateos, Krishna Rajagopal, and Urs Achim Wiedemann. *Gauge/string duality, hot QCD and heavy ion collisions*. Cambridge University Press, 2014.

[32] Edward Witten. Anti de sitter space and holography. *arXiv preprint hep-th/9802150*, 1998.

[33] Robert C Myers. Stress tensors and casimir energies in the ads-cft correspondence. *Physical Review D*, 60(4):046002, 1999.

[34] J David Brown and James W York Jr. Quasilocal energy and conserved charges derived from the gravitational action. *Physical Review D*, 47(4):1407, 1993.

[35] Robert C Myers, Miguel F Paulos, and Aninda Sinha. Holographic studies of quasi-topological gravity. *Journal of High Energy Physics*, 2010(8):35, 2010.

[36] David Lovelock. The einstein tensor and its generalizations. *Journal of Mathematical Physics*, 12(3):498–501, 1971.

[37] Rong-Gen Cai. Gauss-bonnet black holes in ads spaces. *Physical Review D*, 65(8):084014, 2002.

[38] Alex Buchel, Jorge Escobedo, Robert C Myers, Miguel F Paulos, Aninda Sinha, and Michael Smolkin. Holographic gb gravity in arbitrary dimensions. *Journal of High Energy Physics*, 2010(3):111, 2010.

[39] Diego M Hofman and Juan Maldacena. Conformal collider physics: Energy and charge correlations. *Journal of High Energy Physics*, 2008(05):012, 2008.

[40] Aitor Lewkowycz and Juan Maldacena. Generalized gravitational entropy. *Journal of High Energy Physics*, 2013(8):90, 2013.

[41] Joan Camps. Generalized entropy and higher derivative gravity. *Journal of High Energy Physics*, 2014(3):70, 2014.

[42] Aron C Wall. Maximin surfaces, and the strong subadditivity of the covariant holographic entanglement entropy. *Classical and Quantum Gravity*, 31(22):225007, 2014.

[43] Xi Dong. Holographic entanglement entropy for general higher derivative gravity. *Journal of High Energy Physics*, 2014(1):44, 2014.

[44] Ling-Yan Hung, Robert C Myers, and Michael Smolkin. On holographic entanglement entropy and higher curvature gravity. *Journal of High Energy Physics*, 2011(4):25, 2011.

[45] Jason Koeller and Stefan Leichenauer. Holographic proof of the quantum null energy condition. *Physical Review D*, 94(2):024026, 2016.

[46] C Robin Graham and Edward Witten. Conformal anomaly of submanifold observables in ads/cft correspondence. *Nuclear Physics B*, 546(1-2):52–64, 1999.

[47] Sebastian de Haro, Kostas Skenderis, and Sergey N Solodukhin. Holographic reconstruction of spacetime¶ and renormalization in the ads/cft correspondence. *Communications in Mathematical Physics*, 217(3):595–622, 2001.

[48] Andrea Allais and Márk Mezei. Some results on the shape dependence of entanglement and rényi entropies. *Physical Review D*, 91(4):046002, 2015.

[49] Robert C Myers and Aninda Sinha. Seeing a c-theorem with holography. *Physical Review D*, 82(4):046006, 2010.

[50] Srivatsan Balakrishnan, Thomas Faulkner, Zuhair U Khandker, and Huajia Wang. A general proof of the quantum null energy condition. *arXiv preprint arXiv:1706.09432*, 2017.

[51] Xian O Camanho, José D Edelstein, Juan Maldacena, and Alexander Zhiboedov. Causality constraints on corrections to the graviton three-point coupling. *Journal of High Energy Physics*, 2016(2):20, 2016.